Deformation History of the Black Bay Fault, Northwest Territories, Canada

By

Dylan Jamison

A thesis

presented to the University of Waterloo

in fulfilment of the

thesis requirement for the degree of

Master of Science

in

Earth Sciences

Waterloo, Ontario, Canada, 2018

© Dylan Jamison, 2018

Author's Declaration

I hereby declare that I am the sole author of this thesis. This is a true copy of the thesis, including any required final revision, as accepted by my examiners.

I understand that my thesis may be made electronically available to the public.

Abstract

The Black Bay Fault is a major Paleoproterozoic, NE-SW-trending, crustal-scale feature that separates different tectonometamorphic domains of the southern Rae craton in the Canadian Shield. This structure extends from the edge of Lake Athabasca northward for 100's km into the Northwest Territories and was previously poorly constrained. Prior examination of the fault has been limited to small-scale studies in the Uranium City, SK vicinity. The Black Bay fault has previously been associated with rare-earth element and uranium mineralization in northern Saskatchewan, although this relationship is not fully understood. This thesis has focused on understanding the continuation of the Black Bay Fault into the Northwest Territories based on field mapping conducted as part of the GSC/NTGS GEM2 South Rae project. The observations are broken into three study areas: Tazin River, Insula-Labyrinth Lake and Dymond Lake.

The Black Bay Fault has had a cryptic polyphase history. Overall the fault is observed to be a steep, west-dipping structure associated with a strong NE/SW-trending fabric, but there are major disruptions to this trend by two NW-SE-trending segments of this fault. Field observations indicate it was impacted by four main deformational events, D1 to D4. D1 produced sinistral transpression along the fault, resulting in the uplift of the western domains relative to the eastern domains, a steeply west-dipping, NNE-SSW-trending gneissosity and shallowly NE-plunging lineations. D1 is inferred to have occurred ca. 1910 Ma in associated with the Snowbird Orogeny and the collision of the Hearne craton onto the eastern edge of the Rae Craton. D2 is a regionally limited event which modified the geometry of the fault rather than producing deformation along its length and resulted in the development of a left-stepping bend in the fault around Labyrinth Lake and another larger bend around Dymond Lake. D2 fabrics are not observed along the southern extent of the Black Bay Fault. This event remains very poorly constrained but is hypothesized to be associated with the indentation of the Slave craton into the Rae craton, further to the west, at ca. 1860 Ma. D3 was a dextral transpression event resulted in further west-side up movement on the primary Black Bay Fault trend and produced a steeply west-dipping, NE-SW-trending gneissic to mylonitic fabric along with shallowly SW-plunging lineation. D3 began by 1844.4 ±2.1 Ma continued until ca. 1830 Ma and was probably driven through far-field tectonic effects from the Trans-Hudson orogeny to the east. Differential uplift occurred during this event, with the fabrics becoming more ductile moving northward on the western side of the fault. D4

was a brittle-ductile to brittle deformation event associated with dextral movement along the fault and the development of a sinistral, NW-SE-trending conjugate fault/fracture system containing syn-tectonically emplaced mafic dykes. D4 was underway by ca. 1827 Ma and continued until at least ca. 1818 Ma. In addition, fault-associated rare-earth element and uranium mineralization previously discovered in northern Saskatchewan is observed to continue into the Northwest Territories, hosted primarily in S3 and S4 fabrics and possibly associated with the shift from a ductile regime to a brittle regime.

Acknowledgements

I would like to thank my supervisor Dr. Shoufa Lin whose guidance and knowledge introduced me to many features in the field and as well for his patience throughout this long process. I would also like to thank Edith Martel of the Northwest Territories Geological Survey (NTGS) who gave me direction in the field and invaluable feedback throughout the process of synthetizing my data. I thank Dr. Sally Pehrsson of the Geological Survey of Canada (GSC) whose broad knowledge of the region and big picture view helped greatly in understanding the significance of my data. Thanks to Dr. Daniele Regis for his help in processing my geochronological samples and aid in understanding the results.

Furthermore, I would like to thank Dr. Pedro Acosta-Gongora of the GSC for assisting me on my fly camps in the NWT. I also thank Bernadette Knox of the NTGS for introducing me to the geology around Uranium City, SK along with the data provided by Dr. Ken Ashton of the Saskatchewan Geological Survey.

Finally, I would like to thank my family for their support, in particular my father, whose discussions and push kept me focused.

Table of Contents

List of Figures

List of Tables

1. Introduction

1.1 Overview

Shear zones are important and intriguing structural features, accommodating large-scale deformation and providing insight into the tectonic history of an area. The Canadian Shield contains numerous regional-scale shear zones cross-cutting the craton, many of which have had little examination. The Rae craton, forming a central component of the Canadian Shield and composed of amphibolite to granulite facies Archean to Paleoproterozoic rocks (Hartlaub et al., 2005), contains many of these under-examined shear zones. One of these poorly understood shear zones, the Black Bay Fault, is the focus of this study.

Located in the southwestern portion of the Rae craton (Figure 1-1**)**, the Black Bay Fault is a large-scale, NE/SW-trending crustal feature stretching from the Uranium City area in northern Saskatchewan into the southern Northwest Territories. While the Black Bay Fault was initially discovered in the 1950's (Hale, 1954), prior to this study, only the southern extent of the fault in northern Saskatchewan has been examined. The continuation of the Black Bay Fault into the Northwest Territories has previously been based predominately on lineaments present in the aeromagnetic surveys of the area (Pehrsson et al., 2014a). The full extent of the Black Bay Fault was unknown and the fault trace in the Northwest Territories remained poorly constrained.

Previous studies on the Black Bay Fault have revealed a complicated structural history with reactivations and a transition from ductile through brittle-ductile to brittle deformation (Bergeron, 2001). Some attempts at constraining timing of deformation (i.e. Ashton et al., 2009; Bethune et al., 2013; Dieng et al., 2013) have indicated Paleoproterozoic deformational ages ranging from 2.3 Ga to 1.8 Ga. Due to this large time frame, multiple tectonic events have been proposed for the fault development and movement.

The Black Bay Fault has been associated with important mineralization in the area. Around Uranium City, an abundance of vein-type uranium deposits are present, some of which are associated with the Black Bay Fault (Dieng et al., 2013). Further to the north, rare-earth element mineralization at the Hoidas Lake deposit (Figure 1-2) has been emplaced along fault splays off

of the Black Bay Fault (Normand et al., 2009). As with the study of the fault itself, the extent of mineralization into the Northwest territories had not been previously determined.

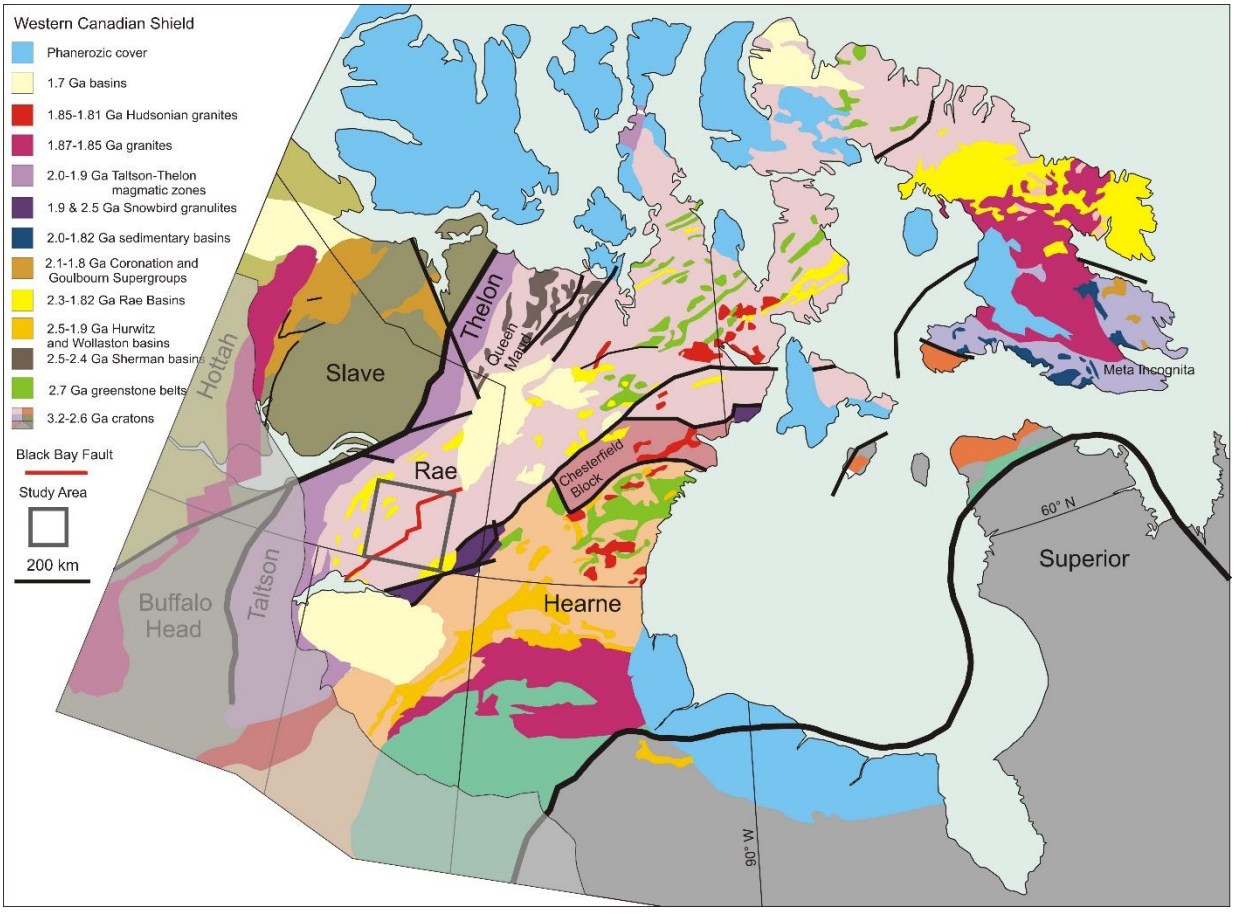

Figure 1-1. Geology of the Western Canadian Shield. The GEM2 South Rae and Black Bay Fault study area is indicated. Modified from Berman et al. (2005) and Martel et al. (2008).

1.2 Study Objectives

The primary goal of this study was to better understand the continuation of the Black Bay Fault into the Northwest Territories. A primary task was to verify whether or not the aeromagnetic lineament and signature accurately represents the fault. More importantly, this study has been designed to better document the structural fabrics associated with Black Bay Fault over a large area. While limited studies from northern Saskatchewan have discussed the Black Bay Fault, most do not have a significant focus on the structural fabrics. Those that do, such as Bergeron's (2001) thesis, examined the fault primarily at the outcrop scale and in a limited area. The study presented here is much more regional in scope and is able to test whether the smaller scale observations agree with the bigger picture of the fault. With a larger-scale view of the structural fabrics, this study also attempted to better constrain the timing of different deformational events

and possible tectonic events (ie. orogenesis, far-field extension, transpression) producing the deformation events. As a minor focus, this study examined whether the fault-associated mineralization present in Saskatchewan extends into the Northwest Territories.

1.3 Project Logistics

Study of the Black Bay Fault in the southern Northwest Territories was completed as part of the GEM2 South Rae mapping project, a joint mapping project between the Geological Survey of Canada and the Northwest Territories Geological Survey. Field work for this large-scale mapping project was completed over two six-week-long field seasons (2015 and 2016). Base camps were located on Wignes Lake and McArthur Lake (Figure 1-2), and mapping was conducted primarily by helicopter-supported traverses and lakeshore work from fly camps. The mandate of the larger project was to map four NTS map sheets (75 A, B, G, and H) at 1:250 000 scale (Figure 1-2). Map sheet 75 B (Abitau) provided the most opportunities to examine the Black Bay Fault in detail, and most of my time in the field was in this area of the project. These map sheets are some of the most poorly mapped sections in Canada and 75B, especially, remains virtually unexplored. It is displayed on the geological map of Canada (Wheeler et al., 1996) as simply a pink square.

In addition to the main study area in the Northwest Territories, a week was spent in Uranium City area, examining some of the outcrops described in previous studies that touched upon the Black Bay Fault. This allowed a clear comparison of deformation in that reference area with our observations further north (Figure 1-2). Uranium-lead geochronology was completed on two samples collected during the 2015 field season in an attempt to better constrain the timing of deformation.

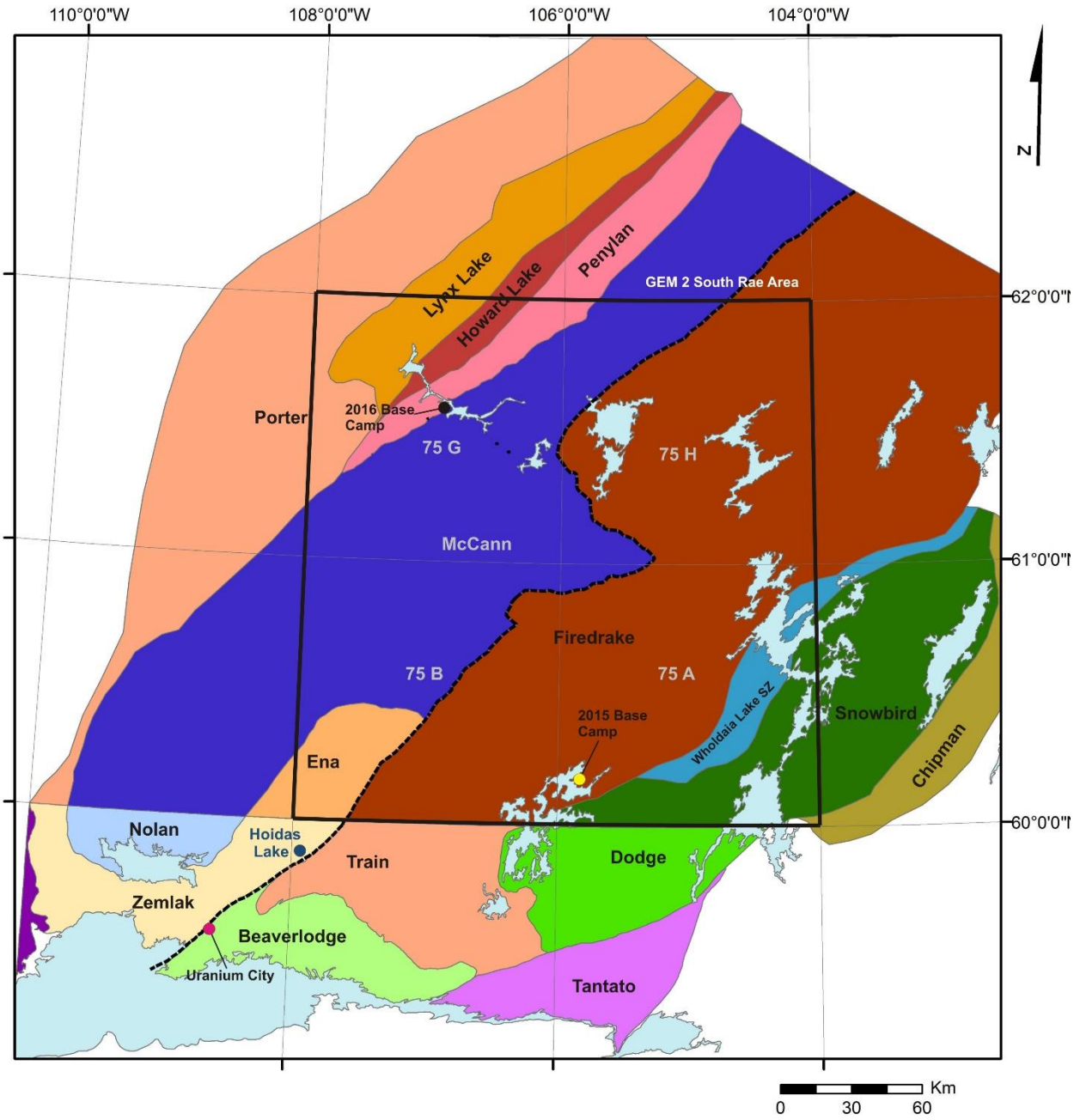

Figure 1-2. Map of the different tectono-metamorphic domains in the southern Rae craton. Domain naming varies across the Saskatchewan-Northwest Territories boundary, but can be easily correlated: Nolan-McCann, Zemlak-Ena, Train-Firedrake and Dodge-Snowbird. The Porter domain may also correlate to the Zemlak domain (Bethune, 2017). The Black Bay Fault is indicated by the dashed line. The GEM2 South Rae project area is highlighted in black. Saskatchewan domain boundaries modified from Sasktchewan Ministry of the Economy,(2010), and NWT domains modified from D Regis et al.,(2017) and Martel et al. (2018)

1.4 Thesis Layout

This thesis is divided into seven chapters including this chapter, the introduction. Chapter two provides a regional context to the study area and introduces the multiple orogenic events which are known to have impacted the southern Rae craton. Chapter three reviews the previous studies

which have been completed on the Black Bay Fault in Saskatchewan. In chapter four, the structural fabrics associated with the Black Bay Fault observed in the field from three study areas, Tazin River, Insula-Labyrinth Lake and Dymond Lake are discussed and an initial deformation sequence is presented. Chapter five focuses on the geochronology in which new U-Pb SHRIMP ages are reported and a synthesis of the published geochronology is presented to build an understanding of the region. Chapter six discusses the observed mineralization surrounding the Black Bay Fault and the fabrics which host the mineralization. Chapter seven attempts to combine the discussions presented in chapter four and five and constrain the timing of the various deformation event while also presenting possible correlations for the deformation events with known tectonic events.

2. Regional Tectonic Setting

The study area, and the postulated extent of the Black Bay Fault, is located entirely within the Rae craton (Figure 1-1). The Rae craton is one of numerous Archean cratons that amalgamated to form the Nuna supercontinent during the mid-Paleoproterozic era (Hoffman, 1988a). Hoffman (2014) proposed that the Rae craton served as a "backstop" for this amalgamation and was impacted by the Thelon-Taltson orogeny on its western margin and the Snowbird orogeny on its southeastern margin. The region of the Black Bay Fault could certainly have been affected by these orogenic episodes. It is possible, however, that the part of the Rae craton encompassed in the study area had already experienced significant deformation during the early Paleoproterozoic Arrowsmith orogeny (Berman et al., 2005).

2.1 Arrowsmith orogeny

Berman et al. (2005) proposed that an early Paleoproterozic orogeny (2.5 Ga to 2.3 Ga), the Arrowsmith, had occurred along the western margin of the Rae craton prior to the formation of the Nuna supercontinent. Previously it was believed that there was a global cessation of magmatism and possibly plate tectonics during this period (Condie et al., 2009) and therefore the Arrowsmith orogeny would not be possible. More recently however; work by Partin et al. (2014) have disproven the theory that a global cessation of magmatism occurred during this period, supporting the possible of the Arrowsmith orogeny.

The Arrowsmith orogeny is thought to represent a Cordilleran-type collision, and the end of high-grade metamorphism is interpreted to have occurred at 2.34 Ga in the northern part of the Rae while the southern portion experienced metamorphism until 2.28 Ga (Berman et al., 2013). A 2.35 Ga metamorphic event observed north of the Thelon basin (Figure 2-1) has been the primary basis behind the postulated Arrowsmith orogeny (Berman et al., 2005), but the corresponding craton or body associated with the orogeny remains ill-defined. Multiple cratons found throughout the world show some evidence of 2.5-2.3 Ga tectonic activity, suggesting they may have all formed a previously unknown supercontinent (Pehrsson et al., 2013), although their paleolatitudes remains poorly constrained.

In northern Saskatchewan a 2.3 Ga magmatic zone present in the Beaverlodge domain of the Rae craton (Hartlaub et al., 2007) may represent the southern extent of the Arrowsmith orogeny

(Figure 2-1). Further work in the Uranium City area has produced similar aged rocks in the adjacent domains (Ashton et al., 2007; Normand, 2014).

A 2012 reconnaissance transect through the planned mapping area for the South Rae GEM2 project by the GSC discovered both crystallization and metamorphic Arrowsmith ages in the domains surrounding the Black Bay Fault (Davis et al., 2015). An earlier and better understood event, the MacQuoid orogeny occurred on the eastern flank of the Rae craton from 2.56 to 2.5 Ga (Pehrsson et al., 2013), but it is believed that either (1) the effects from that orogeny were not felt in the southwest part of the Rae craton where the Black Bay Fault is located or (2) the Black Bay Fault had not been developed at this time.

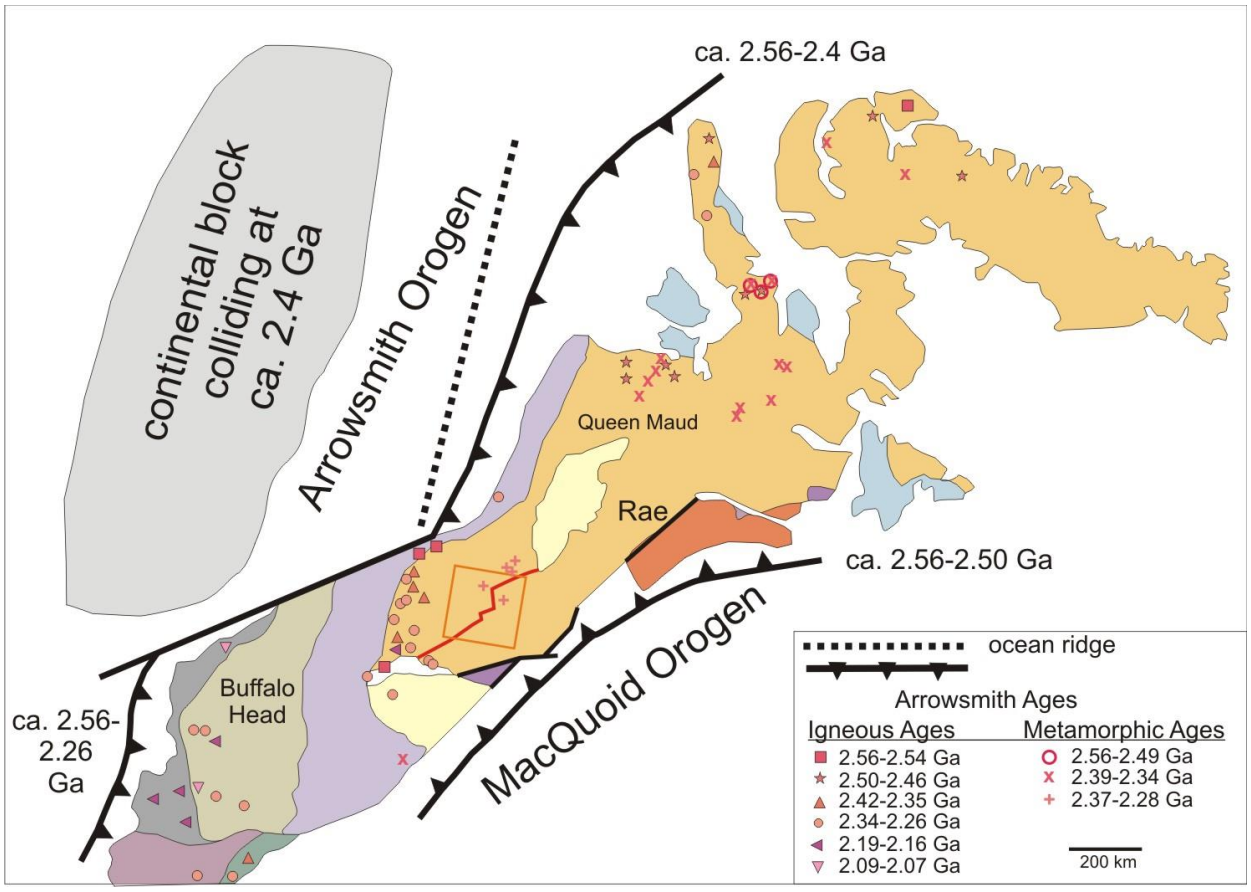

Figure 2-1. Simplified diagram illustrating the Arrowsmith and MacQuoid orogenies on the Rae craton along with the reported ages matching the timing of the Arrowsmith. Band of Arrowsmith ages appear to transect through the project area. Black Bay Fault trace shown in red along with the GEM2 South Rae study area. Modified from Berman et al., (2013)

2.2 Nuna Amalgamation

2.2.1 Thelon-Taltson orogeny

Both the Thelon-Taltson orogeny, which occurred at 1.97 Ga and continued until 1.93 Ga (Hoffman, 2014), and the Snowbird orogeny, which occurred at 1.91 Ga to 1.89 Ga (Berman et al., 2007; Martel et al., 2008), are also potential tectonic drivers for the Black Bay Fault. The older Thelon-Taltson orogeny was the initial orogeny to occur during the amalgamation of Nuna. During this event, the Slave craton was accreted onto the western margin of the Rae craton, with the collision resulting in the development of the Taltson magmatic zone (Hoffman, 2014) (Figure 2-2). Development of the large scale Great Slave Lake shear zone occurred with the collision which produced dextral transpression with east-side up movement along this structure (Hanmer et al., 1992) There is still some controversy around the tectonic setting of this orogeny. Although monazite dating from the magmatic zone suggests a cratonic boundary at this time (Bethune et al., 2013), there has been some debate over this model as the geochemical signatures in this region point, instead, to an intra-cratonic region (Chacko et al., 2000; De et al., 2000). While the eastward extent of the impact of the Thelon-Taltson orogeny in the southern Rae had been uncertain, recent monazite dating around Uranium City, Saskatchewan, close to the Black Bay Fault by Shiels et al. (2016), produced 1.93 Ga metamorphic ages, which falls into the time period of the Thelon-Taltson orogeny.

2.2.2 Snowbird orogeny

The Snowbird tectonic zone divides the western Churchill Province into the Rae and Hearne cratons (Figure 2-2) and extends from Hudson Bay to the Cordilleran orogeny deformation front. This zone was originally identified from aeromagnetic data (Gibb and Walcott, 1971) and was proposed to be a Paleoproterozoic orogenic suture because it truncates the Tatlson magmatic zone (Hoffman, 1988a). Berman et al., (2007) proposed that the Snowbird Orogeny is an early phase of the Trans-Hudson orogeny and is a Paleoproterozoic accretionary event of the Hearne (and Rae-Chesterfield block onto the Rae craton at ca. 1.9 to 1865 Ga.

However, Neoarchean plutonism present in both the Rae and Hearne cratons at ca 2.6 Ga (Regan et al., 2017) has led some to believe these two cratons were already joined by this time, and the that Snowbird tectonic zone is actually the remnant of an Archean orogeny (Flowers et al., 2006; Hanmer et al., 1995; Mahan and Williams, 2005; Regan et al., 2017).

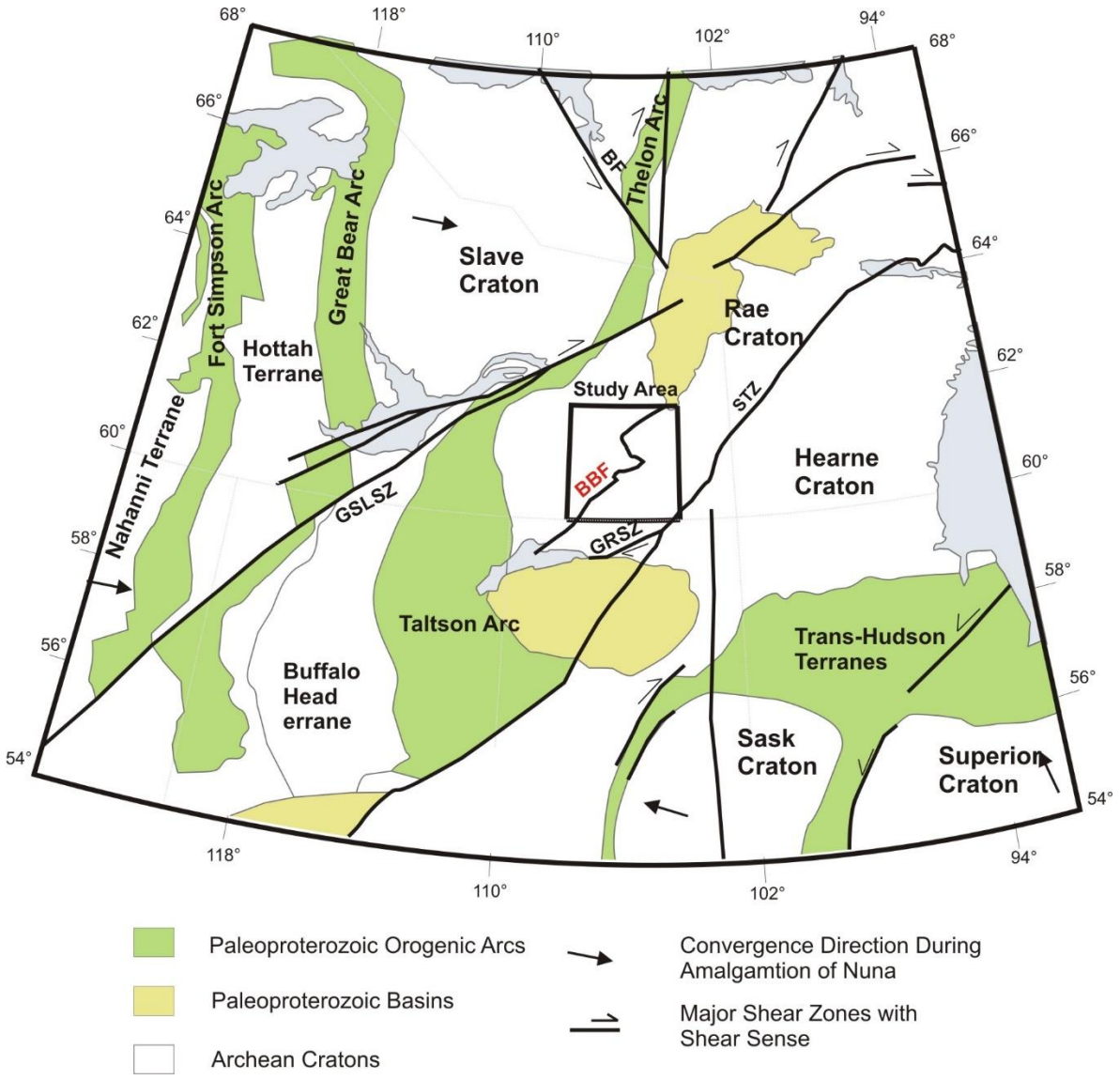

Figure 2-2. Diagram showing the convergence of the various cratons on to the Rae craton during the amalgamation of the Nuna supercontinent (Modified from Ashton et al., 2009)

2.2.3 Trans-Hudson orogeny and other orogenic events

The long lived Trans-Hudson orogeny, 1.9 to 1.8 Ga, had a far reaching tectonic influence and impacted this part of the Rae craton (Ashton et al., 2009; Corrigan et al., 2009). The largest Paleoproterozoic orogeny in the Canadian Shield and probably best known, the Trans-Hudson orogeny involved the collision of the Superior craton onto the Rae and Hearne cratons (Figure 2-2). The orogen extended from the Dakotas up to the Ungava Peninsula, and the orogeny led to the closure of the Manikewan Ocean that was situated between these cratons (Corrigan et al., 2009).

The Trans-Hudson orogeny was long lasting, with the closure of the Manikewan Ocean commencing by 1905 Ma (Corrigan et al., 2009) and terrane accretion onto the Hearne domain initiating by 1.85 Ga (Ansdell, 2005). However, terminal collision of the Superior craton onto the Rae/Hearne craton did not occur until 1.83-1.80 Ga, with collision first starting along the southern margin (Bickford et al., 1990). A large thermal overprint occurred in the Hearne domain at this time, which is known to extend westward to the Snowbird tectonic zone (Schneider et al., 2007) and to have produced dextral reactivation of the zone at 1.83 Ma (Stern et al., 2003). Granites of a similar age have been found further west into the southern portion of the Rae craton, suggesting that the terminal collision impacted this portion of the Rae craton (Ashton et al., 2009).

3. Previous Geological Work

3.1 Early Studies

The feature that has become known as the Black Bay Fault was identified by Hale (1954), who described a zone of mylonitized and deformed rocks in northern Saskatchewan that extends northeast from Black Bay on Lake Athabasca. Further mapping around Uranium City and the larger Beaverlodge mining area by Tremblay (1968) better described the zone of deformation and named the Black Bay Fault.

Although Tremblay's (1968) GSC report offers a fairly comprehensive description of the various geological units and structures of Uranium City, it contains several geological assessments that are not compatible with modern processes or concepts. For example, gneissic compositional banding is (mis)interpreted as sedimentary beds, transposed foliation is not properly described, and granitization is used to describe many different metamorphic and igneous aspects observed in outcrops.

However, Tremblay (1968) did recognize multiple phases of deformation of the Black Bay Fault, and an attempt to measure the lineations was made. Specifically, he found lineations plunging to both the NE and SW at angles of 30-60^{o} on steeply dipping planes with a strike of 050^{o} (Tremblay, 1968), thus providing the first publish geometry of the Black Bay Fault around Uranium City. He also reported evidence of an east-dipping geometry for the Black Bay Fault from shallow trenching of this structure in a uranium mine (Tremblay, 1968), though the location is not described. Further work by Tremblay (1972) identified multiple deformation events, along with recognition of a transition from a ductile regime towards a brittle regime in the deformational fabrics. However, he does not present a kinematic assessment nor discuss the tectonic drivers behind this deformation.

Further publications from the work in the Beaverlodge area by Tremblay (1971 a) produced a detailed geological map and two geological cross-sections. This work was primarily focused on - the more E-W-trending faults like the ABC fault located to the east of the Black Bay Fault in the Beaverlodge region, where uranium mining was ongoing at that time. Two NW-SE-trending cross sections through the Black Bay Fault were produced (Figure 3-1) which show folded basement rocks with eastern fold limbs roughly matching the dip of the Black Bay Fault and

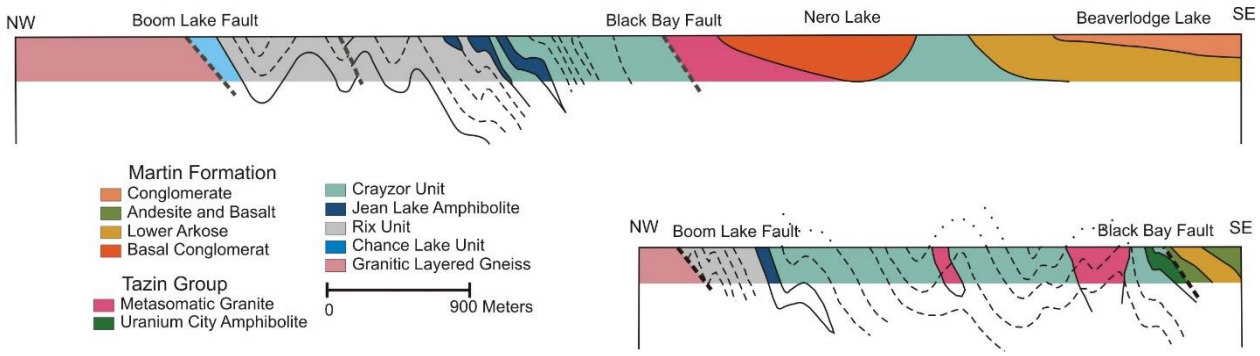

Figure 3-1. Geological cross-sections from the Uranium City area of the Black Bay Fault. A moderate east-dipping fault geometry was proposed for the Black Bay Fault (Modified from Tremblay (1971b))

other parallel striking faults in the area (Figure 3-1). The geological work in the Uranium City area was further improved upon and modernized with a bedrock compilation of the Beaverlodge domain by (Macdonald, 1984).

Published geological surface studies within our study area in the Northwest Territories prior to the commencement of the GEM2 South Rae project is limited to Hoadley (1955), who spent one summer mapping the Abitau map sheet (NTS 75B) through aerial photograph interpretation surveys as well as via canoe. His assessment of structural features is limited primarily to foliations. No faults are indicated on Hoadley's (1955) map nor does he note a change in lithology or boundary where the Black Bay Fault would be expected to continue from northern Saskatchewan. In the southern portion of the Abitau map sheet, the Tazin River was portaged by Hoadley and he recorded foliation aligned with the general course of the Tazin River. While this trend would be expected if the Black Bay Fault is present in this location, very little measurements were made further away from the river's course. Without measurements further out from the river, it is not possible to conclude there is a shear zone present along the trace of the river in this region rather than a regional foliation that that is penetrative through the area. No lineations or kinematic indicators were reported during Hoadley's (1955) mapping of the Abitau sheet.

3.2 Recent studies

Prior to our investigation as part of the GEM2 South Rae project, the most detailed structural information that was clearly related to the Black Bay fault/shear zone comes from a few, spatially limited areas around Uranium City in northern Saskatchewan (Ashton et al., 2000;

Bergeron, 2001; Kraus and Ashton, 2000). Only one structurally focused study has been completed on the fault, viz., a master's thesis at University of Saskatchewan by Julie Bergeron (2001). This study focused on a few well exposed, small (meter-scale) outcrops along with two limited transects south of Uranium City.

Although the trace of the Black Bay Fault had already been identified and examined at spot locations prior to Bergeron's (2001) study, hers was the first major attempt to understand the deformational history and appraise the level(s) of deformation. Her study confirmed that the Black Bay Fault produced significant amount of deformation in the shear zone, with some mylonites to ultra-mylonites being described near to the centre of the shear zone (Bergeron, 2001). Dextral sense of shear was the sole motion observed in the mylonites (Bergeron, 2001), and the shift from ductile through brittle-ductile to brittle deformation was described in the area.

Bergeron (2001) describes a number of outcrops situated in close-proximity to the trace of the fault and made transects across the fault. However, the transects were restricted to the western side of the fault or crossed over only into the Martin Group sedimentary rocks with an depositional age of ~ 1820 Ma (Morelli et al. 2009). The Martin Group has only reached lower greenschist facies metamorphism (Ashton et al., 2001), and only brittle fabrics were measured on the eastern side of the fault, and no shear sense indicators recorded by Bergeron (2001). No measurements from the older and potentially more deformed basement gneisses on the eastern side of the fault were presented. Furthermore, the Black Bay Fault in the study is bordered by the Beaverlodge domain to the east rather than the Train domain (Figure 1-2) which borders the majority of the eastern edge of the Black Bay Fault (Ashton et al., 2001). Consequently, the deformation history observed here may not be very representative of the overall deformation of the fault due to the presence of a lower greenschist facies only observed in the western part of the Beaverlodge domain and not found elsewhere in the area surrounding the Black Bay Fault (Ashton et al., 2001).

A small side study of the Black Bay Fault on the Cracking Stone Peninsula south of Uranium City by Kraus and Ashton (2000) looked at the Black Bay straight belt, which is composed of the Archean aged Murmac Bay Group in the Beaverlodge domain (Shiels et al., 2016). Steep NW-dipping mylonitic fabrics with dextral kinematics were found along with shallowly SW-plunging lineations, which was interpreted to indicate development of the fabrics occurred through a west-

side up dextral transpression event (Kraus and Ashton, 2000). Small, late asymmetrical S-folds were noted in the study and were believed to have formed during a late sinistral shearing event (Kraus and Ashton, 2000). This was the only study in Saskatchewan which reported any evidence of sinistral displacement along the Black Bay Fault.

Beyond the focus around Uranium City, there has been some structurally focused work around the Hoidas Lake rare-earth element deposit ~ 60 km to the northeast by Gunning and Card (2005) and followed up by Normand et al. (2009). In this area, the Black Bay Fault separates the Zemlak (Ena) domain on the west from the Train domain to the east (Normand et al., 2009). These studies reported the Black Bay Fault to be west dipping (Figure 3-2), in contrast to east-dipping reported from the south. However, there remains some disagreement here on the dip direction of the Black Bay Fault as Halpin's (2010) thesis on the Hoidas deposit reports the fault and associated splays as east dipping.

Two generations of ductile fabrics associated with deformation of the Black Bay Fault were noted by Gunning and Card, (2005), plus a subsequent brittle-ductile event. An older event produced southwest-trending, steeply dipping foliation, along with a more mylonitic fabric in some areas (Gunning and Card, 2005). Dextral shear sense indicators were found in this fabric,

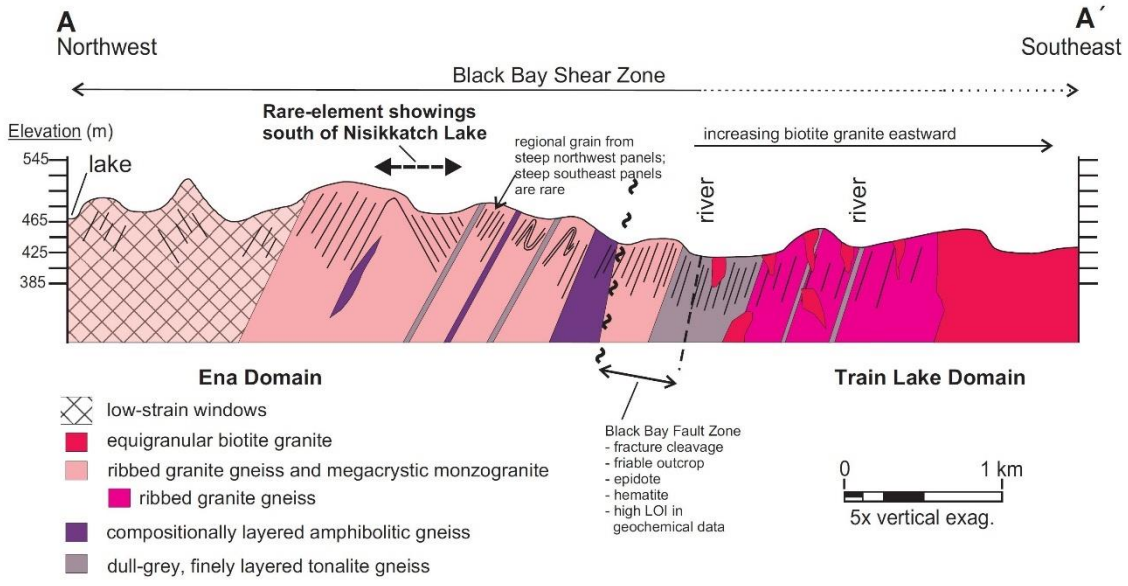

Figure 3-2. Geological cross-section of the Black Bay Fault around the Hoidas Lake area demonstrating a west-dipping fault geometry (from Gunning and Card, 2005)

along with tight, SW-plunging folds. Together these fabrics indicate a west-side up dextral transpression event on the Black Bay Fault (Gunning and Card, 2005).

The later ductile deformation event was more heterogenous and produced meter-scaled mylonitic shear zones aligned either parallel to or overprinting the older fabric counter clockwise (Gunning and Card, 2005). Dextral shear sense indicators were also found in these mylonite zones, along with lineations shallowly plunging to both the southwest and northeast. Gunning and Card (2005) suggest that this fabric developed during a more strike-slip event on the Black Bay Fault.

A final brittle-ductile to brittle event produced a conjugate set of faults and lineaments; a W-NW-trending component and N-NE-trending component, with dextral movement along on the NE component (Gunning and Card, 2005). Later mapping around the Hoidas and Nisikkatch deposits by Normand (2014) revealed two different episodes of NE-SW-trending ductile folding; an earlier event which produce NE-trending, moderately to steeply plunging folds, and a later event which produced SW-trending, moderately plunging folds. While not discussed, the later event described by Normand (2014) appears to correlate with the earlier Gunning and Card (2005) event.

4. Geology of the Black Bay Fault and surrounding areas

4.1 Overview

Data collected from three main study areas, the Tazin River area, the Insula-Labyrinth Lakes area and the Dymond Lake area (Figure 4-1), are utilized as the primary evidence in developing a comprehensive understanding of the Black Bay Fault and its deformation history. The Tazin River and the Insula-Labyrinth Lakes study areas are located in NTS sheet 75 B, and, together, they provide over 110 kilometers of coverage along the Black Bay Fault. The Dymond Lake study area located further to the north in located in NTS sheet 75G. Observations collected from the NTS sheet 75H portion of the Black Bay Fault are included in the Dymond Lake study area. During the examination of the Black Bay Fault for this thesis, the Uranium City area was revisited through a week-long fly camp in order to better understand our observations to the north in the Northwest Territories; however, the Uranium City area will not be discussed in detail in this thesis.

Through the course of the field mapping, fabrics associated with four separate episodes of deformation along the Black Bay Fault (D1 to D4) have been identified, in addition to a regional fabric (pre-D1) that appears to have existed prior to the development of the Black Bay Fault. Foliations associated with these various deformational episodes will be referred to as S1-S4 while L1-L4 will be used for the respective lineations and F1-F4 will be used for the associated folds. Not all generations of structures are well developed in all areas and this will be discussed later on in this section.

The sequencing of the events and the structural fabrics has been established, or inferred, by overprinting relationships at different outcrops throughout this large map region. The supporting overprinting relationships are discussed through the course of the chapter and expanded on in the discussion section (4.5).

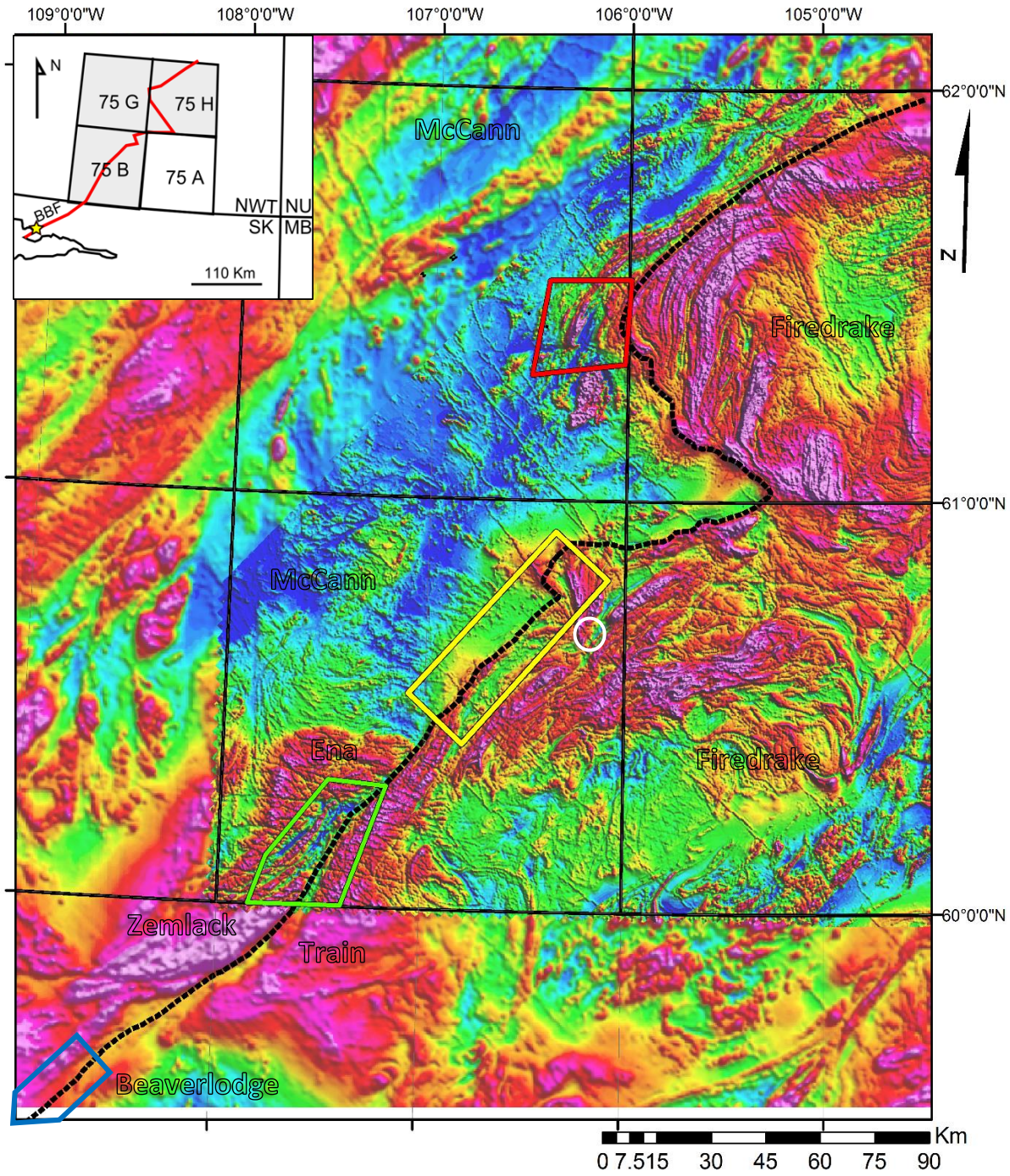

Figure 4-1. Aeromagnetic Map of the South Rae GEM2 study area. Trace of the Black Bay Fault (BBF) is shown in black along with the names of the various tectonometamorphic domains separated by the Black Bay Fault. Study areas for the Black Bay Fault highlighted: Tazin River Area (Green) and Labyrinth and Insula Lakes Area (Yellow). Also shown is the revisited Uranium City study area (Blue) and the Dymond Lake study area (Red)..Gemelo rare-earth element showing circled in white. Aeromagnetic data from Kiss and Coyle (2012)

4.2 Tazin River Area

4.2.1 Introduction

The Tazin River focus area is located in the southwestern corner of the GEM2 South Rae study area, in NTS 75 B (see Figure 4-1). In this region, the Black Bay Fault separates the Ena domain to the west of the fault (described as the Zemlak domain in Saskatchewan) from the Firedrake domain to the east (Figure 4-2). The Black Bay Fault is spatially defined by a pronounced topographic lineament through which the Tazin River flows southerly from the NWT into Saskatchewan (Figure 4-2a). Furthermore, a pronounced magnetic low corresponding with the trace of the Black Bay Fault is visible in the aeromagnetic data of the area, separating the high magnetic signatures of both the Ena and Firedrake domains (Figure 4-2b).

Aeromagnetic data and topography also indicate the existence of several fault splays extending SW from the trace of the Black Bay Fault into the Ena domain. These fault splays are concave to the west, displaying a shift in trend from NE-SW near to the Black Bay Fault to a more ENE-WSW trend as the fault splays extend westward. On the contrary, east of the fault in the Firedrake domain, the first derivative aeromagnetic data suggests the presence of a secondary fault trending parallel to the Black Bay Fault, but no evidence supporting this fault was observed in the field. Also, visible in the aeromagnetic data and satellite imagery are numerous E-W-trending lineaments (Figure 4-2 B). These are interpreted to be late (D4 or post-D4) brittle fractures and faults.

Outcrops throughout the Tazin River area generally have low relief, are limited in extent, and tend to be heavily covered by lichen. The geology in the area around the Black Bay Fault was examined in detail in one limited region using a four-day fly camp situated adjacent to the fault on the western side (Figure 4-2) from which multiple overland traverses were completed.

In addition to the fly camp, five helicopter-supported traverses were completed in the Tazin River vicinity. The majority of the structural measurements were collected from the Tazin River fly camp area as the surrounding traverses were less focused on the structure of the area. The latter were used to establish a better regional picture of the deformation marginal to the Black Bay Fault. Unfortunately, due to the width of the Tazin River, establishing continuous traverses crossing the fault was problematic. Consequently, the western side of the fault (Ena domain) had greater examination than the eastern region (Firedrake domain). Additionally, exposure near to

the river was relatively poor due to the significant deposition of overburden along the Tazin River. Several Pleistocene esker systems as well as the Tazin River followed the topographical low expression of the Black Bay Fault.

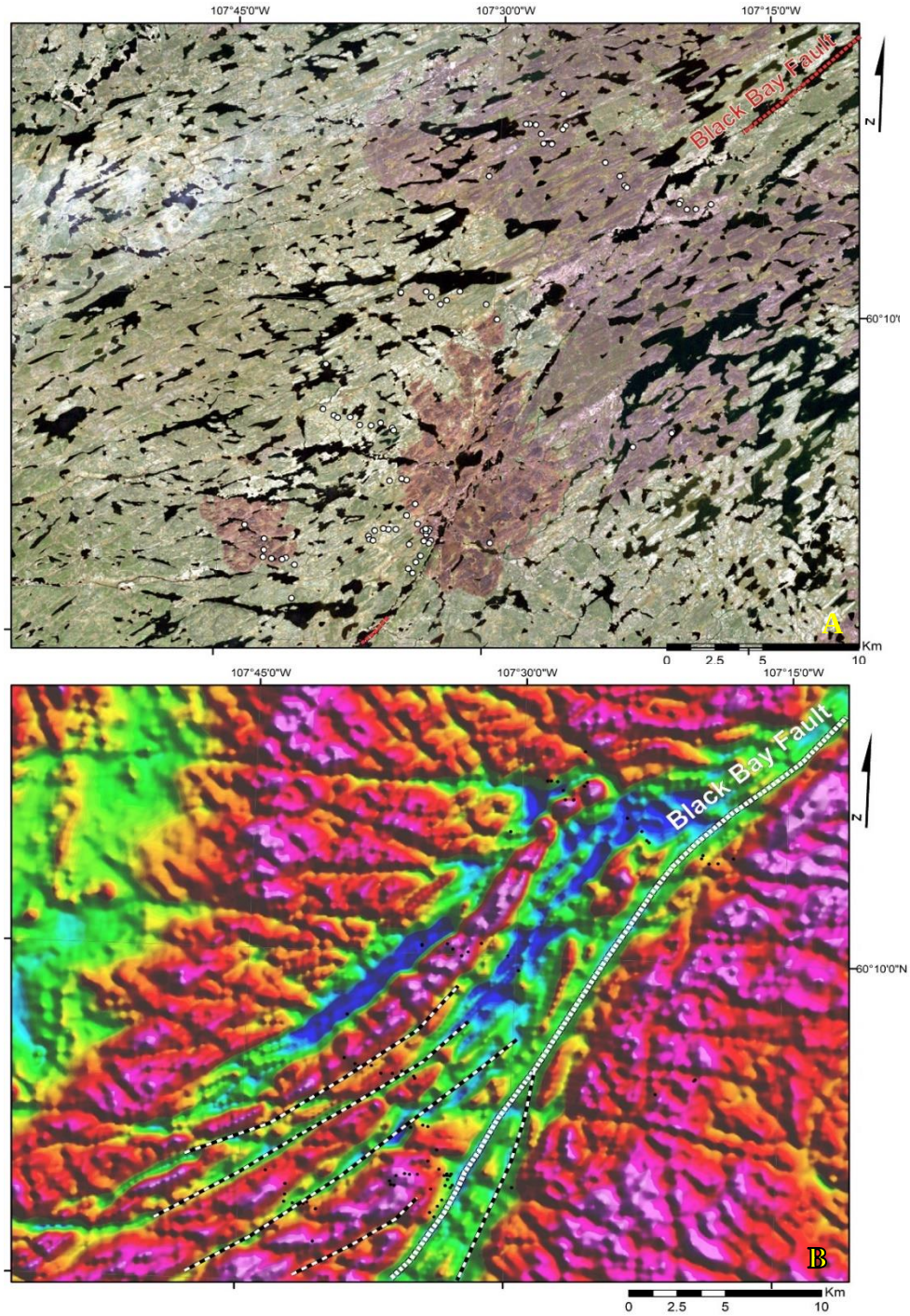

Figure 4-2. (A) CanImage satellite imagery of the Tazin River Area illustrating the topographical lineament of the Black Bay Fault.(B) Aeromagnetic Survey Map of the Tazin River Area, with area of focus during a 4-day fly camp highlighted in black. Fault splays extending westward from the fault into the Ena domain. Field stations shown in black. Aeromagnetic data from Kiss and Coyle (2012).

4.2.2 Geology

Ena domain

Through our field observations, the Ena domain in the Tazin River area is subdivided into five map units based on lithology and structure: (1) orthogneiss, (2) foliated felsic rocks, (3) metasedimentary rocks, (4) paragneiss, (5) foliated mafic rocks and (6) mylonite zones (Figure 4-6). The different map units are intended to capture variations in the deformational fabric, from foliated to gneissic to gneissic with mylonitic zones.

The majority of the rocks in the Ena domain are of upper amphibolite to granulite grade. There is a general compositional variance between the igneous and sedimentary protolith zones that is reflected in the aeromagnetic data of the area (Figure 4-2). This relationship is relied upon in the development of the geological map for the Ena domain, with many of the contacts inferred from the aeromagnetics data (Figure 4-6). Specifically, in the low magnetism regions, garnetiferous rocks ranging from weakly foliated to well-developed gneissic banding are commonly observed and assumed to be metasediments to paragneisses (Figure 4-3) (although aluminosilicates such as sillimanite were only rarely observed). Comparatively, in the regions with a higher magnetic signature, the rocks lack garnets and are well foliated to gneissic meta-plutonic rocks.

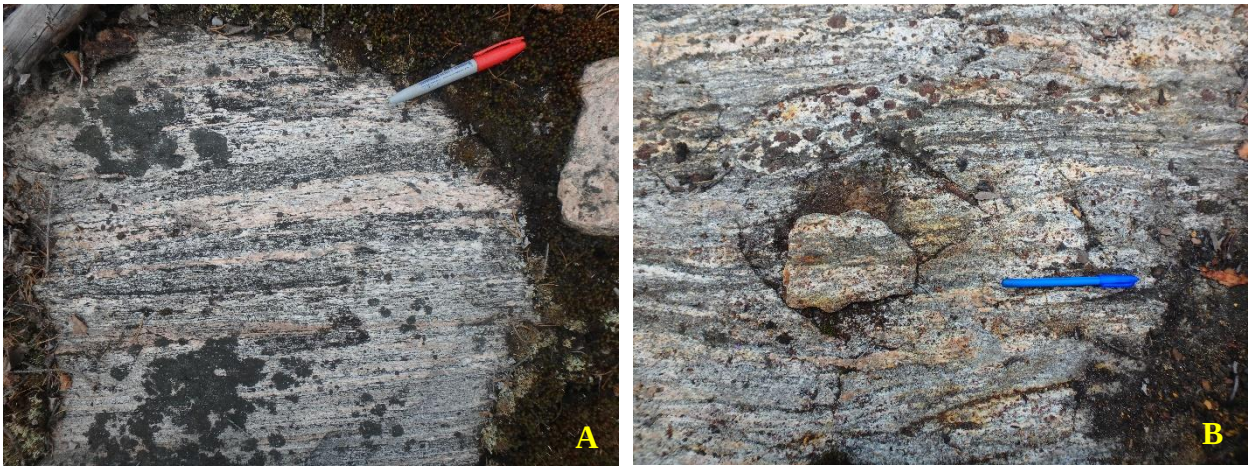

Figure 4-3. Field photos of typical rocks of the Ena domain, intermediate orthogneiss (A) and paragneisses (B)

A regression in the metamorphic grade is observed moving towards the Black Bay Fault from the interior of the Ena domain, with orthopyroxenes found in the rocks outside of the fault zone area. Additionally, unstable and altered garnets are observed in the metasediments closest to the Black Bay Fault, whereas garnets appear more stable in the other bands of metasediments further west.

Pegmatitic dykes rich in hyalophane, a barium-rich alkali feldspar, are commonly observed in the Ena domain both in deformed and undeformed intrusions (Figure 4-4). Additionally, orthopyroxene-bearing syenitic intrusions were observed in a few outcrops. These appear to be unique to the Ena domain. In addition to the felsic intrusions, a NW-trending mafic dyke swarm which has undergone metamorphism up to amphibolite facies was observed to crosscut the deformed gneisses in a few outcrops. Multiple generations of late syn-tectonic to post-tectonic felsic intrusions are observed to cut the various basement rocks, with some intrusions appearing to have been injected parallel the Black Bay Fault fabric. For example, a distinctive, undeformed, chalky-white and pink, aplitic granite intrusion is observed to transect all deformational fabrics.

Figure 4-4. Field photos of hyalophane-bearing granitic pegmatite. Note grey-blue feldspars (A) and mafic xenoliths altered to a diopside-allanite composition (B)

The orthogneisses often contain mafic xenoliths that show alteration to diopside-allanite. This alteration appears to be exclusive to the Ena domain (Figure 4-4). Hydrothermal veins with the same diopside-allanite composition was also observed cutting basement rock. With the exception of the metasediments and paragneisses, the majority of the rocks situated in the Ena domain are strongly magnetic, and magnetite crystals up to 3mm in diameter are commonly observed in hand samples. The meta-sediments are variably magnetic.

There is a significant amount of hydrothermal alteration throughout the Ena primarily seen as discoloration of the host rock adjacent to fracture and veins sets. This alteration was primarily potassic, with plagioclase in the host rock showing partial to full alteration to a salmon pink k-feldspar or epidotization associated with pistachio-green veins. A minor amount of hematization

was seen in the Tazin River area, but it is much less than what is seen in the Uranium City area further to the south, which shows significant amounts of hematization.

Firedrake Domain

Outcrops examined in (the southwestern portion of) the Firedrake domain in the Tazin River focus area are primarily composed of orthogneisses. Although the ground observations stations are few and widely separated through the Firedrake domain, these orthogneisses are tentatively divided into three map units: (1) migmatitic granodiorite gneiss, (2) intermediate orthogneiss and (3) mylonitic gneiss. The migmatitic gneisses appear to have undergone a significant amount of partial melting, and the resulting melt has produced a soupy or migmatitic texture (Figure 4-5). The orientation of a pre-existing layering in the gneisses is highly variable in the migmatitic gneiss; however, a NW-SE alignment begins to develop when approaching the Black Bay Fault from the east. This fabric defines the intermediate gneiss map unit. A clearly mylonitic fabric was observed at only one field station, near to the trace of the Black Bay Fault. Mafic xenoliths in the Firedrake domain do not show the diopside-allanite alteration observed in the Ena domain, but often contain resitite of older gneissic layering.

Figure 4-5. Field photos of rocks from the Firedrake domain: (A) Soupy gneiss to migmatitic rock (intermediate in composition). (B) Gneissic rock with significant granitoid intrusions, some injected along gneissosity.

Overall the metamorphic grade of the Firedrake domain in the Tazin River area is upper amphibolite. Garnet-bearing rocks are rare in the southern portion of the Firedrake domain due to the strong retrogression and were only observed in one location near to the Black Bay Fault (though, as noted above, outcrop examination of this part of the Tazin River focus area was relatively limited). Similar to the Ena domain, multiple felsic intrusions were observed to cut the

orthogneisses. Many of the intrusions in the vicinity of the Black Bay Fault appear to be syn-tectonic, with granitoid material having been injected aligned with the gneissosity (Figure 4-5). Based on one observation from the air, the amphibolitic dykes noted in the Ena domain appear to extend across the Black Bay Fault into the Firedrake domain. As in the Ena domain, the rocks in the Firedrake domain show significant potassic alteration, but epidote veining is less abundant and diopside-allanite veins are not present. Quartz tension gashes were also occasionally observed whereas quartz was only found in boudin necks in the Ena domain. In all the outcrops, the rocks were found to be strongly magnetic using a hand magnet. Due to the lack of stations and the relatively smooth aeromagnetic pattern, the lithology of the Firedrake domain in the Tazin area could not be as well divided as for the Ena domain.

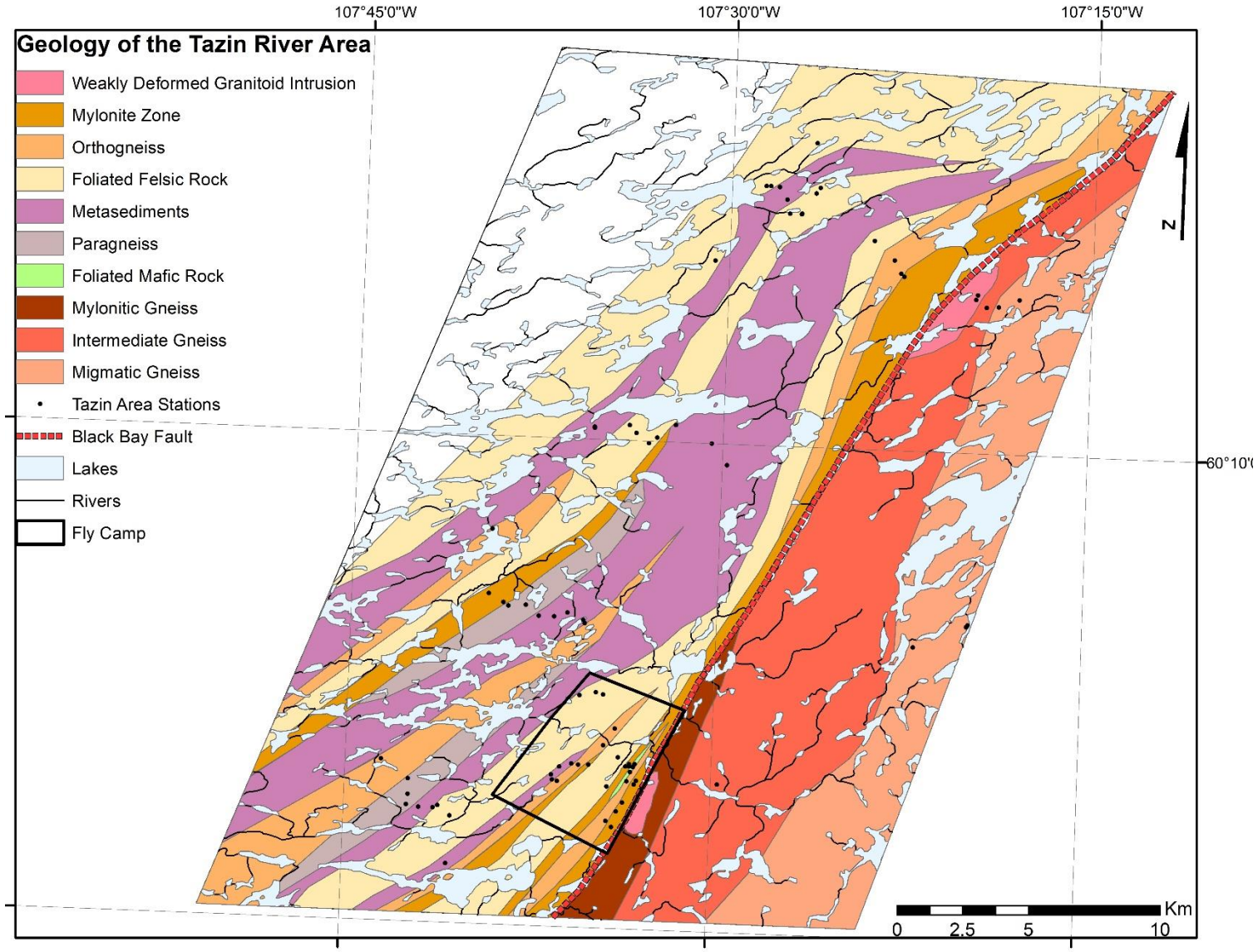

Figure 4-6. Simplified Geological Map of the Tazin River Area, compiled from the 2015 traverses and extrapolation from the aeromagnetic data of the area.

4.2.3 Structural Fabrics

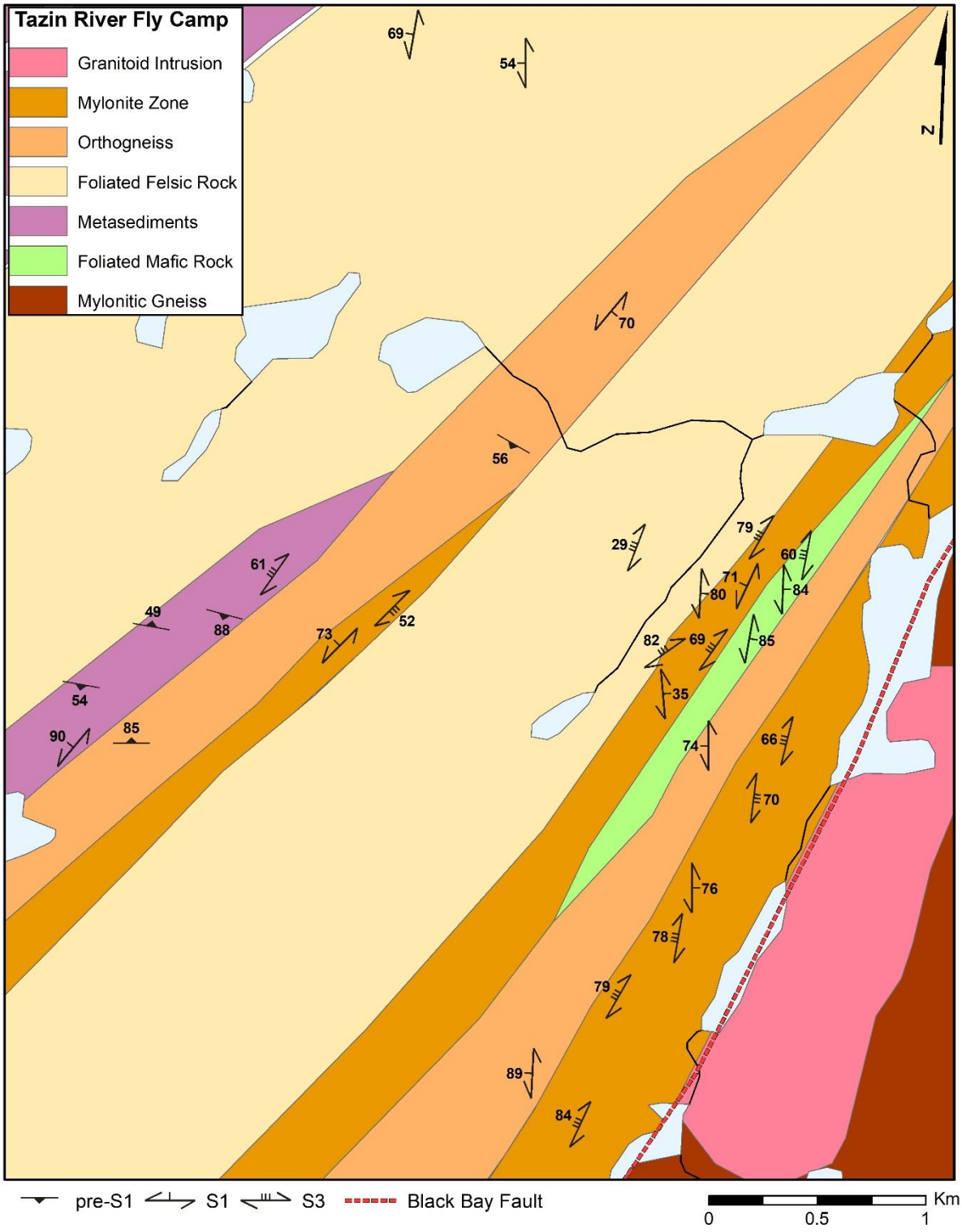

Figure 4-7. Geological map showing the various generations of foliations measured around the Tazin River fly camp

Overview

The Tazin River area predominately contains three generations of deformational fabrics (S1, S3 and S4) associated with the Black Bay Fault and are described in the following section. Notably, the Tazin River area is devoid of evidence of D2. The Tazin River area provides the best insight into the D1 and D4 out of the two main study areas. In addition, a pre-existing fabric (pre-S1), is present in the region and is discussed briefly.

Pre-D1

In the Tazin River area, an older fabric, pre-S1, is occasionally found, preserved in locations which have undergone the least amount of deformation (Figure 4-7). This is assumed to represent the fabric that existed in the area preceding the development of the Black Bay Fault. Preservation of pre-S1 is more frequent moving further west of the Black Bay Fault into the Ena domain (Figure 4-7). The character of the pre-S1 fabric here is variable, ranging from gneissic to weakly foliated and varying in strike from E-W to WNW-ESE (Figure 4-7 and Figure 4-8). Note that pre-S1 seen in the metasediments does not appear to represent primary bedding, which was not identifiable in the Ena domain. Pre-S1 was only observed in one outcrop east of the fault, in the Firedrake domain, with an ENE-SWS trend.

D1

S1 is a well-developed, steeply dipping, NNE/SSW-trending proto-mylonitic to gneissic fabric (Figure 4-7, Figure 4-8, Figure 4-9). There are locations along both sides of the Black Bay Fault in the Tazin River area where S1 fabrics and F1 folds overprint the pre-S1 fabric (Figure 4-9). Specifically, several outcrops that display a prominent pre-S1 gneissosity, also contain a strong S1 foliation that is axial planar with F1 folds of the pre-S1 gneissosity (Figure 4-9). Both shallowly plunging SW and NE F1 folds (S- and Z-fold asymmetry, respectively) are found throughout the Tazin area, but overall there is a predominance of S-fold asymmetry (indicating sinistral kinematics) (Figure 4-9). In additional to the S-folds, sheath folds aligned with S1 are found preserved in a few outcrops, ranging from decimeters to meters in scale (Figure 4-10).

In general, preservation of lineations is poor in the Tazin River area, and differentiating the generations is difficult. In many of the outcrops few stretch lineations were easily measurable due to the low relief of the outcrops. L1 lineations associated with S1 were easier to identify and F1 fold axes were more abundant than the corresponding L3 and the majority of lineations preserved belong to L1. Many of the L1 lineation are parallel to the opposing fold axes the of the doubly plunging sheath folds, and the L1 lineations are found to plot in two weak clusters, some shallowly plunging to the NE lineations along with some shallowly SW-plunging lineations aligned parallel with the non-cylindrical fold axis (Figure 4-8). Additionally, a couple steeply NNE-plunging to sub-vertical lineations were measured. These lineations occur closer to the Black Bay Fault, near to where S-folds were also present.

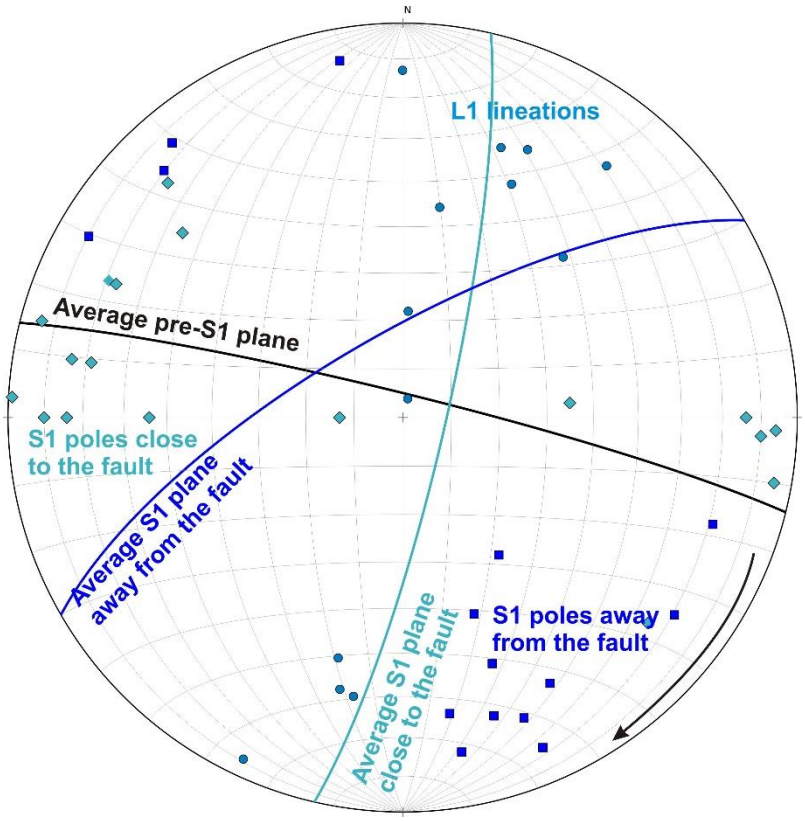

Figure 4-8. Equal-area lower hemisphere projection of poles to S1 and pre-S1 and L1 lineations. Note the transition of the S1 foliation from SSW-trending near the fault to SW-trending away from the fault. The S1 fabric overprints the older background gneissosity pre-S1 at high angle.

Beyond the S-folds, other sinistral kinematic indicators are occasionally found in the S1 fabric, such as a mafic xenolith in a dioritic gneiss showing sinistral rotation (Figure 4-9 D). These sinistral indicators are most commonly found in the more gneissic sections of the Ena domain, and often a couple kilometers away from trace of the Black Bay Fault, rather than in mylonitic zones.

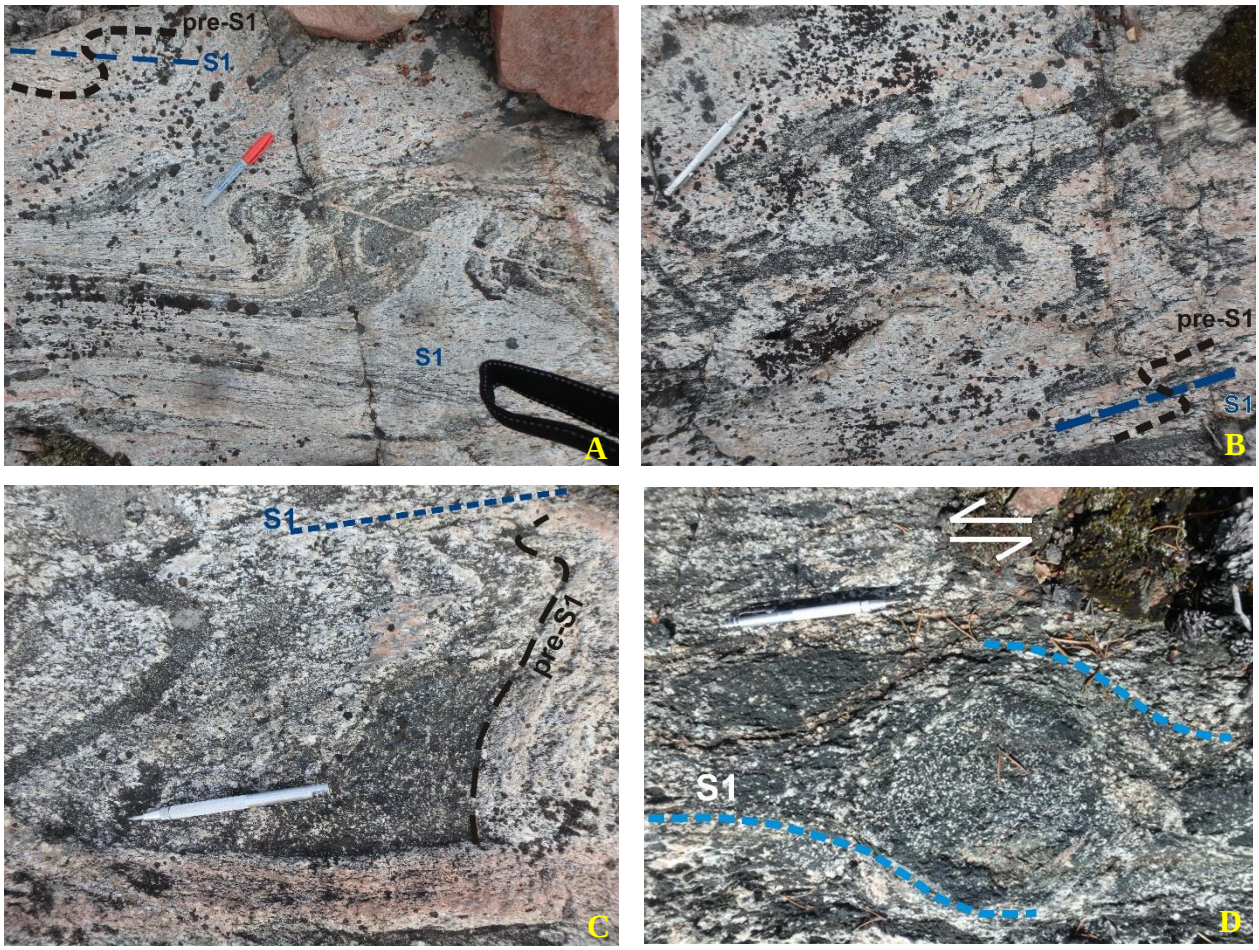

Figure 4-9. Examples of the S folds found within the Tazin River area. S folds contain a strong axial-planar S1 foliation trending parallel to the axial planar of the folds overprinting the deformed pre-S1 gneissosity (A, B, C). A larger mafic xenolith defines a δ-clast in the S1 fabric, indicating sinistral motion (D). Pen indicates north

Within the Ena domain, the trend in the S1 fabric is observed to undergo a clockwise shift moving westward away from the fault, shifting from a NNE/SSW towards an ENE/WSW trend (Figure 4-8). The westward shift in the S1 fabric and the lithological patterns follow the pattern of the interpreted fault splays. Although rare, a few sinistral kinematic indicators are present in the fabric adjacent to the magnetic lows. Based upon the change in trend and sinistral kinematics,

the aeromagnetic lows in the Ena domain are inferred to follow a set of synthetic D1 sinistral fault splays.

Figure 4-10. F1 Sheath folds found in the Tazin River Area ranging from 10's cm (A) to meter scale (B) deforming the pre-S1 gneissosity. Sheath folds are found within the S1 fabric.

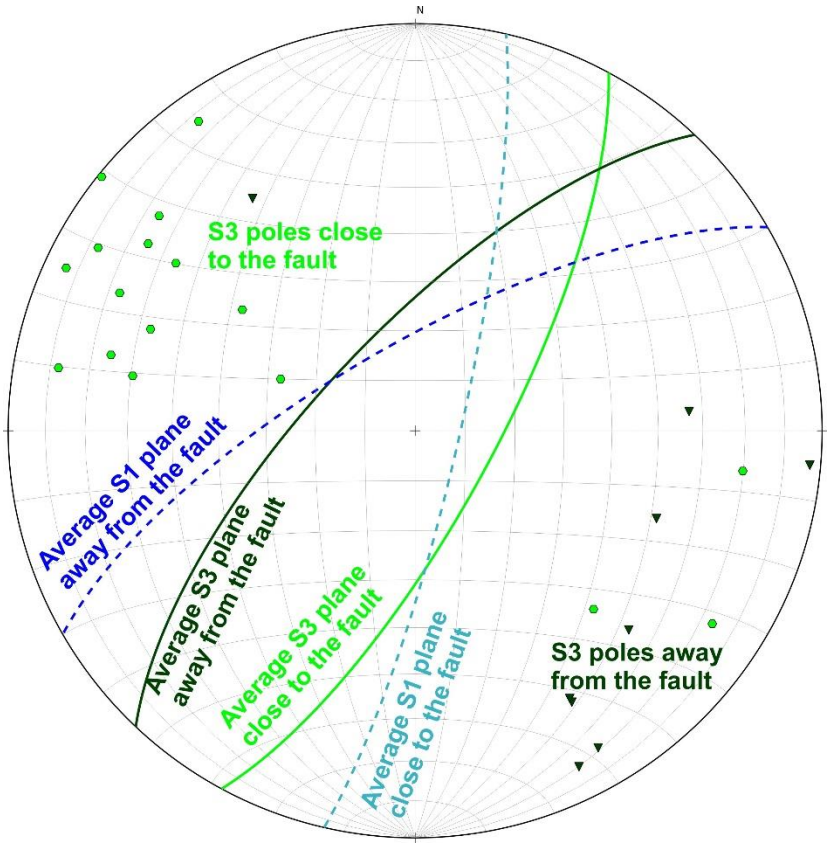

Figure 4-11. Equal-area lower hemisphere projection of poles to S3 along with the S1 average panes as reference. Unlike S1 which becomes more E-W-trending moving westward from the Black Bay Fault, S3 undergoes a smaller rotation in strike.

D3

S3 is a pervasive NE/SW-trending, steeply dipping mylonitic fabric that overprints S1 (Figure 4-12). The general trend of the S3 fabric shows a discernible, clockwise rotation moving westward, away from the Black Bay Fault zone, but this shift is less than what was noted in the S1 fabric (Figure 4-11).

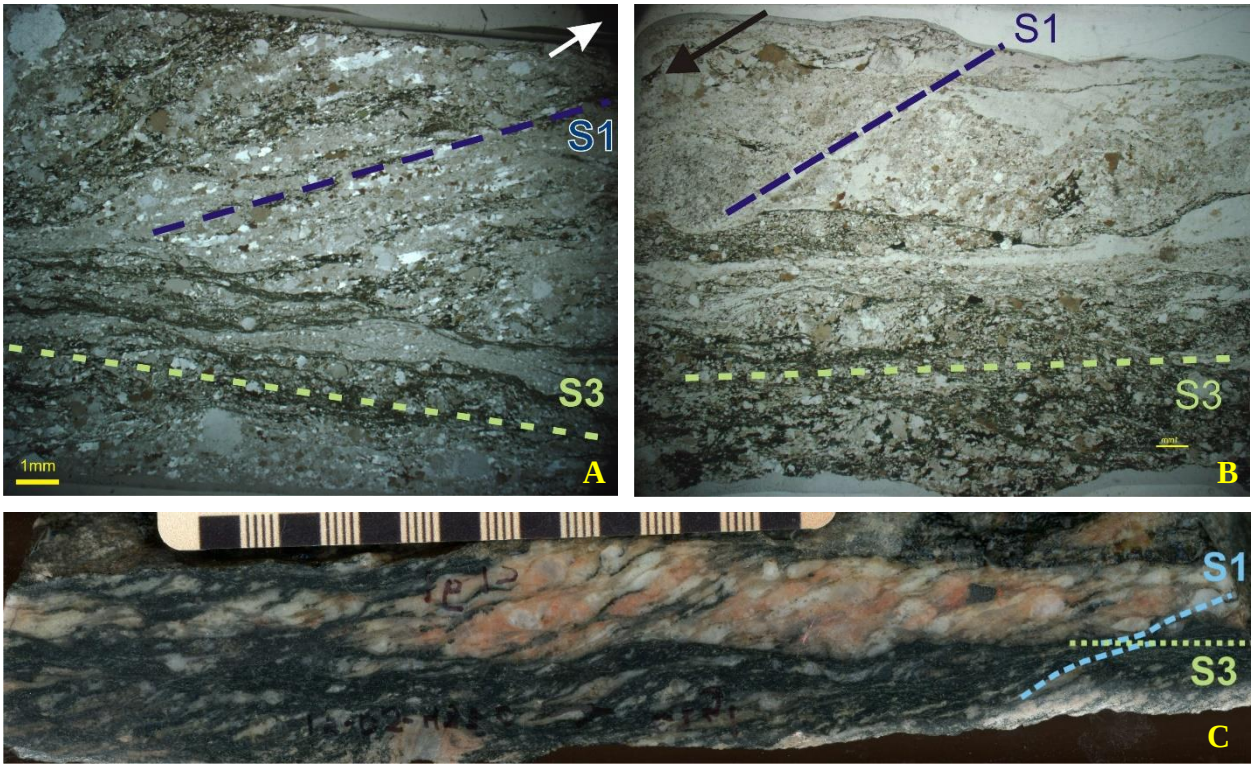

Figure 4-12. Thin sections from outcrops at both the north and south ends of the Tazin River area, close to the Black Bay Fault showing a clockwise overprinting of S3 on S1 (A,B). Hand sample showing S1 fabric preserved in coarser sections transposed and cut clockwise by finer grain S3 fabric (C).

S3 is found with increasing frequency when approaching the Black Bay Fault, and it is most common in the mylonitic zones of the Ena domain (Figure 4-7). S3 is more heterogeneously developed compared to S1, predominantly found in more strongly deformed, mylonitic sections and bands in the more gneissic or foliated outcrops (Figure 4-16). Consequently, some outcrops only contain an S1 fabric.

L3 lineations are difficult to identify in the Tazin River area and differentiating the L3 lineations from L1 is difficult. Only a few outcrops showing a well-developed and clear L3 stretching lineation are observed, though the limited data show a consistent trend. At locations where S3 is clearly differentiated from S1, the L3 lineation plunges moderately SW. (Figure 4-13, Figure 4-17 B).

Figure 4-14. Field photos showing mafic layers that have been boudinaged and dextrally sheared.

Kinematic indicators associated with D3 are well developed. For example, there are multiple occurrences of mafic layers that show evidence of boudinage with dextral asymmetry and pull apart shearing (Figure 4-14). In outcrops in close proximity to the Black Bay Fault where both S1 and S3 are observable, a geometrical relationship indicates dextral shear (Figure 4-12). In these cases, the coarser grained fabric that preserves the older S1 fabric is cut by a finer grained and stronger small scale D3 shear zones (Figure 4-12 C). Some transposition of S1 into S3 is seen in these outcrops, providing further evidence of dextral kinematics with S3.

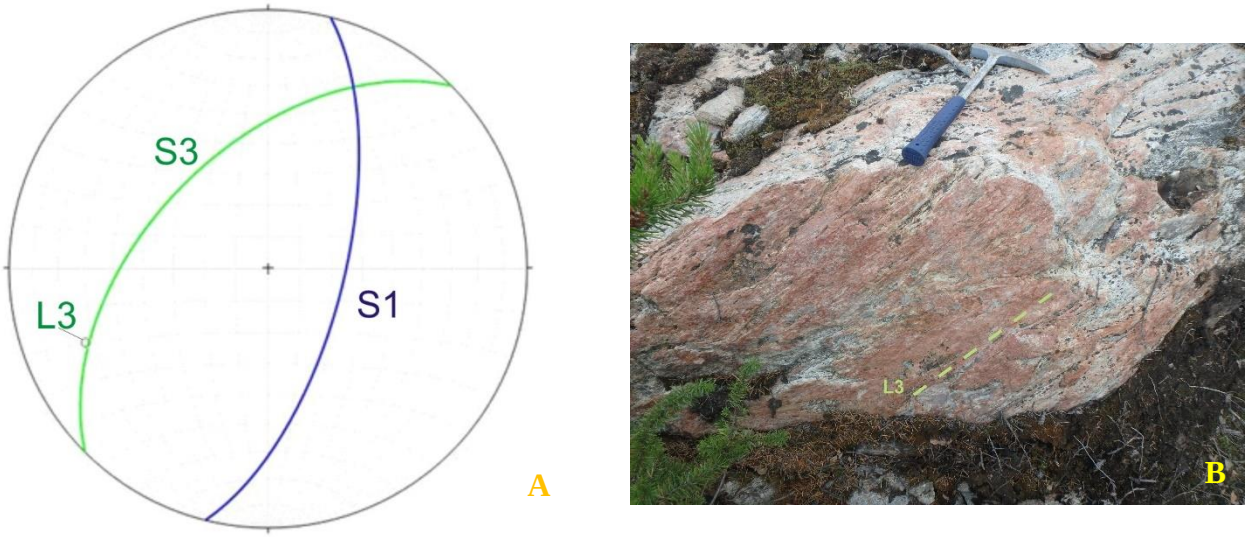

Figure 4-13. (A) Equal-area lower hemisphere plot showing S1 (blue), S3 (green) and a moderately SW-plunging L3. (B) Field photo of an exposed S3 plane showing the SW-plunging L3 stretching lineation.

Figure 4-16. (A) Mylonitic S3 zone with dextral C-S fabric in the more deformed portion of the outcrop. (B) Large dextral D3 shear band cutting the S1 fabric clockwise. Deformation is less ductile, approaching a more brittle-ductile rheology.

In the Firedrake domain, one outcrop a kilometer away perpendicularly to the Black Bay Fault contains a dextral S3 shear band adjacent to some quartz-filled tension gashes which are aligned at a high angle to the S3 foliation (Figure 4-15). These two features are assumed to be synchronous and are the product of dextral transpression as demonstrate by Sanderson and Marchini, (1984). Weak Z-folding of a syn-tectonic granitic intrusion is found near the tension gashes supporting that the development of the tension gashes occurred with the dextral S3 fabric.

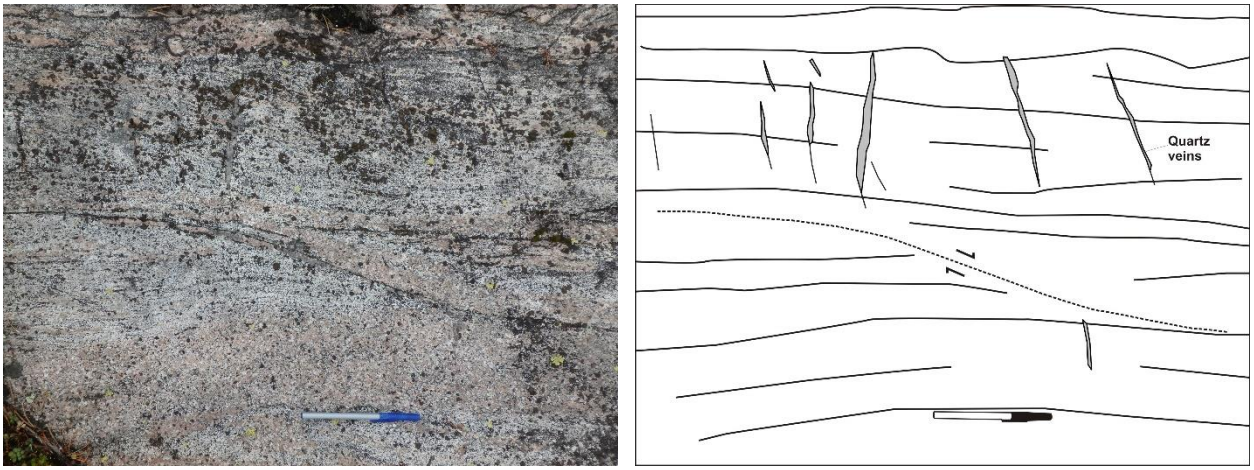

Figure 4-15. Field photo and rough sketch illustrating a D3 dextral shear band adjacent to some quartz-filled tension gashes cutting the S3 fabric at high angles. These strucutres are assumed to be synchronous and formed in a transpressive environment (Sanderson and Marchini, 1984).

D4

At several locations through the Tazin River region, steeply dipping, NW/SE-trending, discrete sinistral shears, D4, cut the ductile gneissic to proto-mylonitic S1 and S3 fabric. These NW/SW-trending shears have a brittle-ductile appearance. The frequency of the discrete shears increases with proximity to the Black Bay Fault, and they occur in both the Ena and Firedrake domains. Some of these shears are filled by leucosome melts and felsic dykes. In addition, three outcrops contain NW/SE-trending shears which have been intruded by mafic dykes. Mafic dykes were much rarer in the South Rae mapping area compared to the felsic dykes which have numerous generations and types and intruded into the bedrock in a variety of orientations. Consequently, the mafic dykes were more diagnostic in understanding the deformation of the region.

A large, unfilled NW/SE brittle-ductile, sinistral shear was observed from the air (Figure 4-17 A), adjacent and trending parallel to one of the mafic dykes that had intruded along another NW/SE-trending shear. At another outcrop, sinistral drag folds transposing the S3 gneissosity into S4 are observed along the margins of a mafic dyke (Figure 4-18 (1,2)). Some pieces of host rock that are present in the dyke have preserved the remnants of the sinistral drag folds (Figure 4-18 (5)). The presence of host rock pieces along with unfilled sinistral shears suggest that the dykes themselves were probably not responsible for the development of the drag folds, but, rather the dykes were emplaced along pre-existing NW/SE-trending sinistral shears.

Beyond having been intruded along the NW-SE-trending sinistral shears, the dyke also contains a well-developed NW/SE-trending foliation (Figure 4-17 C, D and Figure 4-18) which suggests syn-tectonic emplacement. Additionally, weakly developed S-folds are found in the dykes. The dykes' foliation is similar in orientation to the shears with a strike and dip (165/73). A moderately NW-plunging lineations was measured (Figure 4-17B) providing a better geometry for the S4 fabric. The mafic dykes are also observed to have been intruded into dextral S4 NE/SW- trending shears and have developed a corresponding NE/SW foliation (Figure 4-18 (3,4)). Dextral drag-folds are found along the edge of the NE/SW-trending dyke portion.

While the NE-SW-trending shears show dextral motion, like the D3 shears, both the brittle-ductile shears and mafic dyke must post-date D3 due to the presence of a well-developed S3 mylonitic fabric is observed to be cut by a foliated dyke (Figure 4-17 D). A late granitic

pegmatite which has been boudinaged intrudes into the NE/SW portion of the mafic dyke (Figure 4-18 (4)) indicate D4 deformation was ongoing post mafic dyke emplacement.

The dykes are likely part of a dyke swarm rather than one interconnected dyke based upon the orientation of the dyke contacts at the other observed locations. Due to the smaller size of these dykes, the aeromagnetic data does not highlight these dykes due to the resolution of the data.

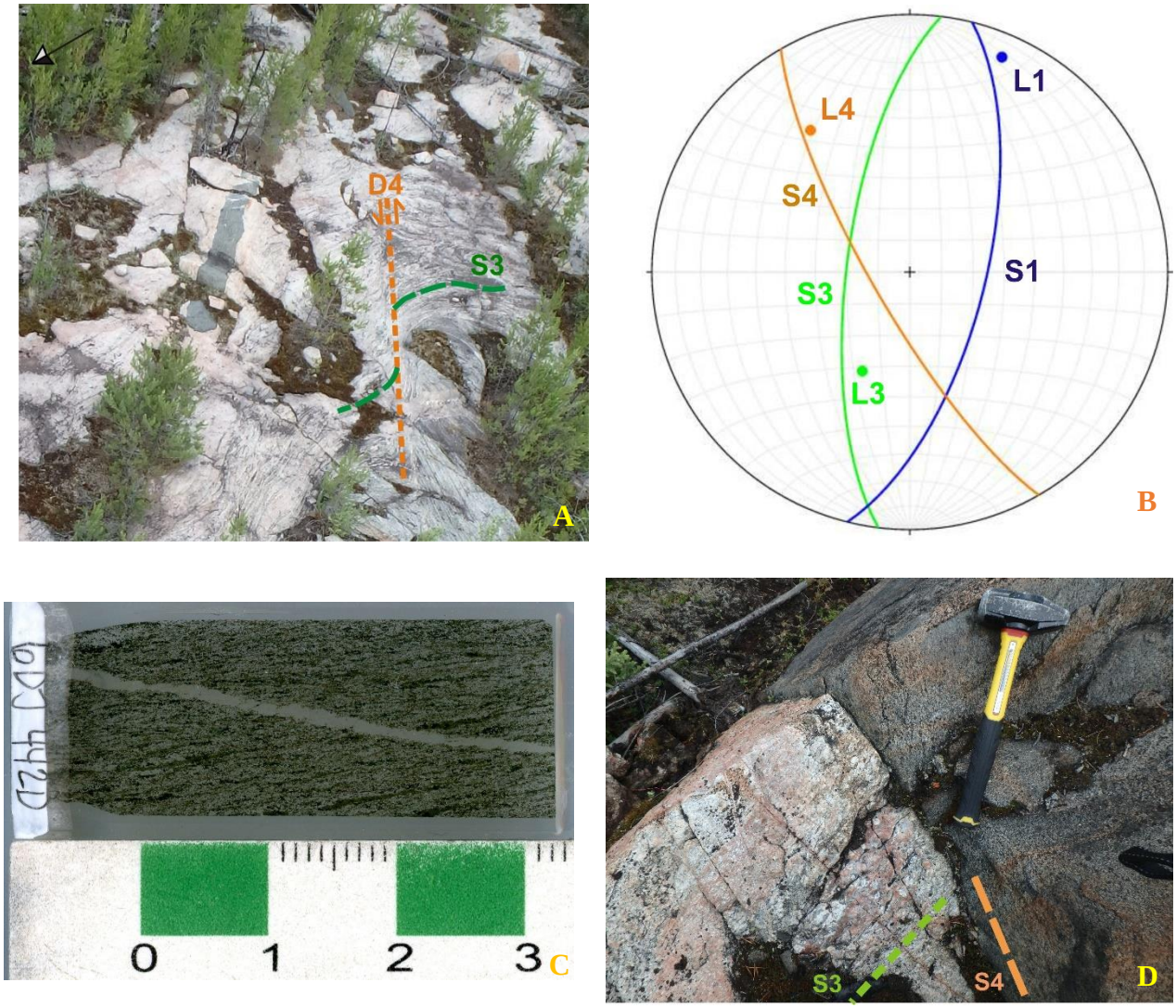

Figure 4-17. (A) Aerial photo of a mafic dyke cutting the S3 fabric in the Firedrake domain (east side of the Black Bay Fault). Dyke trends sub-parallel to a NW-SE-trending sinistral shear that deforms the S3 fabric. (B) Stereonet plot of the fabrics observed in a dyke containing outcrop shown further in Figure 4-18. L1 and S1 blue, L3 and S3 green, L4 and S4/dyke trend orange. (C) Thin section from a mafic dyke showing a well-developed NW-SE-trending fabric. Felsic dyke oriented parallel to Black Bay Fault. (D) Photo of mafic dyke with strong foliation cutting a more mylonitic, likely S3 portion of the host rock). B, C,and D are all from the same outcrop in the Ena domain which is shown in detail in Figure 4-18.

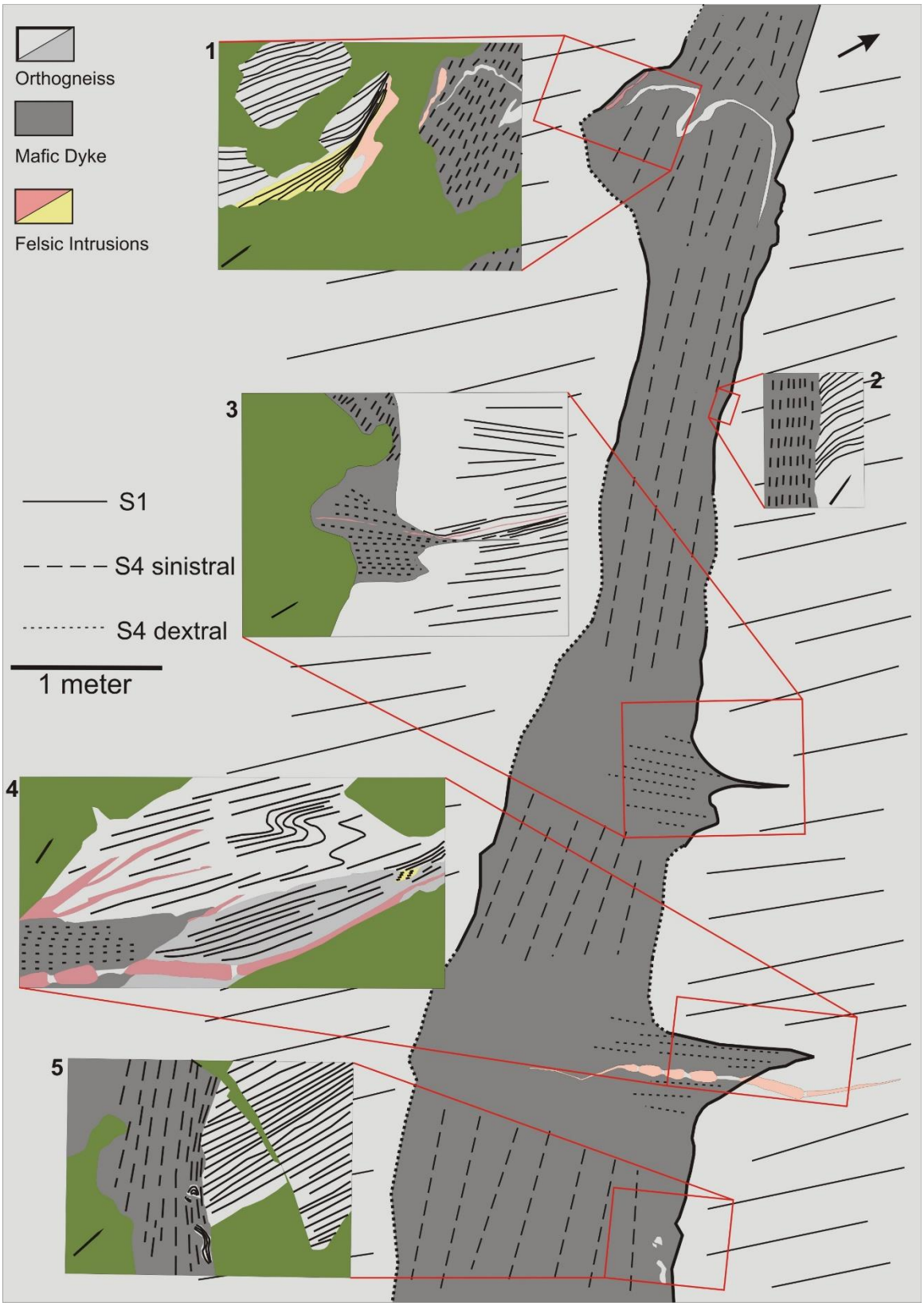

Figure 4-18. Sketch of a metamorphosed mafic dyke which has been emplaced along brittle-ductile sinistral S4 shear. The mafic dyke has developed a similarly oriented fabric, signifying syn-tectonic emplacement. Evidence of the shear zone is observed along the margins (1,2) while host rock pieces contain remnants of the drag folds (5). The dyke also intrudes along a dextral S4 NE-SW conjugate shears, developing a NE-SW foliation (3) which also contains a boudinaged granitic dyke (4).

In addition to the sinistral NW-SE brittle-ductile shears, a conjugate set of NE-SW-trending brittle-ductile shears is found in the Tazin River area (Figure 4-19). The dextral component has a very similar orientation to S3, with a trend similar to that of the Black Bay Fault. The NE-SW fabric found in certain areas of the dyke is assumed to be this S4 dextral fabric (Figure 4-18). Meter-scale offsets along the dextral brittle-ductile shear zones are observed in a few locations close to the Black Bay Fault in the Ena domain (Figure 4-20). While these shears are observed to cut the majority of the felsic intrusions in the area, the brittle-ductile shear in Figure 4-20 B is cut by an undeformed felsic intrusion elsewhere in the outcrop. No breccias or brittle deformation beyond small scale mineralized joints are observed in the Tazin river, in contrast to the Uranium City area, which contains an abundant amount of brittle deformation primarily seen as fracture sets, breccias and topographic lineaments. The brittle deformation in the Uranium City area predominately indicates dextral motion along the Black Bay Fault.

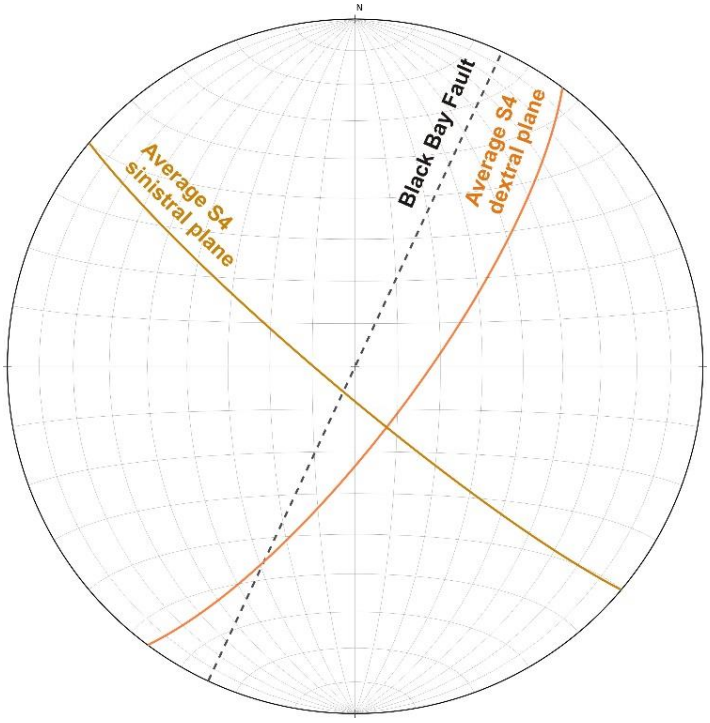

Figure 4-19. Equal-area lower hemisphere projection of the average S4 dextral and sinistral brittle ductile shear planes. As reference, the trend of the Black Bay Fault is also shown.

Figure 4-20. Brittle-ductile shears trending parallel to the the Black Bay Fault showing (A) 10's cm to (B) 0.5 meter scale dextral offset.

4.3 Insula-Labyrinth Lakes Area

4.3.1 Introduction

The Insula-Labyrinth Lakes area is situated in the northeastern portion of the Abitau map sheet (NTS 75B) (Figure 4-21). This area provided our densest coverage of structural data relating to the Black Bay Fault and the surrounding region. This region encompasses a roughly 60 km by 20 km area, which was investigated with transects across the Black Bay Fault spaced less than 10km. Additionally, fly camps with zodiac support were located on both Insula Lake and Labyrinth Lake.

During 2015, a four-day fly camp on Insula Lake was used as the base for several shoreline traverses around this lake. Insula Lake contains many NE-SW-trending islands and bays with well-exposed shorelines. The data collected from these shoreline traverses provided a more complete view of the regional geology than the more linear and laterally restricted overland traverses. The Labyrinth Lake area was revisited during the 2016 field season with a fly-camp to investigate the geology related to a major shift in the aeromagnetic signature of the Black Bay Fault beneath the lake, as well as to further examine rare-earth element mineralization identified during the previous field season (Acosta-Góngora et al., 2018). Coverage of this area was further enhanced with a few helicopter transects that were conducted in this area during the 2012 field reconnaissance for the larger mapping program, with samples collected for geochronology (Davis et al., 2015; Regis et al., 2017).

In the Insula Lake and Labyrinth Lakes area, the Black Bay Fault marks the boundary between the McCann domain and the Firedrake domain. In this area, the trace of the Black Bay Fault is less distinct on the aeromagnetic data than in the Tazin River area, to the south, where it is clearly marked by a linear magnetic low between two magnetic highs. In the Insula Lake and Labyrinth Lake area, the Firedrake domain is generally marked by higher magnetism than the McCann domain, which is commonly non-magnetic (Figure 4-21). However, the border between the high and low magnetism did not always prove to be the location of the Black Bay Fault when examined in the field and determining which side of the Black Bay Fault an outcrop was in was occasionally problematic. An abrupt change in trend of the fault to the northwest at the north end of Labyrinth Lake is indicated in the aeromagnetic data (Figure 4-21), which further complicates the placement of the Black Bay Fault.

We also found that the topography and hydrographic features of the area do not highlight the Black Bay Fault as clearly as in the Tazin River area, where the course of the Tazi River marked the fault. While the northeast flowing Labyrinth River and Labyrinth Lake were initially assumed to mark the trace of the Black Bay Fault, field observations revealed that these waterbodies are not a good proxy for the trace of the fault. Only the northern end of Labyrinth Lake was clearly situated over the fault trace.

This same limited reliability with topography was observed around Insula Lake, where all the islands and inlets showed similar NE-SW orientations across a ~ 15 km wide region, with no dominate feature indicating the fault zone. The poorer reliability in the topography as a structural tool is probably due to the smaller angle between past glacial movement responsible for the majority of the landforms in the area and the fault trace in this area which can be seen in the air photos of the region. In the Tazin River area there is a larger angle between the fault and glacial features seen with the numerous drumlins (Figure 4-2 A).

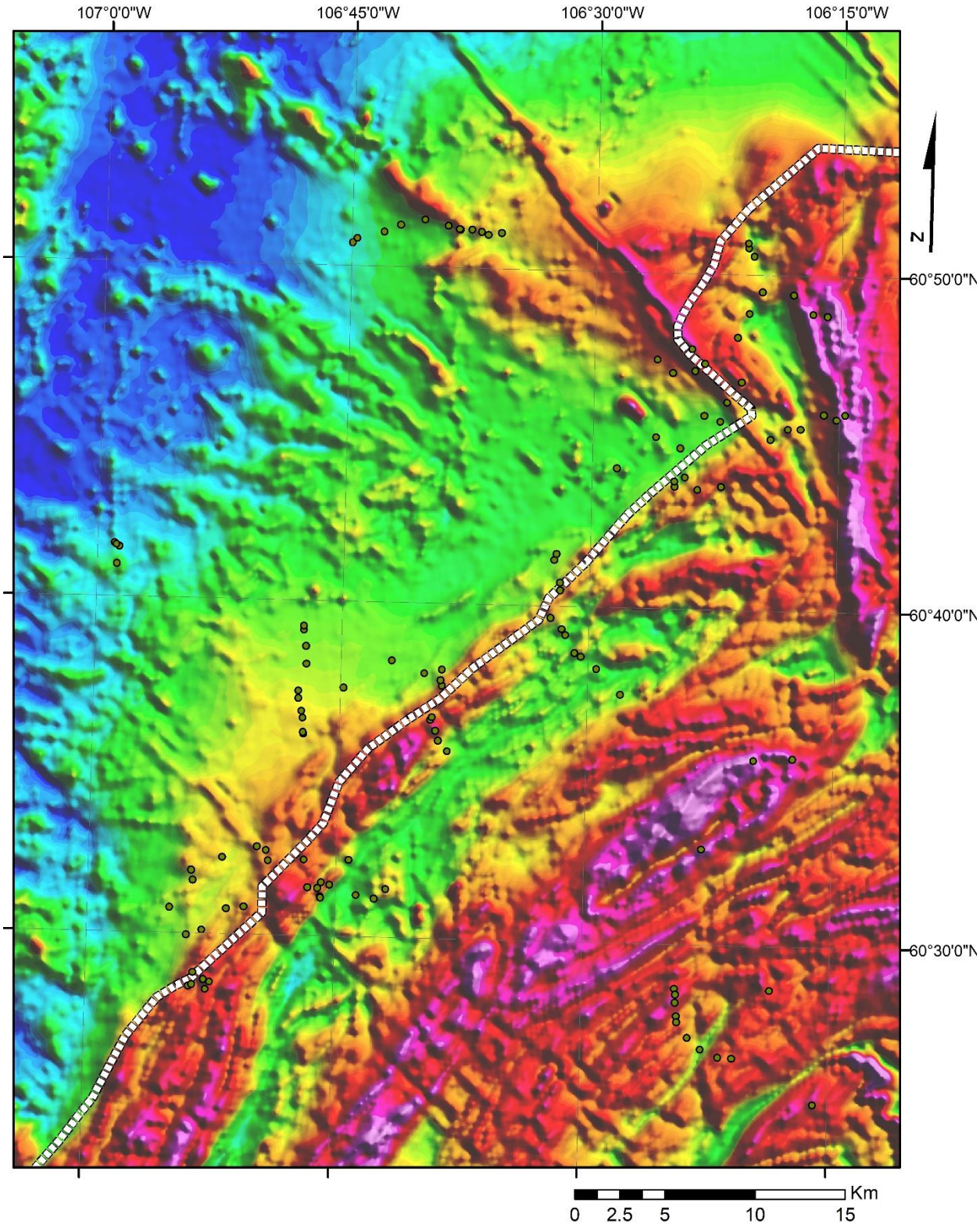

Figure 4-21. Aeromagnetic survey of the Insula and Labyrinth Lakes area. Trace of the Black Bay Fault is observed to undergo a jog to the northwest. Raised linear feature where the fault undergoes a northwest shift is due to the presence of a Mackenzie Dyke which post-dates deformation in the area and does not outcrop. Large scale sheath folds can be seen in the Firedrake domain. Aeromagnetic data from Kiss and Coyle (2012)

4.3.2 Geology

McCann domain

Based on our field observations, the McCann domain in this area has been subdivided into five lithological-deformational units, namely, (1) pyroxenite, (2) blue-quartz monzonite, (3) blue-quartz gneiss, (4) megacrystic granite and (5) ultramylonite (Figure 4-23). These units are primarily granulite facies rocks, but there is some retrogression to upper amphibolite facies rocks in areas near to the Black Bay Fault with garnets retrogressing to amphiboles .

At locations more than 3-4 km away from the Black Bay fault (and the domain boundary), the dominant lithology of the McCann domain is a blue-quartz monzonite (Figure 4-23). There has been some confusion in the determination of the lithology classification for this rock unit through the course of the mapping campaign. During the 2012 transect this rock was identified as blue-quartz diatexite (Pehrsson et al., 2014b). However, during our subsequent mapping it was discovered that the vast majority of outcrops did not contain any of the associated resitite nor xenoliths of the protolith (Figure 4-22). During the 2015 mapping season the rock was initially thought to be a tonalite, but it was discovered that what was visually identified as plagioclase was instead a white alkali feldspar. The blue quartz ranges in colour from a blue to a more commonly observed greyish blue, more closely resembling a smoky quartz. This unit often contains garnets along with a varying component of ferromagnesian minerals (primarily clinopyroxenes and biotite, but also hornblende and orthopyroxenes). However, in the Insula-Labyrinth Lakes area, garnets were not commonly observed, and hornblende was the primary ferromagnesian mineral in the blue-quartz monzonite.

Closer to the domain boundary and Black Bay Fault, the rock is a variably deformed megacrystic granite (sensu stricto), occasionally approaching a granodiorite in composition (Figure 4-22). In strain shadows, feldspars in the megacrystic granite were observed to be up to 5 cm in diameter. In regions of higher strain, the feldspar megacryst have been deformed into an augen texture, but in some regions, it has been deformed up to a straight gneiss or to a mylonite (Figure 4-22). In deformed areas, this unit was difficult to discern from a gneiss unit of the Firedrake domain that contains stronger augen texture. The megacrystic granite is generally non-magnetic, though the aeromagnetic maps show increased regional magnetism around Insula Lake. An ultramafic pyroxenite to grabbroic unit is also observed in a few locations near to the fault (Figure 4-22)

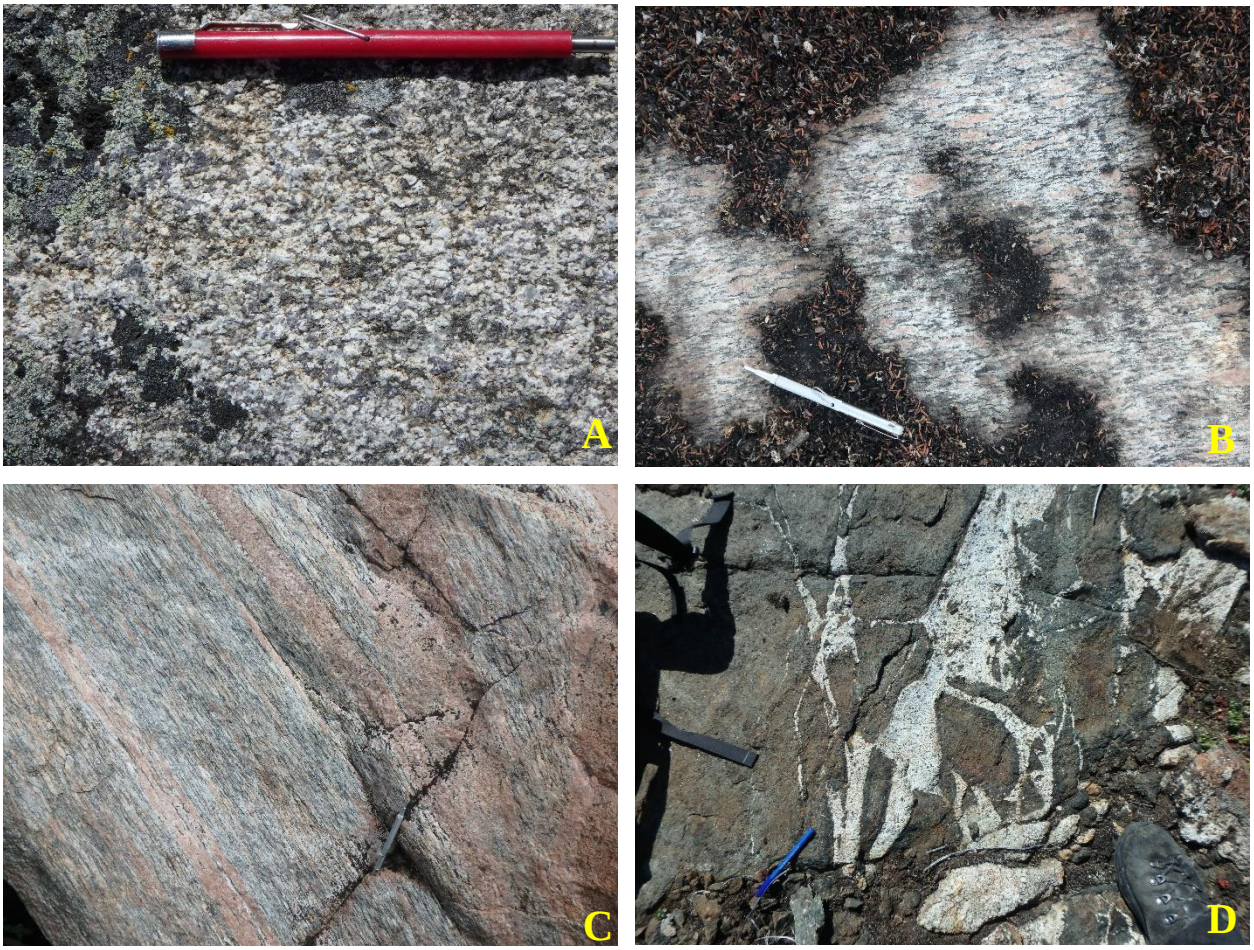

Figure 4-22 Rocks found in the McCann domain around the Insula-Labyrinth Lakes Area: (A) blue-quartz monzonite, (B)moderately deformed megacrystic granite,(C) granodioritic mylonite, and (D) ultramafic pyroxenite unit.

and is moderately deformed. Unlike the other units that have good lateral continuity, this mafic unit was difficult to trace and appears to be more spatially restricted, primarily found as lenses adjacent to the fault.

Hyalophane-bearing pegmatites were occasionally observed in the McCann domain, but were not nearly as common as in the Ena domain and are rare near to the Black Bay Fault. Later granitoid intrusions are commonly observed injected into the gneissosity as well as cutting all the main units near to the Black Bay Fault in the Insula Lake region. These granitoid intrusions closely resemble in composition the younger granitoids observed intruding the Ena domain in the Tazin River area. However, the very late, chalky-white, pink, aplitic granitic intrusion of the Ena domain was not observed in the McCann domain. Unlike in the Ena domain, the large-scale potassic alteration and epidotization was not readily observed in this part of the McCann domain. The diopside-allanite veining observed in the Tazin River area was also absent here.

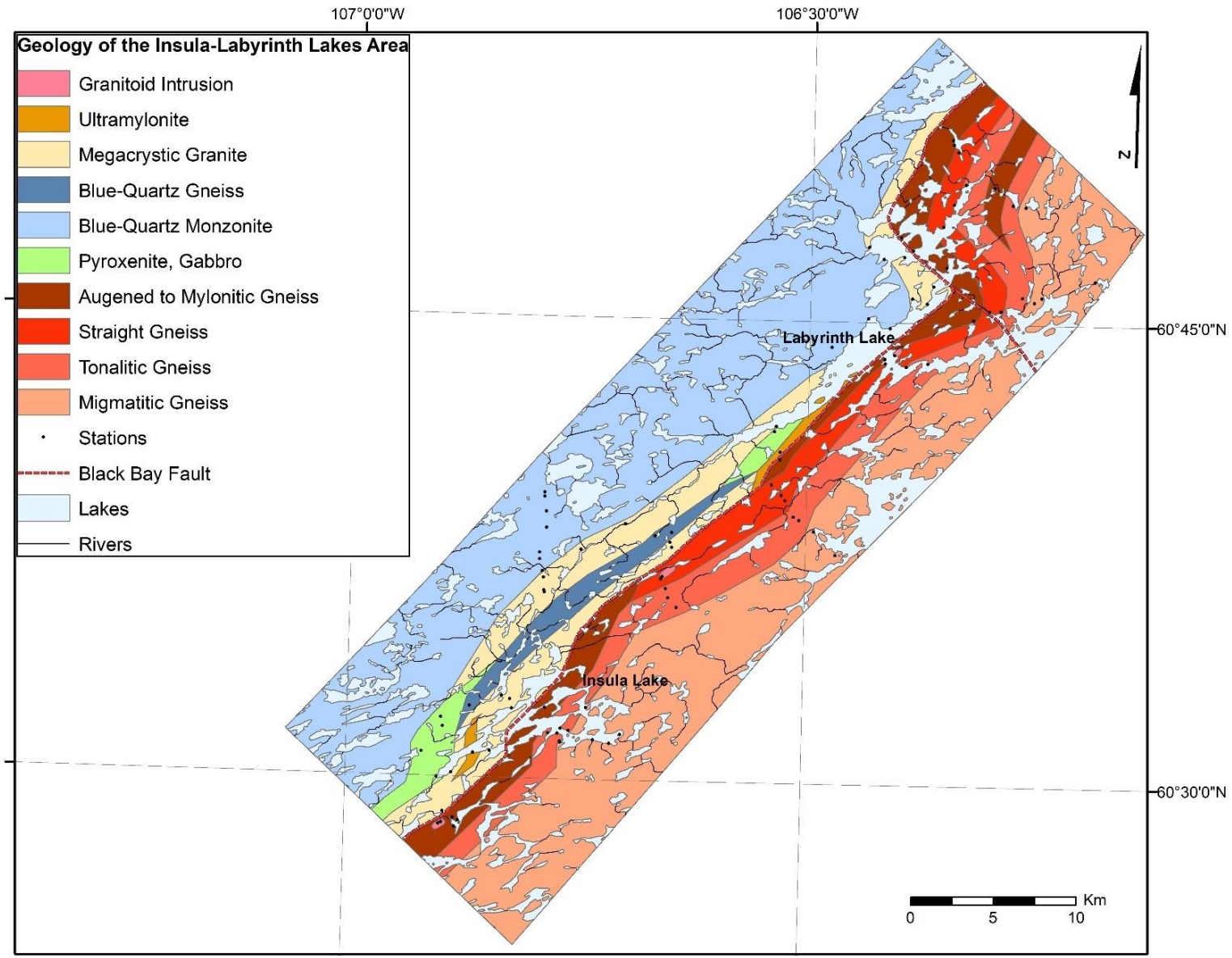

Figure 4-23 Simplified geological map of the Labyrinth and Insula Lake area. Compiled from the 2015 and 2016 traverses and extrapolation from the aeromagnetic surveys of the area

Firedrake domain

The lithological characteristics of the Firedrake domain around the Insula-Labyrinth Lakes area are similar to those found around the Tazin River area to the south, with a migmatitic orthogneiss comprising the majority of the outcrops outside of the deformation zone associated with the Black Bay Fault (Figure 4-24). Near the edge of the Black Bay Fault deformation zone there is a transition in the migmatitic gneisses; they become more banded, mafic xenoliths are well oriented or absent, and the overall rock resembles a deformed tonalitic gneiss.

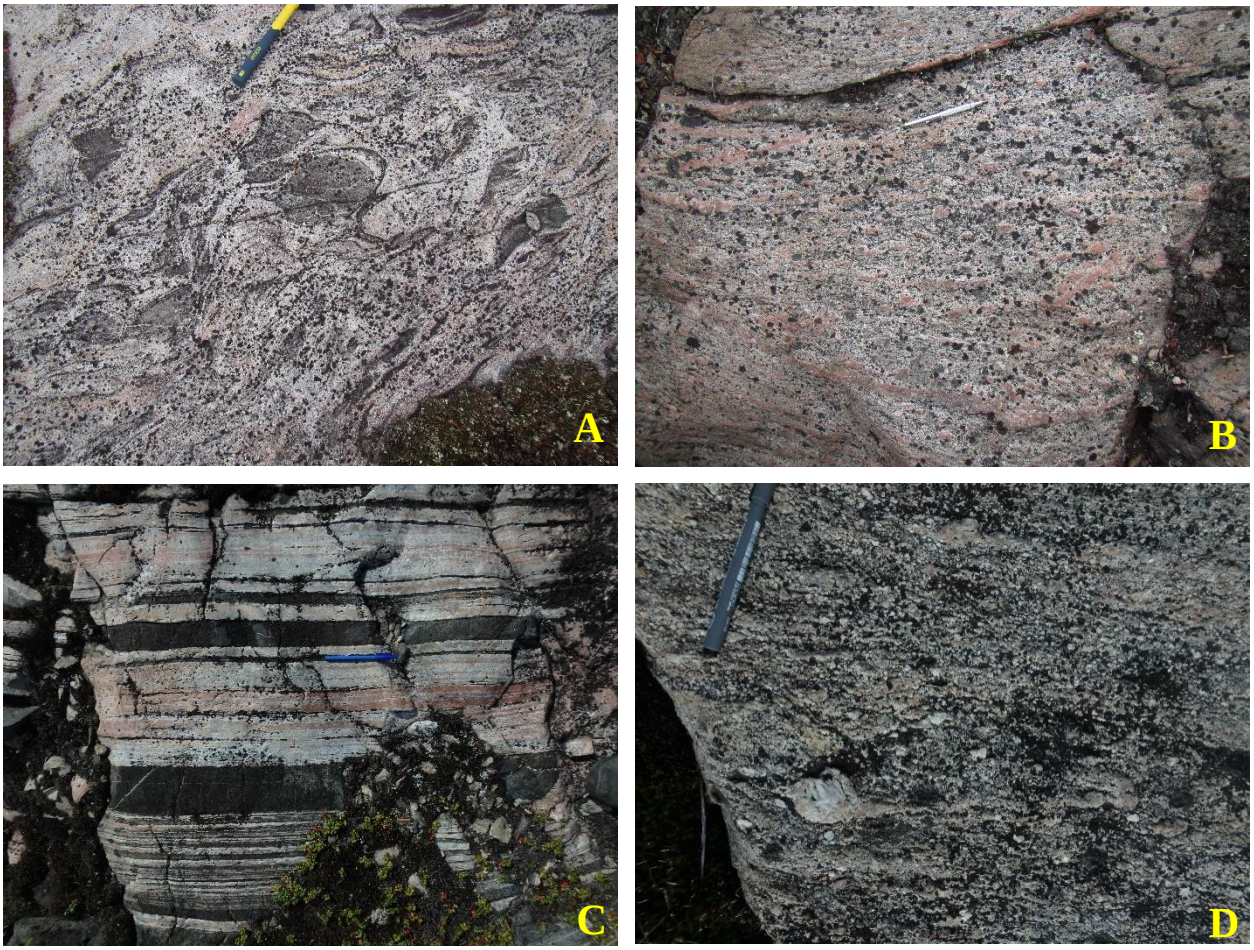

Figure 4-24 Rock types found in the Firedrake domain in the Labyrinth and Insula Lakes area. (A) Classic Firedrake tonalitic soupy to migmatitic gneiss, (B) granodioritic gneiss developing an augen texture, (C) straight gneiss with rectilinear banding, (D) heavily recrystallized gneiss with polygonal quartz.

Closer to the domain boundary, a variably deformed, augen granodioritic gneiss to straight gneiss was found adjacent to the interpreted fault trace. More mafic, dioritic bands and portions were also found within the augen gneiss. In many locations, this unit resembles the deformed megacrystic granite of the McCann domain; however, this unit contains more granitic intrusions, which cut the gneissosity at a high angle, and K-feldspar rich layers were less continuous (Figure

4-24). Geochronology results were also used to determine whether the rock belongs to the augen gneiss of the Firedrake versus the megacrystic granite of the McCann domain.

Approaching Labyrinth Lake from the south, straight gneiss belts with long, continuous rectilinear gneissic bands were encountered (Figure 4-24) at a distance of ~500 m to 2 km from the Black Bay Fault. A large amount of dynamic recrystallization of the quartz is observed where these straight gneiss bands show multiple deformation sequences, with the growth of polygonal quartz, resulting in the destruction of the earlier fabrics (Figure 4-24).

4.3.3 Structural fabrics

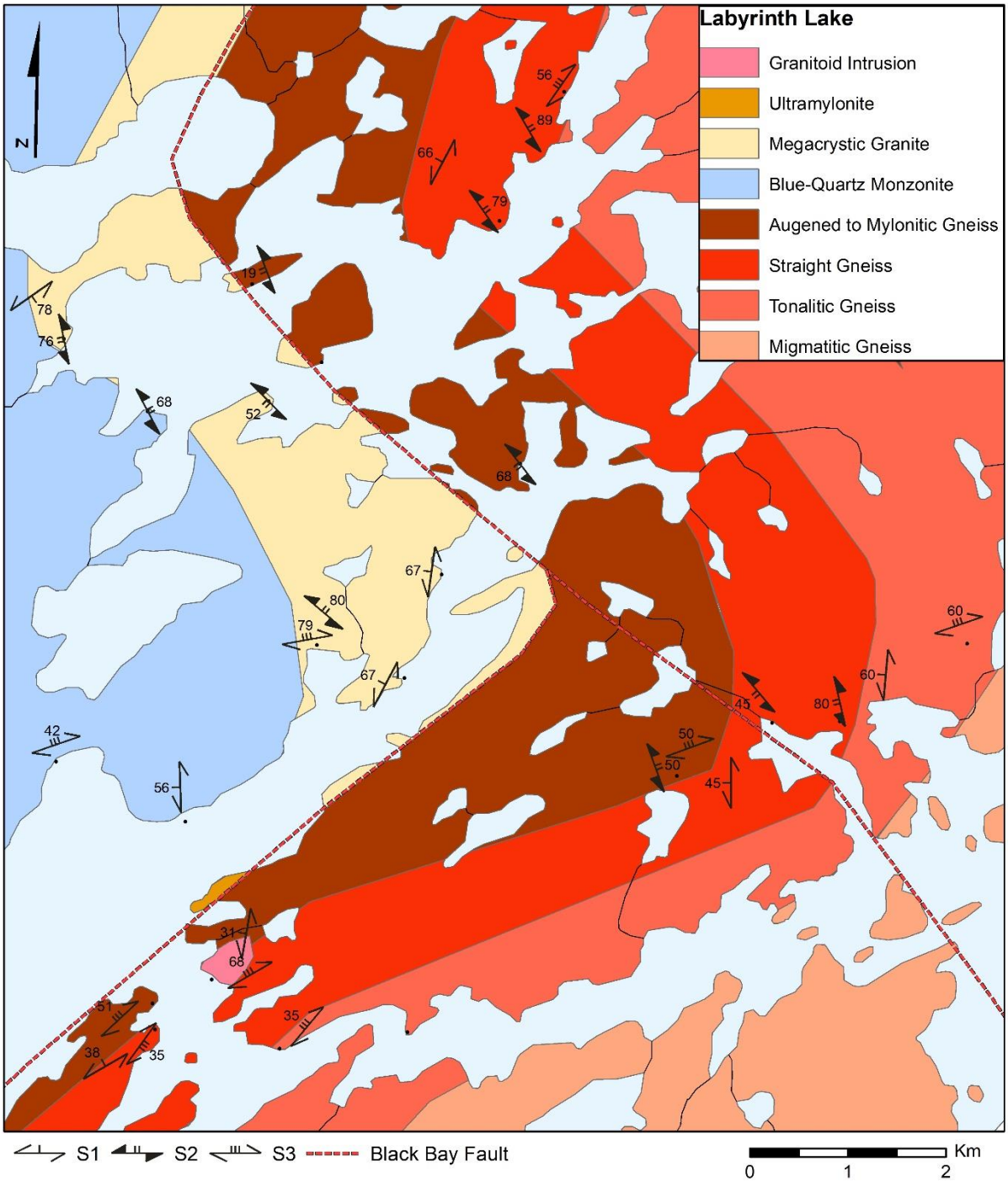

Figure 4-25. Map of the northern end of Labyrinth Lake where the Black Bay Fault undergoes a change in trend. Various generations of fabrics observed in this area are plotted. Pre-S1 was not identifiable in this area.

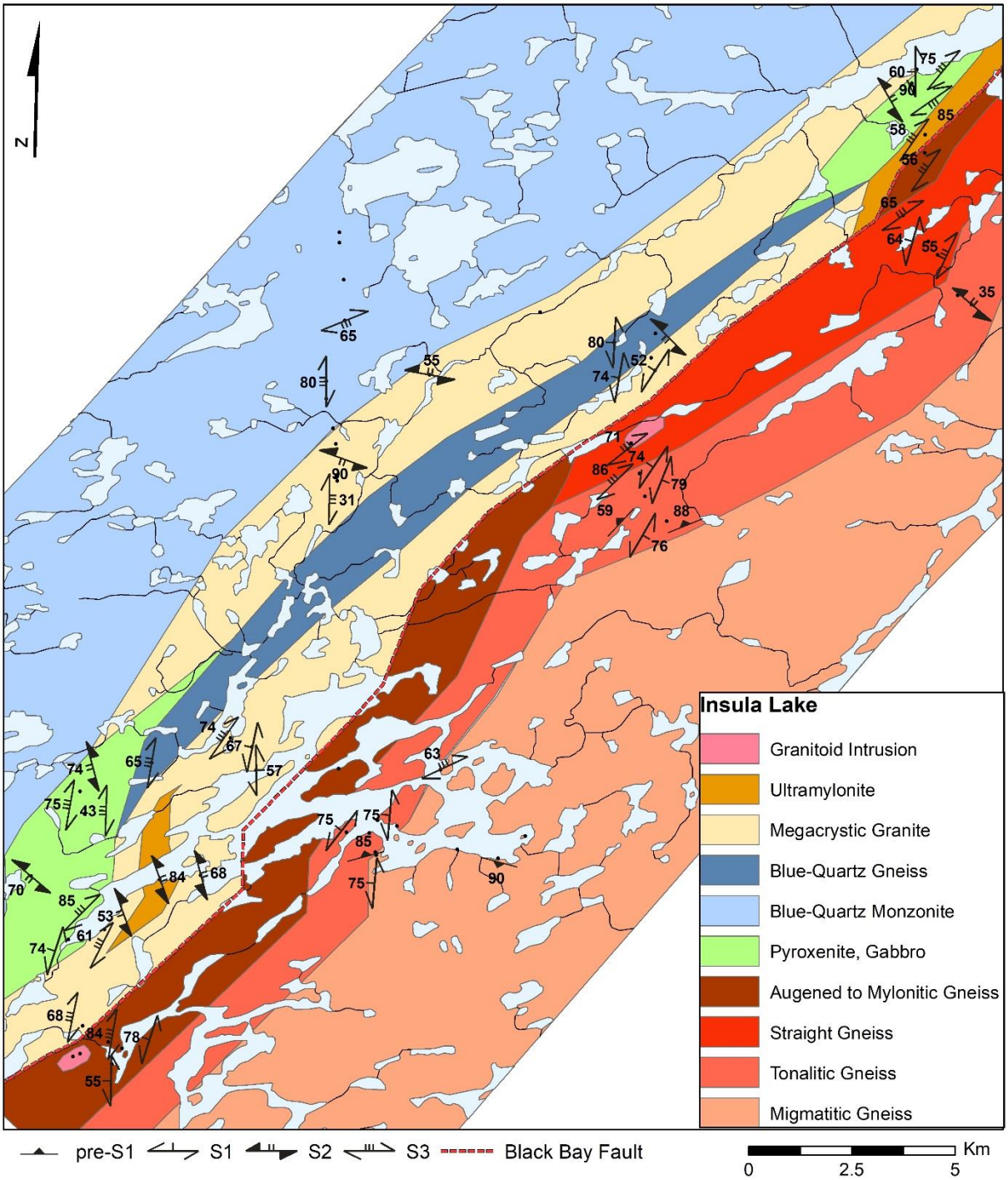

Figure 4-26. Geological Map of the Insula area showing the various fabrics observed in the area. S2 was primarily found around the southern part of Insula Lake. Pre-S1 was measurable close to the boundary between the tonalitic and migmatitic gneiss of the Firedrake domain.

Overview

The Insula-Labyrinth Lakes area contains all four main deformational fabrics (S1, S2, S3 and S4) along with a pre-S1 fabric. In addition to containing D2 deformation, the Insula-Labyrinth Lakes area has better preserved D3 compared to the Tazin River area. The various fabrics are described below.

Pre-D1

The oldest fabric in the Insula-Labyrinth Lakes area is a background gneissosity, pre-S1, which is rarely preserved and primarily only found, in both domains, away from the fault, towards the edges of the Black Bay Fault deformation zone (Figure 4-25, Figure 4-26). The orientation of the pre-S1 gneissosity varies across the fault. In the Firedrake domain, the pre-S1 gneissosity primarily trends E-W to ENE-WSW (Figure 4-27, Figure 4-26). In the McCann domain, the pre-S1 gneissosity trends WNW-ESE. Pre-S1 was only found as a weak foliation in the blue-quartz monazite (Figure 4-23) and is considered too weak to be placed on the structural maps of the area. Due to distribution of the traverses and outcrop exposure, pre-S1 was better observed on the eastern side of the fault, in the Firedrake domain. Consequently, a representative average pre-S1 plane can only be plotted on the Firedrake side of the Black Bay Fault in this area (Figure 4-28). No lineations were found associated with the pre-S1 fabric.

Figure 4-27. Migmatitic tonalitic gneiss in the Firedrake domain, east of Insula Lake, showing the background pre-S1 fabric of the area.

D1

S1 is the oldest structural fabric associated with the Black Bay Fault in the Insula and Labyrinth Lake area. S1 is observed on both sides of the Black Bay Fault in both the Insula Lake and Labyrinth Lake regions. Although it can be recognized in the majority of the mapped lithologies, it is mainly found preserved in the more strongly deformed straight gneisses and mylonites ((Figure 4-25, Figure 4-26). Throughout the region it occurs as a moderately to steeply dipping, NNE/SSW-trending gneissosity (Figure 4-28). There is a moderate dispersion in the orientation data, but the dominant dip direction of S1 is to the west.

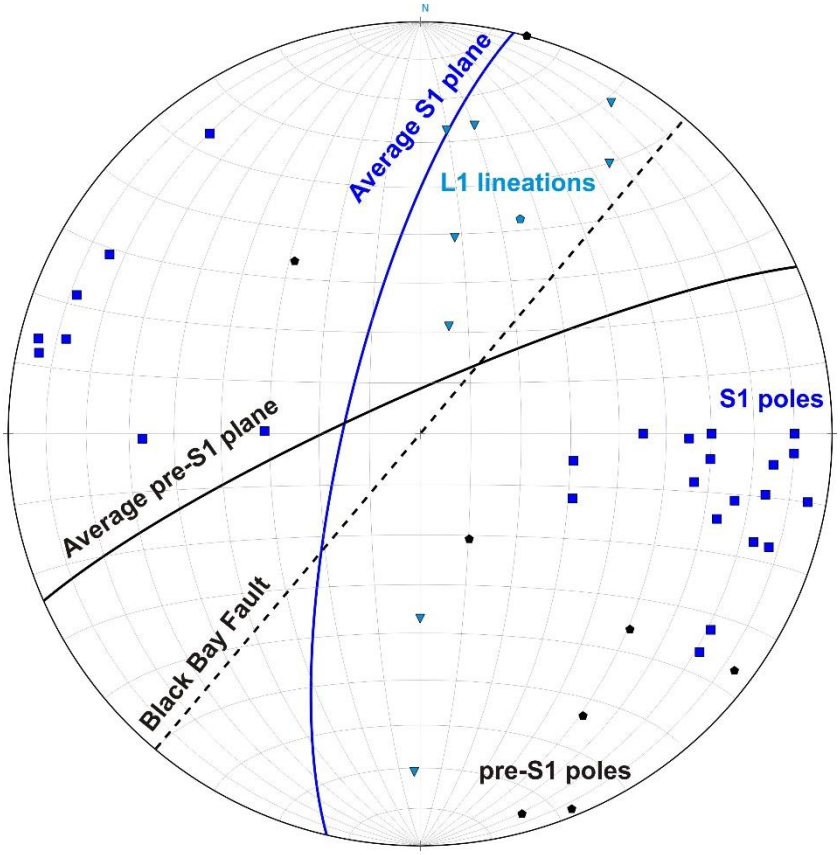

Figure 4-28. Equal-area lower hemisphere projection of poles to S1 and pre-S1 along with the L1 lineations found in the Insula-Labyrinth Lakes area. Also shown is the trend of the Black Bay Fault from the aeromagnetic data in area.

Distinct L1 lineations are rarely observed in the Labyrinth Lake area. Consequently, due to the small sample size over a large area, the lineations do not produce a very tight cluster on the average S1 plane. However, the L1 lineations are found to plunge to the NE and lie relatively close to the average S1 plane. In the tonalitic gneiss of the Firedrake domain, some L>>S

tectonites with moderately NE-plunging lineations (035/21) were measured adjacent to locations containing sinistral indicators (Figure 4-29 F). Additionally, a few S1 dominate outcrops contain meter to decameter size, NE-trending isoclinal folds.

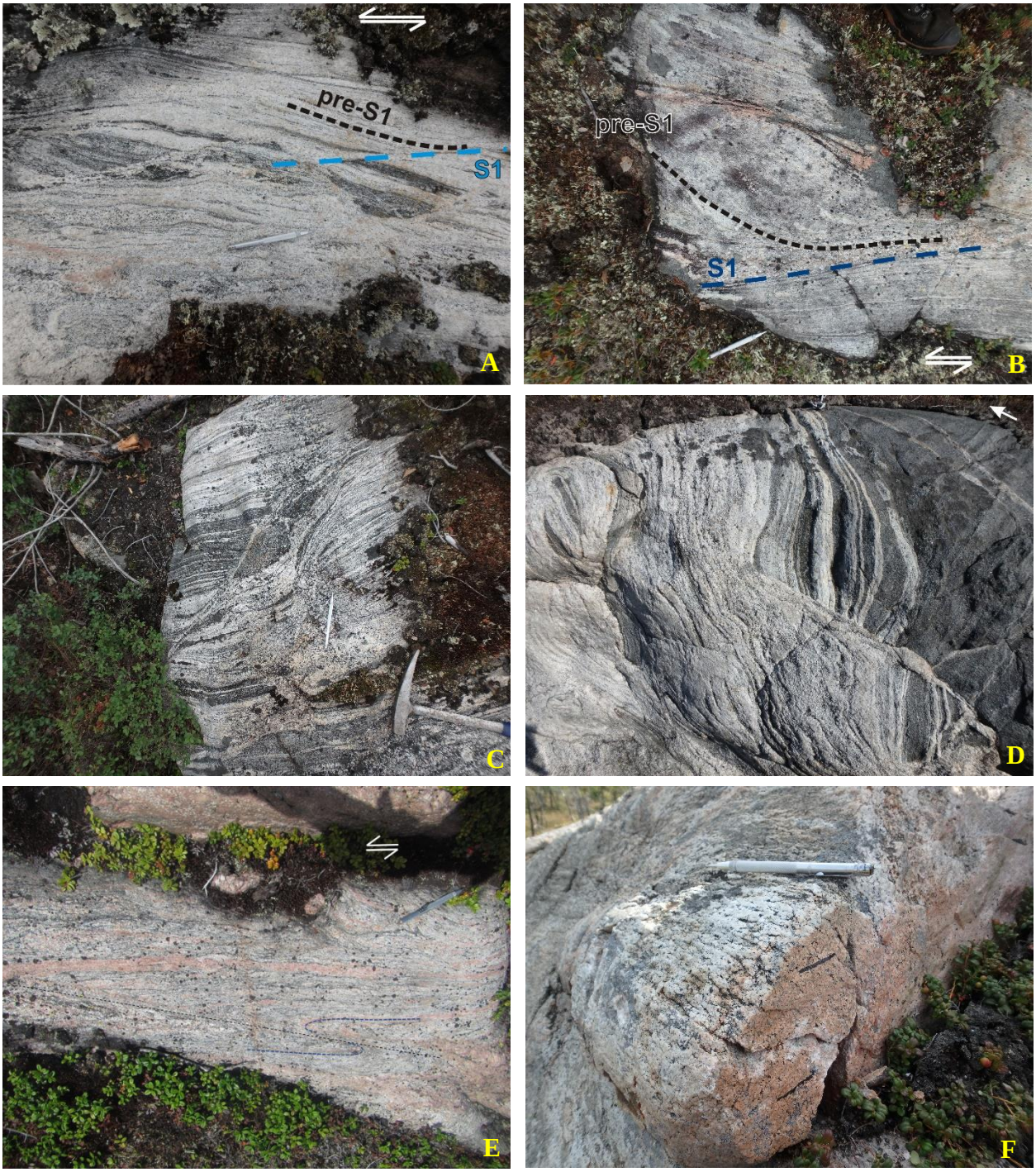

Figure 4-29. Field examples of the S1 fabrics found in the Insula-Labyrinth Lake area (A,B) Sinistral shears transposing pre-S1 fabrics into S1 orientation. (C,D) Sinistral anastomosing S1 shears cutting pre-S1 gneissosity. More mafic sections are less ductily deformed and instead contain melt along the offsets. (E) A normal S-type flanking fold indicating sinistral motion. (F) Tonalitic L-tectonite associated with S1. Lineation plunges shallowly to the NE.

Shear sense indicators associated with S1 were primarily found preserved towards the boundary between the tonalitic and migmatitic gneisses that occurs at the margin of the deformed zone in the Firedrake domain (Figure 4-26). Here, sinistral drag folds are found transposing the pre-S1 gneissosity (248/88) into the Black Bay Fault orientation (030/76) (Figure 4-29 A, B). Anastomosing S1 sinistral shears are also found crosscutting Pre-S1 gneissosity and rotating lozenges containing pre-S1 fabrics (Figure 4-29 C, D). Closer to the Black Bay Fault around Labyrinth Lake, where S1 is found in higher strained rocks, most porphyroclasts are φ-types that show little asymmetry and, thus, cannot be used to determine the shear sense. However, some normal S-type flanking folds (Passchier, 2001) that support a sinistral shear sense were observed (Figure 4-29 E).

The S1 fabric is less well preserved in the McCann domain, generally occurring only as a weak NE-SW foliation, and shear sense indicators are more difficult to identify.

D2

The S2 fabric is most strongly developed at the northern end of Labyrinth Lake (Figure 4-25). The aeromagnetic survey indicates an abrupt, 90-degree deviation in the orientation in the McCann-Firedrake boundary (and Black Bay Fault trace) to the northwest for a distance of 5 km. The lithological units in both the Firedrake and McCann domains follow this deflection into the NW orientation (Figure 4-23).

A well-developed, steeply west-dipping, NW-SE-trending foliation (S2) was encountered at multiple locations in this region (Figure 4-30). The rocks on the Firedrake side of the Black Bay Fault display very strong D2 strain fabrics, with well developed straight gneisses resembling those associated with S1 (Figure 4-24 C). The NW-trending S2 fabric locally contains well developed blastomylonites. Approaching the boundary/fault from the Firedrake side, older, NE-SW-trending S1 fabric was observed to be rotated CCW into a NW-SE orientation (Figure 4-25). However, elsewhere in the Insula-Labyrinth Lakes area, the S1 fabric is observed to be crosscut by S2 shears (Figure 4-31 A) or sinistrally transposed into S2 (Figure 4-31 B).

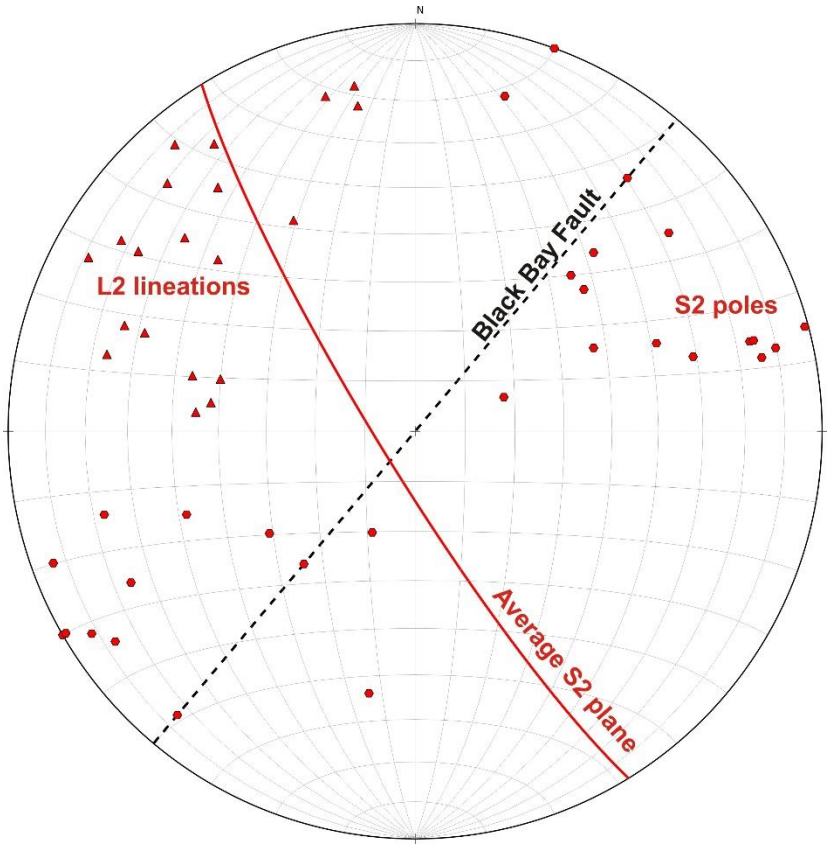

Figure 4-30. Equal-area lower hemisphere projection of poles to S2 and L2 lineations observed in the Insula-Labyrinth Lakes area

Shallow NW-plunging L2 stretching lineations (Figure 4-30) were commonly observed in the felsic gneiss lithology (Figure 4-32 B). In areas where multiple generations of structures are preserved, the more dioritic layers and xenoliths often contain a well preserved mineral lineation (315/23), similar in geometry to the stretching lineations (Figure 4-32 A). While vertical sections with kinematics were rarely found in the study area, one outcrop contains a NW-SE-trending (140/55) blastomylonite with a C-C' fabric recording west-side up motion (but this may belong to a later (D3) fabric based on the more brittle and fractured nature of the sample.

In the southern part of the Insula Lake area, mylonitized megacrystic granites were observed with S2 fabrics that are NW-SE to N-S, contrasting to the surrounding NE-SW S1 and S3 (see below) fabrics. Sinistral kinematics with strong C-S fabric were also observed associated with these S2 fabrics, along with NW-plunging lineations (Figure 4-31 C). The aeromagnetic surveys do not show as substantial of a shift in the trace of the Black Bay Fault in this region as at the north end of Labyrinth Lake, but a small offset in the orientations of the lithologies to the NW is observed (Figure 4-26).

Figure 4-32. Examples of the shallowly NW-plunging lineations. (A) The more dioritic rocks appear better preserve this fabric as a mineral lineation with felsic crosscutting dykes containing the overprinting S3 fabric. (B) Shallow NW plunging stretch lineations on S2 gneissosity.

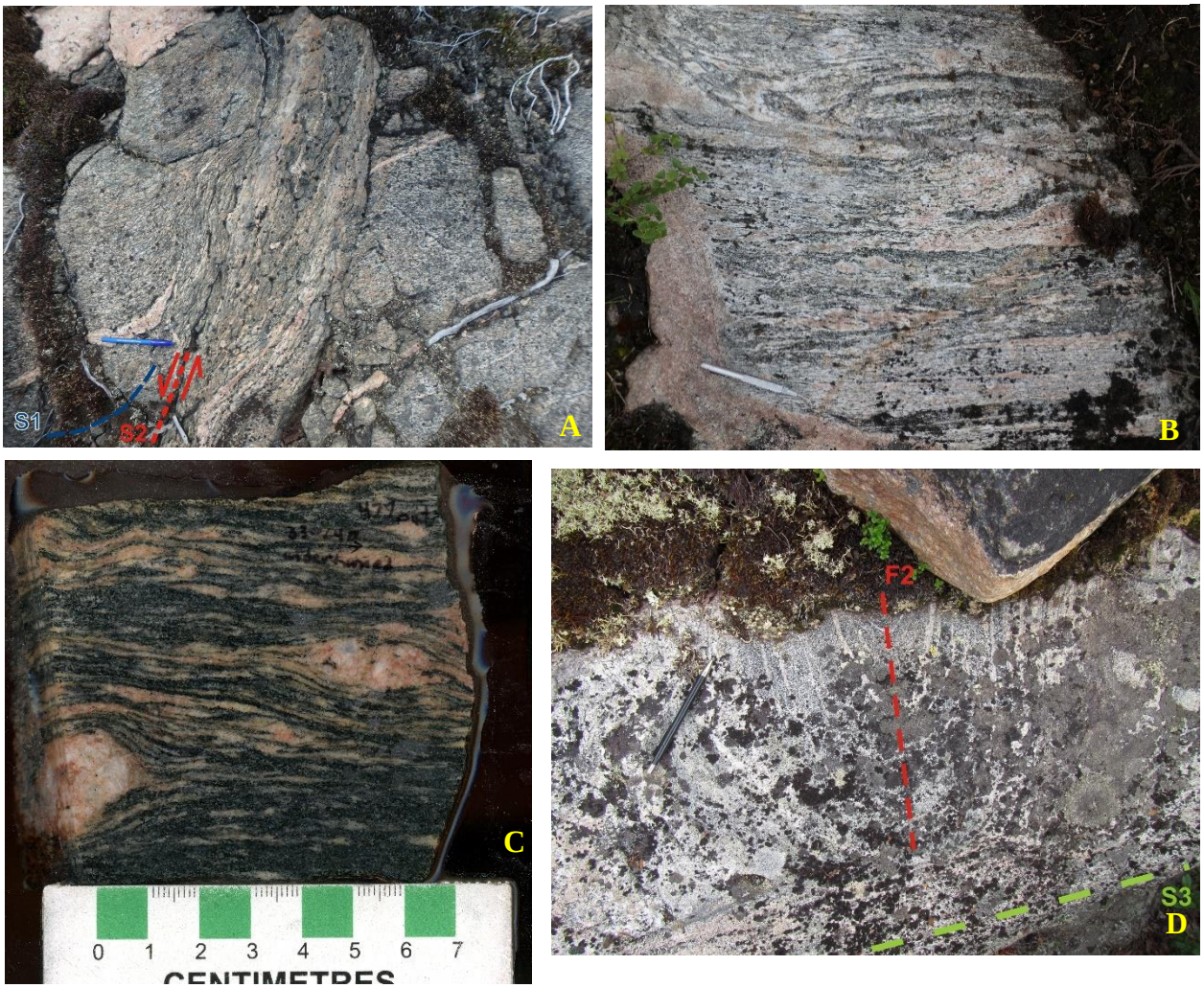

Figure 4-31. Photos of the S2 fabric found in the Insula and Labyrinth Lake areas. (A) Sinistral S2 shear band cutting S1 foliation. (B) Sinistral c-s fabric with a normal S-type flanking fold. (C) Dextral indicators on underside of hand sample indicating sinistral motion. (D) NW-SE-trending F2 fold. A later NE-SW-trending S3 fabric can be observed cross-cutting the edge of the fold nose and dextral kinematics were found in the crosscutting fabric elsewhere in the outcrop.

D3

A steeply west dipping NE-SW fabric, S3 occurs throughout the Insula-Labyrinth Lakes area in rocks that are mylonitic to gneissic. This fabric is observed to crosscut both S1 and S2 foliations at several locations (Figure 4-34 E), thus providing its temporal context. The S3 fabric is found to consistently dip to the west, in contrast to the S1 and S2 fabrics, both of which show some variability in the measured dip directions. Where the (older) NE-SW S1 fabric is preserved, the S3 fabric is observed to overprint counter-clockwise (Figure 4-33) and closely follow the aeromagnetic lineament of the Black Bay Fault (Figure 4-26).

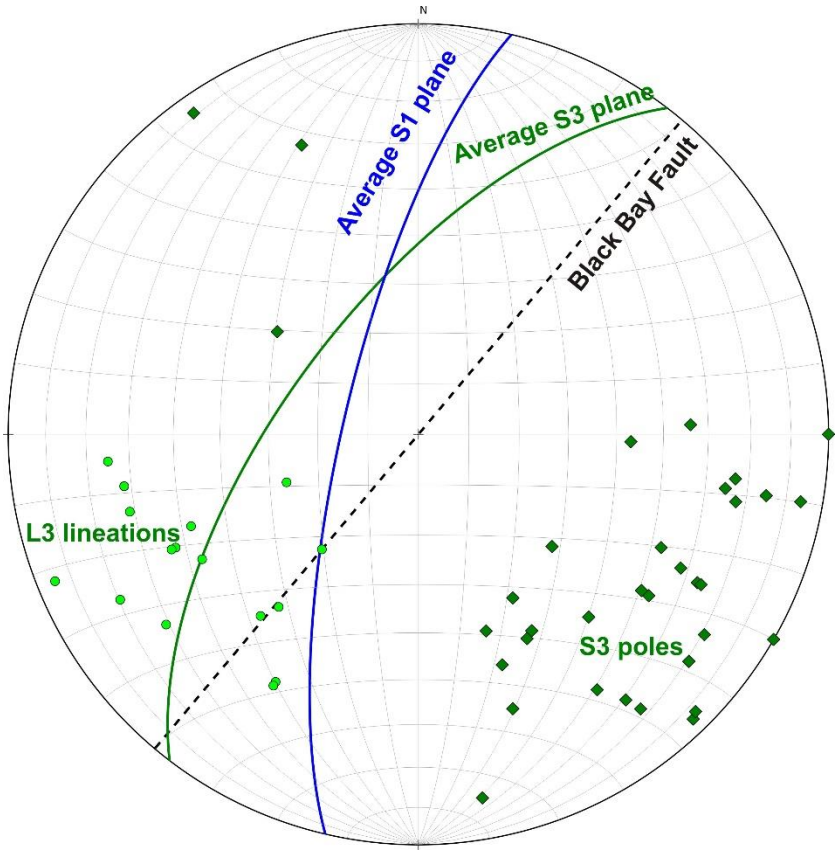

Figure 4-33.. Equal-area lower hemisphere projection of poles to S3 in the Insula-Labyrinth Lakes area. L3 lineations are moderately SW-plunging. S3 is observed to overprint S1 clockwise.

L3 stretching lineations were commonly found within the S3 fabric, plunging moderately to the SW (Figure 4-33). Like the other generations of lineations in the area, they do not form a tight cluster. Dextral shear sense indicators are frequently found associated with the S3 fabric, including a strong C-C' fabric along with dextrally rotated porphyroclasts in outcrops in the Labyrinth Lake area (Figure 4-34 A, B, C). Elsewhere, dextral pull-apart shears are present

(Figure 4-34 D) along with Z-folded granitoid dykes. Some of the Z-folded dykes are boudinaged as well, indicating syn-tectonic emplacement (Figure 5-1).

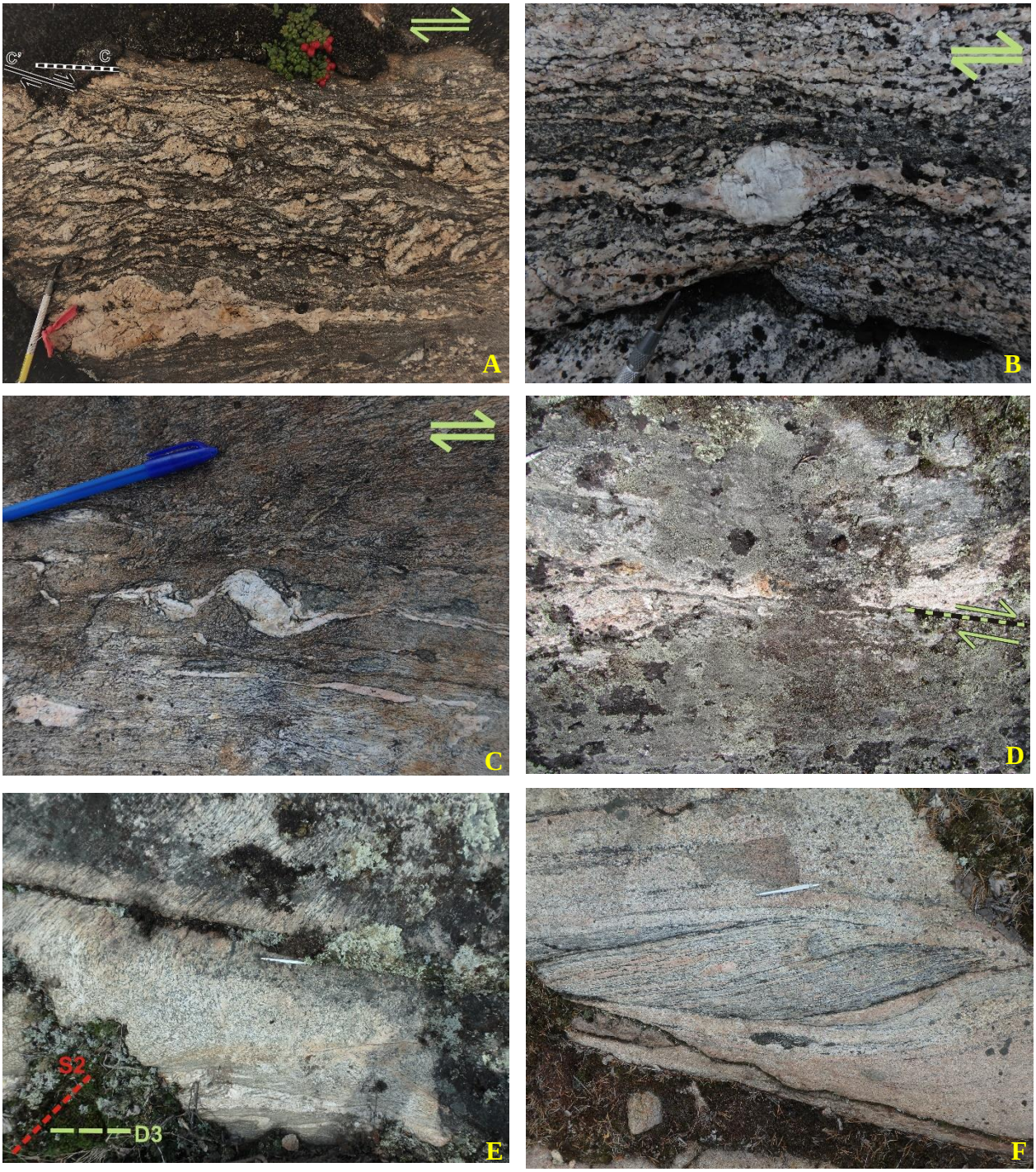

Figure 4-34. Field photos of the S3 fabric from the Labyrinth Lake area. (A) Well developed C' fabric indicating dextral motion along with small z-folds. (B) Dextral σ-clast and (C) δ-clast. (D)Dextral shear cutting a more felsic layer. (E) D3 shear band and Z-folds cutting S2 fabric. (F) Gneissic lenses undergoing dextral rotation into S3 fabric.

Around Insula Lake, granitoid intrusions comprise a large portion of the outcrops, with the granitoids having been injected along S3 gneissosity (possibly syn-tectonic with D3). Some of the outcrops contain lenses of the orthogneiss host rock that have preserved the older S1 sinistral C-S fabric and sigma clast, while the contact between the orthogneiss lenses and injected granitoids show dextral drag folding and shearing (Figure 4-34 F). Some locations that contain a dominate S2 fabric are found to be cut by the S3 fabric. Felsic intrusions containing a moderate S3 fabric are observed to cut a dioritic rock containing a S2 foliation (Figure 4-32 A). Elsewhere, another diorite outcrop containing a S2 foliation is cut by larger S3 shears containing Z-folds (Figure 4-34 E). NW-plunging F2 folds are also observed to be truncated by S3 shears (Figure 4-31 D) while and S2 fabric is found on some F3 folds.

D4

Evidence for a late brittle-ductile to brittle D4 deformation is rare in the Insula-Labyrinth Lakes area and primarily occurs in the Firedrake domain surrounding Labyrinth Lake (Figure 4-35). A primary example is a conjugate system of small discrete shears with a NE-SW dextral component and NW-SE sinistral component. These discrete shears cross-cut the more pervasive foliation and gneissosity (and, thus, appear to post-date the majority of deformation) and are occasionally filled by leucosome (Figure 4-35 A). Some of the blastomylonites near the NW offset in the fault show more evidence of brittle-ductile deformation compared to the rest the other ductilely deformed rocks in the surrounding area, through the form of heavily fractured quartz and felspar porphyroclasts (Figure 4-35 B). Brittle fractures and small faults with a similar conjugate set geometry are also found, rarely with offsets greater than 10 cm (Figure 4-35 D). There are also some E-W brittle fault surfaces that are heavily brecciated and display fault polish. The brittle fault system seems to contain the majority of the hydrothermal alteration in the area: epidotization, silicification, and potassic alteration in the region are predominately associated with the brittle faults. The trend of the sinistral component in both the brittle-ductile and brittle faults is similar to that of the more widespread S2 fabric (Figure 4-36) while the dextral faults predominately follow the Black Bay Fault orientation and S3 fabric.

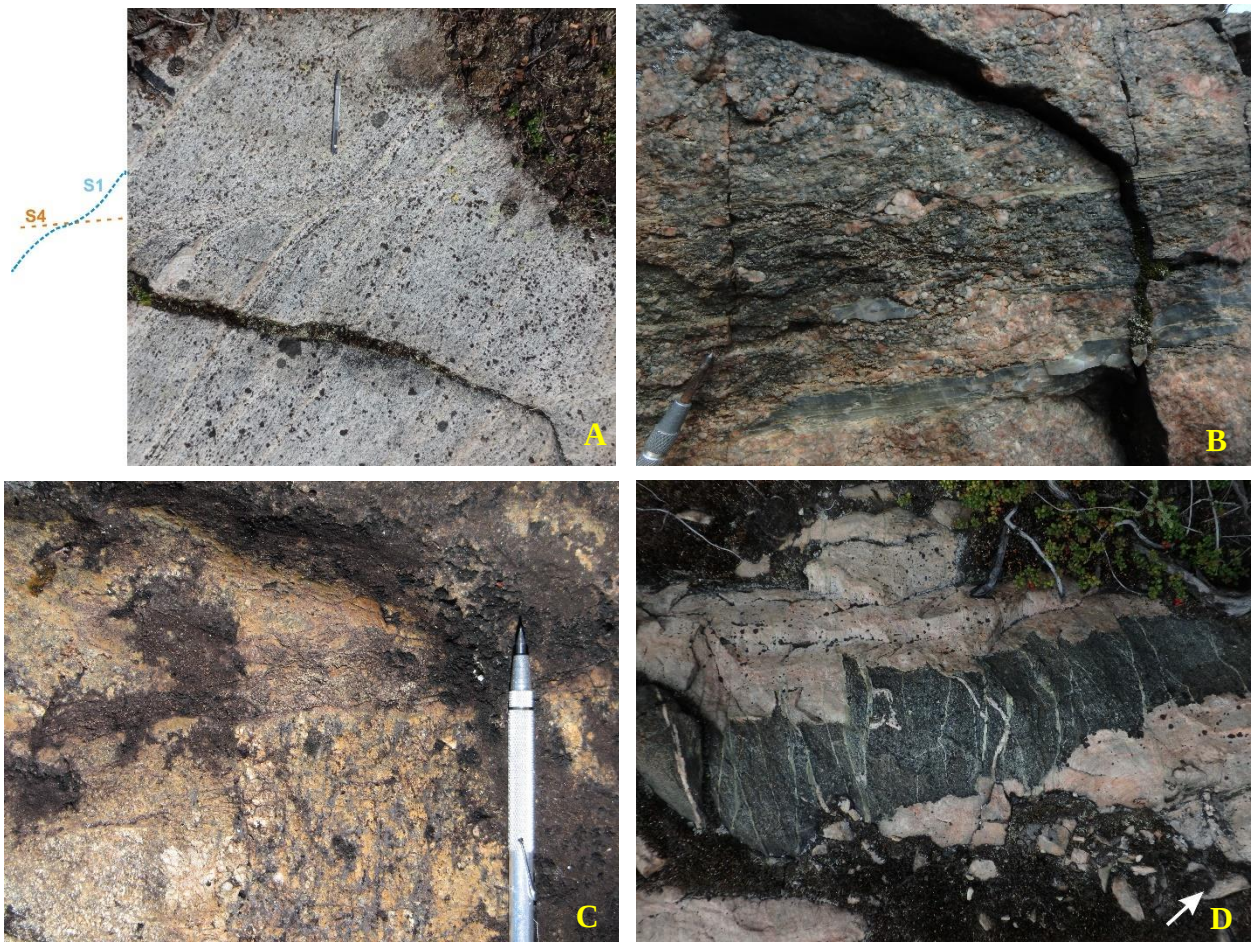

Figure 4-35. (A) Brittle to brittle-ductile deformation in the Insula-Labyrinth Lakes area. Discrete dextral shear. (B) Heavily fractured and alter blastomylonites. (C) E-W-trending brittle fault with breccias containing epidotization and silicification. (D) Set of Sinistral NW/SE- trending brittle fractures with epidotization.

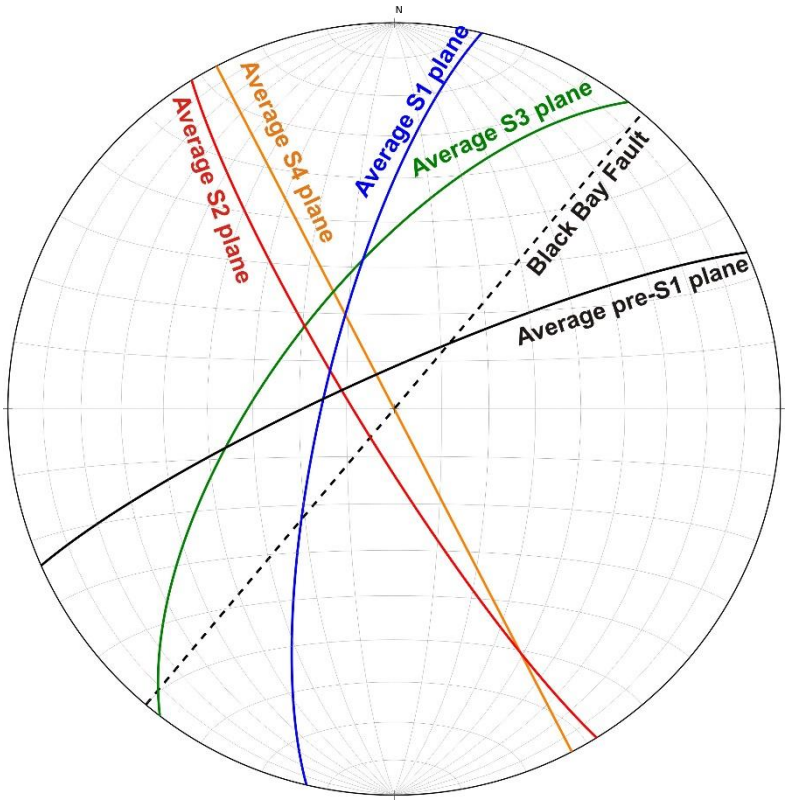

Figure 4-36. Equal-area lower hemisphere projection of the multiple generations of planar fabrics in the Labyrinth and Insula Lake Area summerizing the previous stereonet plots.

4.4 Dymond Lake and other northern traverses

4.4.1 Introduction

In addition to the two Black Bay Fault study areas in the NTS map sheet 75B, the fault was also examined further to the north around the Dymond Lake area in map sheets 75G and H, approximately 75 km north of Labyrinth Lake. In this area, the Black Bay Fault undergoes a large bend to the NW, similar to what was observed at Labyrinth Lake but much larger in scale (over 65 km), before returning to a NE/SW to ENE/WSW trend. In the vicinity of Dymond Lake, the Black Bay Fault marks the division between the northern extent of the Firedrake domain on the east side of the fault and the McCann domain on the western side. The Firedrake domain contains an elevated magnetic signature compared to the low magnetic signature of the McCann domain, similar to the Insula-Labyrinth Lake areas. However, the use of the aeromagnetic transition as a proxy for the fault trace was found to be unreliable in the Dymond Lake area. Specifically, the main fault trace and domain boundary was, in places, found offset from the aeromagnetic change, located further east in smaller magnetic lows in the high aeromagnetic signature areas (Figure 4-37). This discrepancy is particularly pronounced where the fault returns to a NE-SW trend (Figure 4-37). Here, an elevated magnetic signature extending 10's of kilometers into the McCann domain.

Unlike the fault bend around Labyrinth Lake, the NW-SE-trending portion of the fault trace in this area is observed to undulate, with several E-W and N-S-trending segments. These undulations appear to delineate large-scale (>40 km) NNE/SSW-trending folds in the aeromagnetic pattern of the Firedrake extending outward from the domain boundary. The relationship between these features and the Black Bay Fault is unknown.

One five-day fly camp was spent at Dymond Lake during the 2016 field season, with several shoreline traverses completed (Figure 4-37). Unfortunately, the Black Bay Fault was belatedly discovered to be located ~ 5 km east of Dymond Lake, and the study at the fly camp was solely situated in the McCann domain. In addition to the fly camp at Dymond Lake, two traverses crossing the Black Bay Fault were completed north of Dymond Lake around Damant Lake (Figure 4-37), and five traverses were completed along the main offset segment to the south. Helicopter sampling by other project members surrounding these traverses supplemented the structural understanding in this region. Outcrop exposure in the Dymond Lake area was poorer

than in the Insula-Labyrinth Lake area, due to less recent forest fire burns and a shift towards more open tundra, resulting in outcrops heavily covered in lichens.

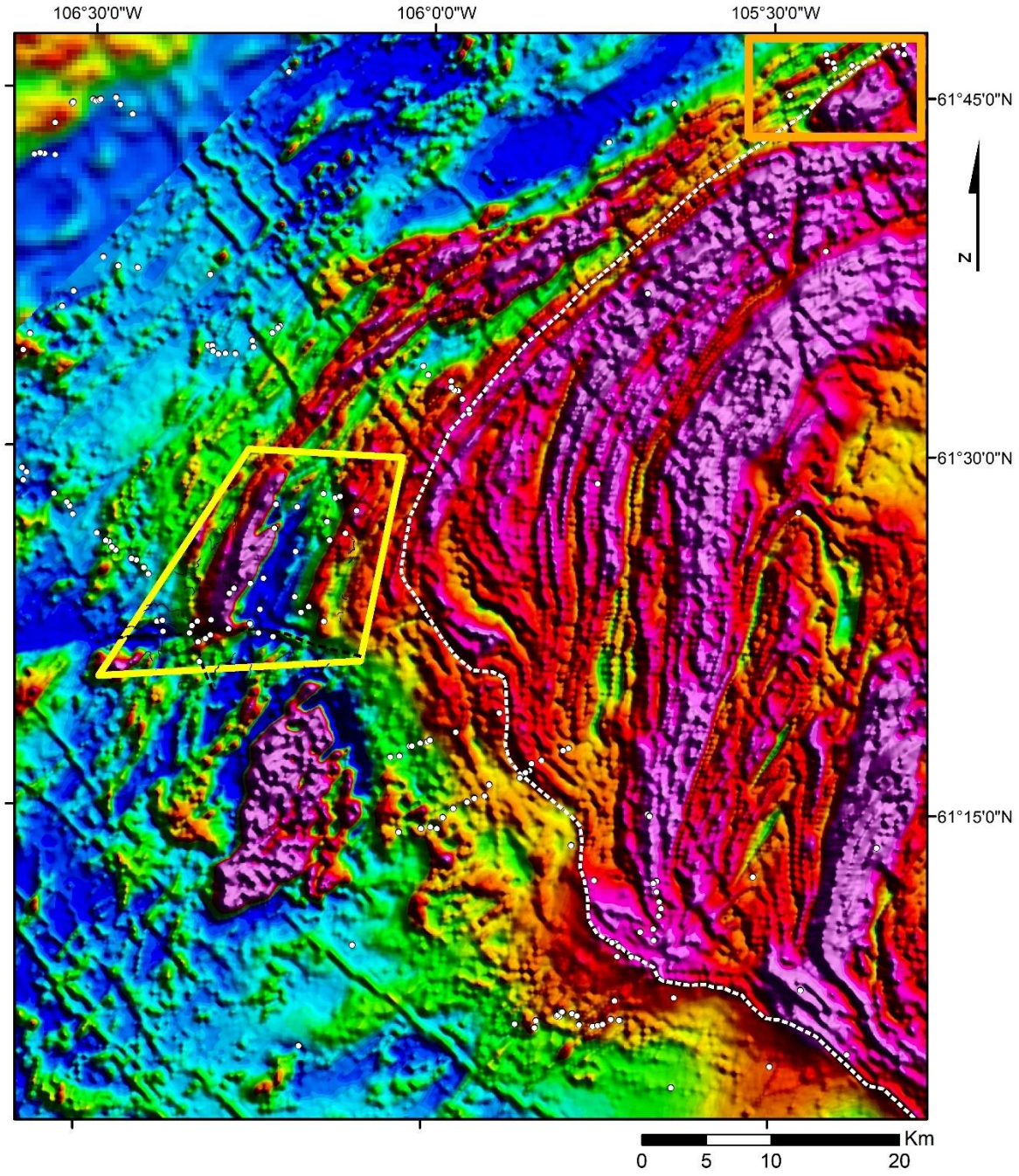

Figure 4-37. Aeromagnetic map of the Dymond Lake area and surrounding northern extent of the Black Bay Fault. Black Bay Fault indicated by the white line. Field stations shown in white. Dymond Lake fly camp area highlighted in yellow. Damant Lake area in orange.

4.4.2 Geology

McCann domain

Work in the Dymond Lake area provided an opportunity to better subdivide the various lithological units present in the McCann domain compared to the work done further to the south around the Insula-Labyrinth Lakes area. Overall, the majority of the units around Dymond Lake are garnet-bearing tonalites to monzonites with variations in the composition of their ferromagnesian mineral components (Figure 4-40), viz.: (1) orthopyroxene-clinopyroxene-rich tonalite, (2) clinopyroxene-rich tonalite, (3) hornblende rich tonalite, (4) a ferromagnesian mineral poor leucotonalite, and (5) a quartz diorite (Figure 4-41). Additionally, the (6) blue-quartz gneiss, (7) megacrystic granite, and (8) ultramylonite units observed in the Insula-Labyrinth Lakes area are also present around Dymond Lake. An E-W-trending grabbroic unit (9) and cpx-syenite (10) are also present and appear to be structurally associated with large late-stage brittle to brittle-ductile faults in the region.

Quartz found in the majority of all the rock units in the Dymond Lake area has a dark grey to bluish colour, resulting in a more distinct blue hue than observed in the McCann domain in the Insula-Labyrinth Lakes area. The blue hue of the McCann quartz in the Dymond Lake area was found to be the best differentiator from rocks of the Firedrake domain, rather than a lack of garnets or magnetism.

The megacrystic granite is primarily found close to the Black Bay Fault and was not observed towards the centre of the McCann domain. Bands of metasediments (Figure 4-38 C) along with occurrences of metamorphosed banded iron formation (Figure 4-38 D) are found sporadically throughout the domain, but are more prevalent along the large NW-SE-trending Black Bay Fault segment.

Apart from the megacrystic granite and late intrusives, the majority of the rock units in the McCann domain contain garnets or evidence of relic garnets. The garnets are primarily red to red-brown in colour, although the metasediments contain two populations of garnet: a more purple to pink garnet population and a red garnet population. Sillimanite is commonly found with the more purple to pink garnets.

A strong brittle deformational overprint is present in this region of the McCann domain. Large brittle faults, trending E-W and NNW-SSE (Figure 4-40), produce the greatest relief in the GEM2 South Rae mapping area, with 100's of metres high cliffs. Metamorphic grade is observed to change across some of these late faults, and a change of the ferromagnesian minerals in the tonalites occurs across the faults at Dymond Lake. North of the E-W secondary fault a granulite-grade tonalite of orthopyroxene-clinopyroxene composition is present, but south of the fault the tonalite has a clinopyroxene or hornblende composition (Figure 4-40). A strong cataclastic overprint is visible surrounding these faults (Figure 4-54), and the fault zone displays fault polish and brittle fractures. Evidence of hydrothermal alteration is strong with epidote and potassic alteration observed.

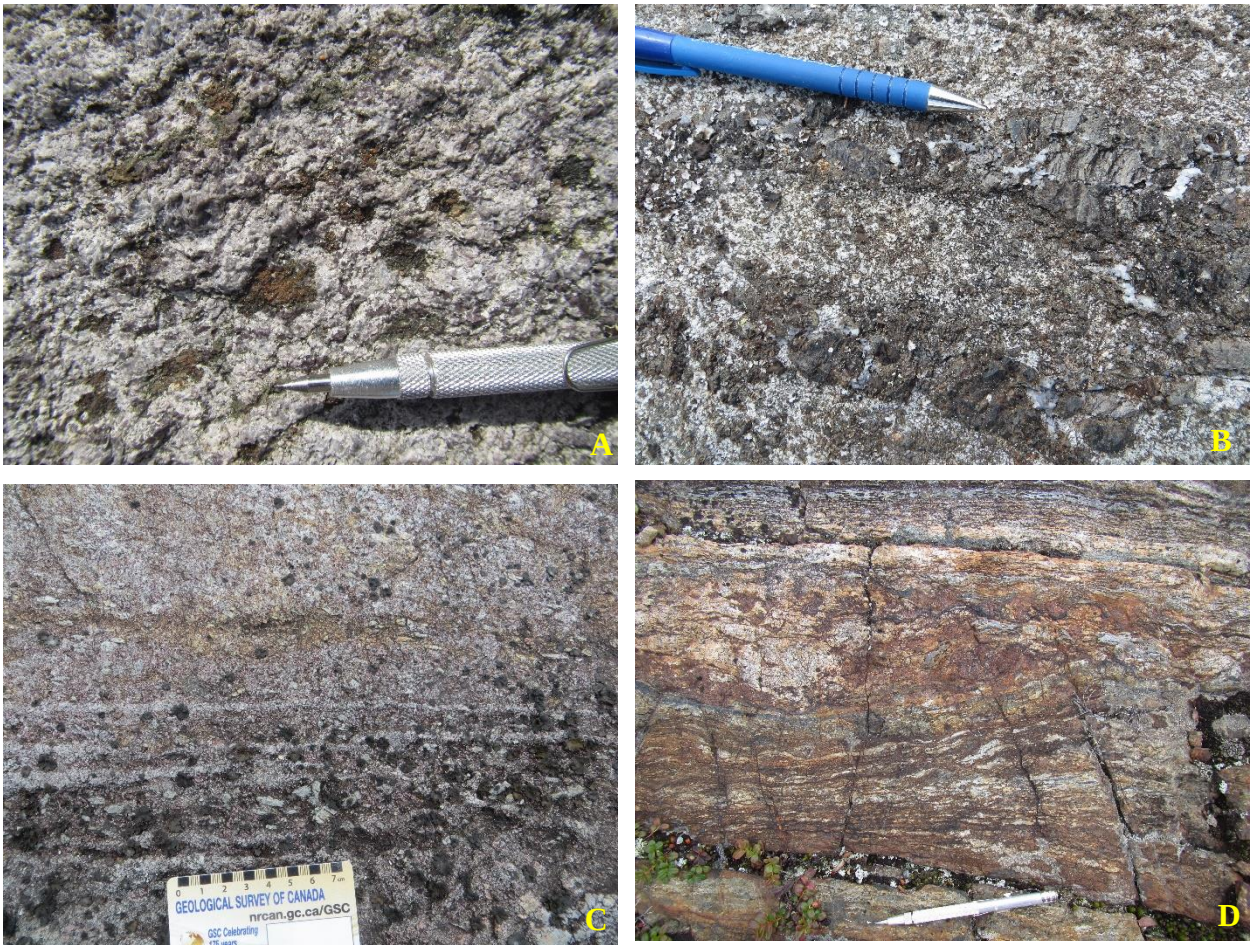

Figure 4-38. Example of the McCann rock units in the Dymond Lake vicinity. (A) Blue-quartz tonalite with red-brown garnets rimmed by clinopyroxene and hornblende. (b) Orthopyroxene-clinopyroxene quartz-diorite with large orthopyroxene crystals. (C) foliated metasediments with large sillimanite crystals and pink garnets. (D) Metamorphosed banded iron formation with magnetite layering, rich in pyroxenes.

Firedrake domain

Overall much less time was spent in the northern Firedrake domain than in the adjacent McCann domain, both in my traverses focusing on the Black Bay Fault and in the general regional mapping by other project members. As a result, the lithology of the Firedrake domain in this area remains largely undifferentiated.

The northern portion of the Firedrake domain in the Dymond Lake region appears to contain more compositional variance than noted in the Insula-Labyrinth Lakes area and the Tazin River area. While the characteristic migmatitic to soupy orthogneiss of the Firedrake domain of those areas was still present, it was primarily found further away from the domain boundary, and our transects examining the Black Bay Fault rarely encountered it. Instead, around the domain boundary and the Black Bay Fault, garnet-rich paragneisses are present (Figure 4-39), preventing a clear determination of the boundary. The more typical migmatitic Firedrake gneisses are present further east, away from the boundary and placement of the boundary was initially rough. The placement of the boundary was refined through P-T-t work done by Regis et al. (2017). Some straight gneiss packages are also found close to the Black Bay Fault, although much less common compared to the Insula-Labyrinth Lakes area of the Firedrake domain. The late brittle overprint observed in the McCann around Dymond Lake does not appear to extend significantly into the Firedrake domain.

Figure 4-39. Firedrake paragneiss unit found close to the Black Bay Fault, resembling some of the McCann paragneisses found nearby.

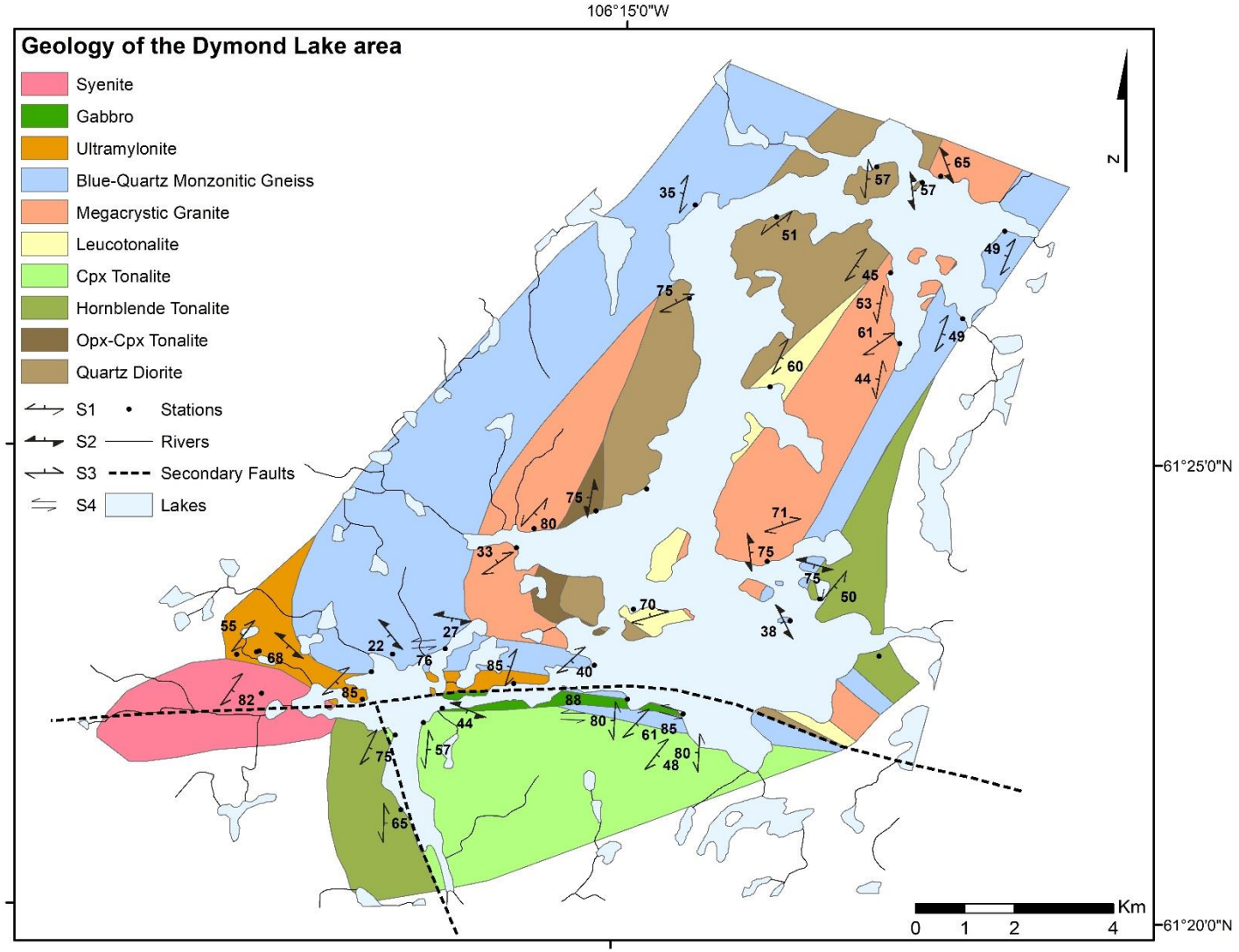

Figure 4-40. Simplified geological map of the Dymond Lake area.. The Black Bay Fault is located approximately 5 km east of the edge of the mapping area.

4.4.3 Structural Geology

Examination of the structural fabrics in the Dymond Lake region provided the opportunity to better understand the NW-SE S2 fabrics previously identified in the Insula-Labyrinth Lake area and the relationship with the S1 and S3 fabrics. Work in this area was more focused on the western side of the Black Bay Fault, in the McCann domain, whereas observations in the Insula-Labyrinth Lake areas were concentrated in the eastern, Firedrake domain. Preferential mineral alignment in some of the outcrops has preserved the later overprinting fabrics, allowing for better differentiation of the deformational events. In the Dymond Lake area, all four deformation events are well preserved with many crosscutting relationships along with the preservations of a background fabric, pre-S1.

Pre-D1

Separating the pre-S1 fabric in the McCann domain from the later S2 fabric was difficult in the Dymond Lake area. Here we found evidence of the impact of the Black Bay Fault over 10 km west of the Black Bay Fault. Additionally, as the majority of the 2016 GEM2 field season was focused on characterizing the structures near the domain boundary, few measurements were collected in the centre of the domains. This made assessment of the background (pre-D1) fabrics difficult. However, in the transects between McArthur Lake (further to the west, where the 2016 base camp was located) and Dymond Lake, the foliation and gneissosity was observed to be generally WNW-ESE-trending, with no overprinting fabrics. It is assumed that these outcrops were not impacted by Black Bay Fault deformation. Structural measurements recorded in Taylor's (1959) mapping of the region support the assumption of a pre-existing fabric trending WNW-ESE.

In the Firedrake domain, in contrast, fabrics associated with the Black Bay Fault are rapidly lost moving eastward, away from the fault trace. Away from the fault, the pre-S1 fabrics in the Firedrake domain are mainly aligned with the regional-scale folds visible in the aeromagnetic survey of the region. Although the regional-scale folds are oriented in a similar orientation to some of the fabrics associated with the Black Bay Fault deformation events, their association with the Black Bay Fault is unclear and the fabrics in the rocks surrounding the regional-scale folds differ from the fabrics associated with the fault. Near to the Black Bay Fault in outcrops impacted by the fault, the resistites are well-aligned and the leucosome melts often sheared, both

predominately oriented with the trace of the fault whereas the rocks surrounding the regional-scale folds contain a large amount of unoriented leucosome.

D1

The oldest fabrics associated the Black Bay Fault, S1, are best preserved in the area north Dymond Lake, where the aeromagnetic signature of the Black Bay Fault returns to a NE-SW trend. Preservation of D1 fabrics is limited around Dymond Lake proper and rarely found further south along the large NW-SE-trending section of Dymond Lake.

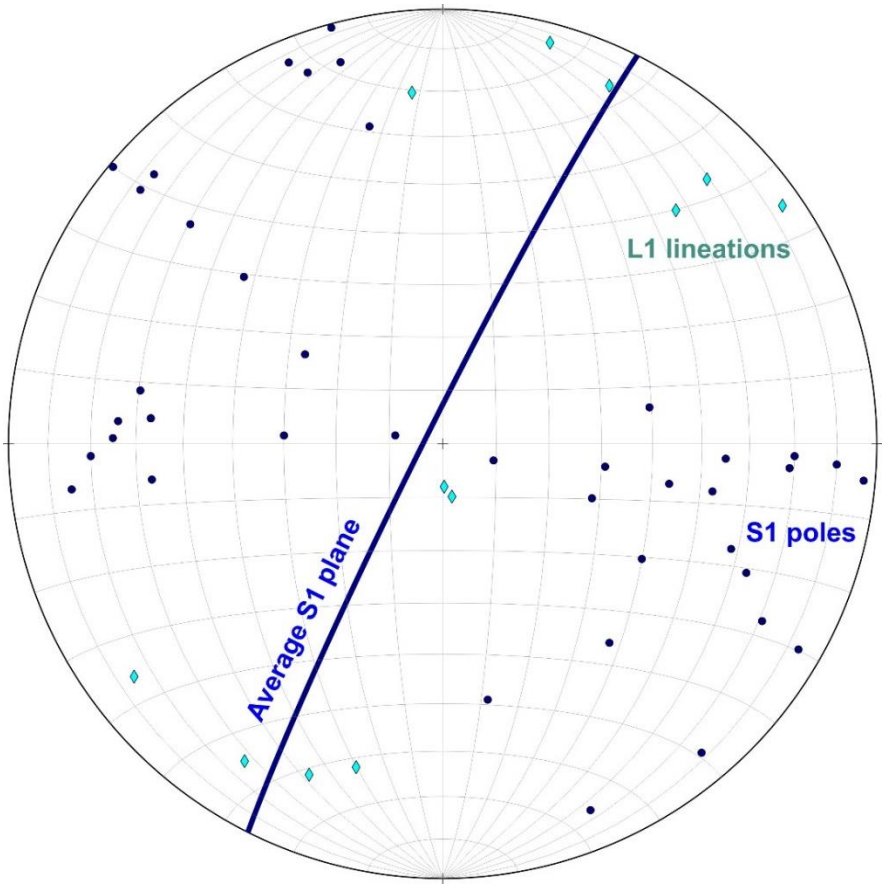

Figure 4-41. Stereonet plot of the S1 planes and L1 lineations found in the Dymond Lake region. The larger spread in S1 poles is a result of the larger study area.

Overall, S1 is found as a steeply dipping, well developed NNE-SSE-trending foliation to gneissosity in the Dymond Lake region (Figure 4-41). Around Damant Lake, further to the northeast (Figure 4-37), the S1 fabrics were found to become more NE-SW-trending, paralleling the Black Bay Fault trend, but are still steeply dipping. The clockwise shift in S1 fabrics around Damant Lake may be due to rotation that occurred during a later deformational event, or

potential bias introduced due to the limited number of traverses in this area. The relatively large dispersion in S1 poles (Figure 4-41) is likely due to the larger size of the Dymond Lake region.

D1 fabrics is preferentially preserved in rocks with a more tonalitic composition. This pattern is observed in both the Firedrake and McCann domains. The preferential preservation of D1 fabrics in more tonalitic compositions was also observed in the Insula-Labyrinth Lakes study area. Tonalitic L-tectonites are relatively common in the Dymond Lake area (Figure 4-42) and account for the majority of the L1 lineations recorded. L1 lineations are found to be primarily shallowly plunging to both the NE and SW (Figure 4-41). The variance in trend observed with these lineations is likely due to the shallow plunges, which can amplify variation in the trend when collecting the data. In addition, around Damant Lake, isoclinal, NE-trending, upright F1 folds contains sub-vertical lineations.

Figure 4-42.. L-tectonites associated with D1 found throughout the Dymond Lake region.

Sinistral kinematic indicators are preserved in some of the fabrics, primarily as small s-folds (Figure 4-43 A) and c-c' fabrics (Figure 4-43 B), although some sinistral σ- and δ-porphyroclasts (Figure 4-43 C, D) are found. More sinistral kinematic indicators are found in the fabrics on the western side of the Black Bay Fault (McCann domain) compared to the Insula-Labryinth Lakes area where most of the sinistral kinematic indicators were observed during the transects on the eastern side of the fault (Firedrake domain) Transposition of the older pre-S1 fabrics into S1 is not observed in the Dymond Lake area, but this may be due to overall poor preservation of S1 or pre-S1 fabrics.

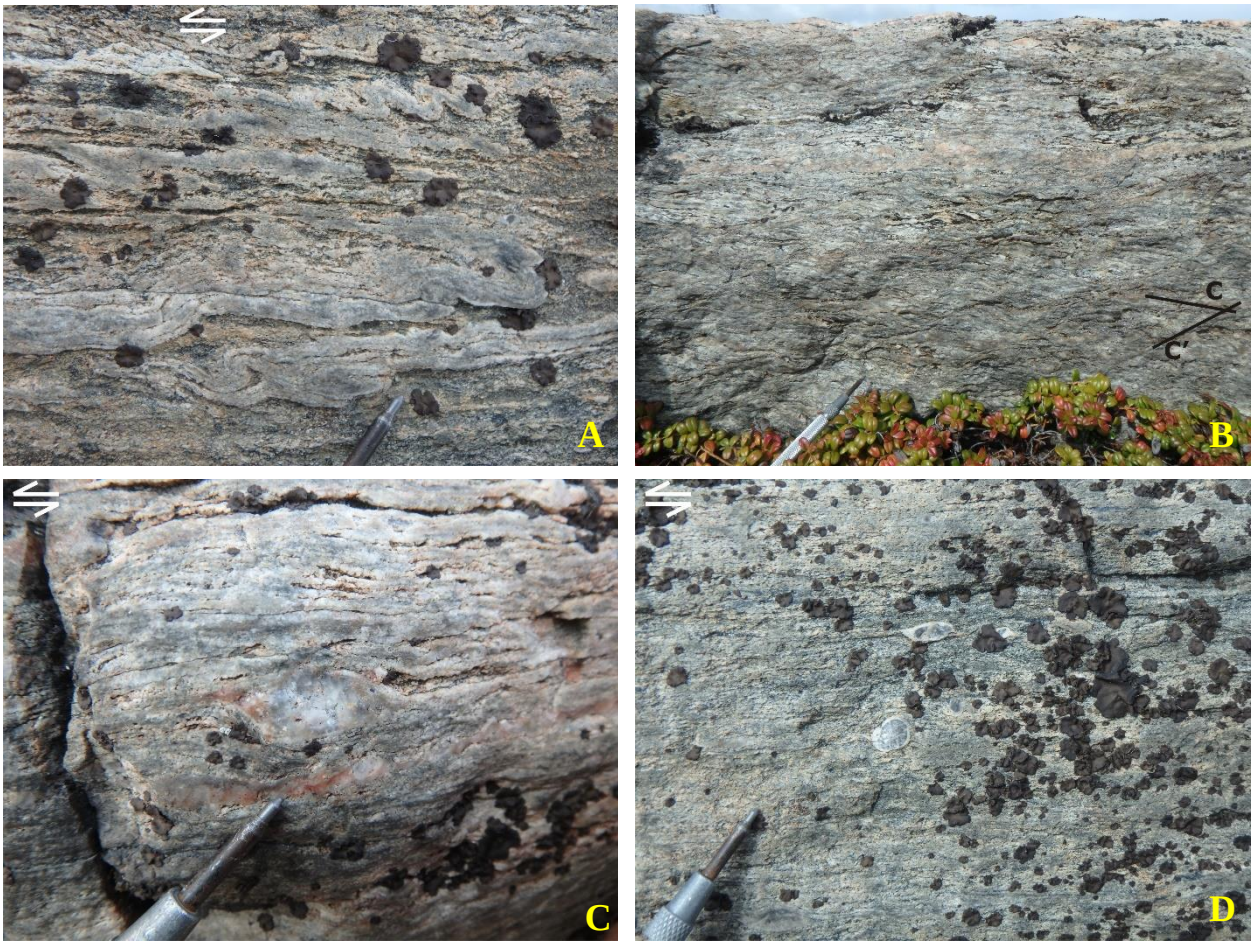

Figure 4-43. Sinistral kinematic indicators observed in the S1 fabric. (A) Small S folds. (B) C-C' fabric indicating sinistral shear. (C,D) Sinistral σ-clast along with δ-clast.

D2

The D2 deformational event is well preserved in the Dymond Lake region, with a prevalent NW-SE-trending, overall moderate to steeply west-dipping S2 foliation to gneissosity (Figure 4-44 A). S2 is best preserved south of Dymond Lake along the large NW-SE-trending segment of the Black Bay Fault and domain boundary (Figure 4-37). The undulating pattern seen in the aeromagnetic trace of the fault is also observed in the strike of the S2 fabric and, consequently, there is a large spread in the S2 pole distribution (Figure 4-44 A).

Around Dymond Lake proper, preservation of S2 improves moving westward away from the fault where the impact of the subsequent D3 event was not as strong. Around Damant Lake, where the trace of the Black Bay Fault returns to a NE-SW trend, little evidence of D2 was observed. S2 was more commonly found preserved in the megacrystic granite and other more

gneissic units compared to the tonalite, where D2 has not overprinted the pre-existing structures as strongly.

Crosscutting relationships of the S2 fabric over S1 are observed around Dymond Lake, with the older S1 NNE-SSW-trending fabric defined by compositional banding overprinted by a NW-SE-trending S2 foliation defined by preferential mineral alignment (Figure 4-45 A). Elsewhere, an S2 shear is observed to crosscut a D1 L-tectonite (Figure 4-45 B). Folding of the S1 fabric into S2 suggests sinistral kinematics. Also present are garnet amalgamations which have acted as δ-clast which also show sinistral motion (Figure 4-46).

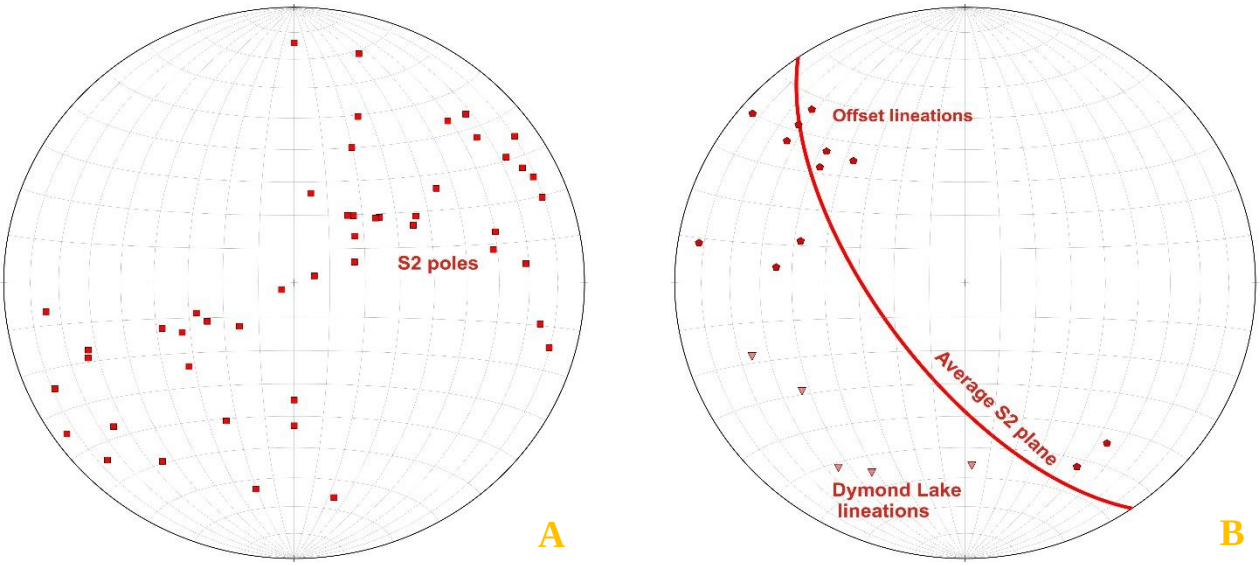

Figure 4-44. (A) Equal-area lower hemisphere plot of the S2 poles in the Dymond Lake area.. (B) Equal-area lower hemisphere plot of the lineations measured on S2. Lineations around Dymond Lake plunges to SW while south along the larger offset they are found to plunge shallowly to the NW/SE.

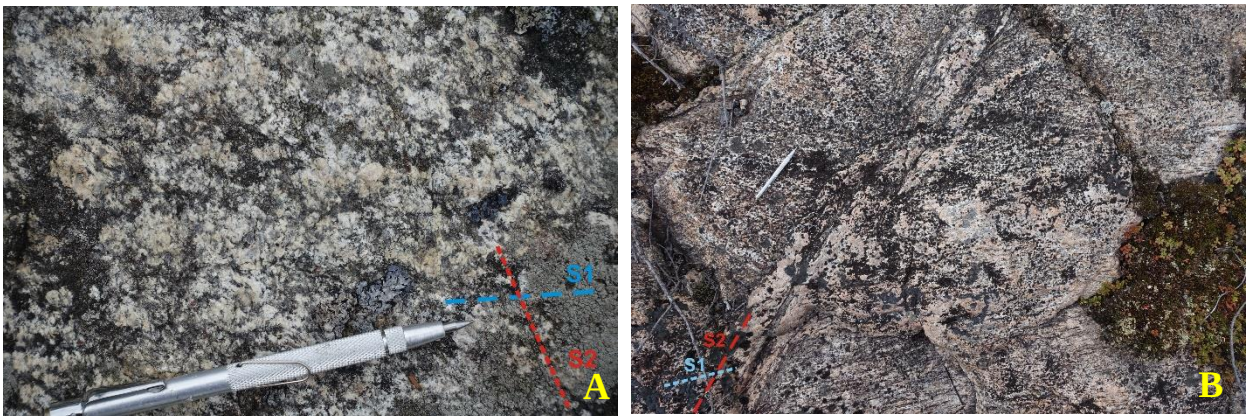

Figure 4-45. Outcrop photos where S2 overprints an older fabric assumed to be S1. (A) NNE-SSW-trending compositional banding overprinted by NW-SE-trending S2 fabric defined by preferential mineral alignment. (B) Tonalitic L-tectonic with S1 fabric cut by an S2 shear with small sinistral shearing observe along the edges.

Figure 4-46. Rare sinistral kinematic indicators found in the S2 fabric. Delta clast composed of a garnet amalgamation.

One outcrop adjacent to the NW-SE-trending section of the Black Bay Fault contains evidence of NE-plunging L1 lineation which has been refolded by a F2 open fold, producing a doubly plunging fold with a shallowly plunging, porpoising hinge with a trend of 320/140 (Figure 4-47). The deformed L1 lineations here are delineating the trace of the F1 fold hinges. The oblique angle between the L1 and F2 hinge suggest that L1 was pre-existing and did not develop during D2. Open, shallowly plunging F2 folds were also found at Dymond Lake, with both NW and SE trends. The range in recorded dip of the S2 fabric is likely due to measurements collected on the limbs of the open folds in locations where the fold hinge or nose is not exposed.

South of Dymond Lake, the majority of L2 lineations were observed to plunge shallowly to the NW, with stretching lineations paralleling the F2 fold axes (Figure 4-44 B). However, around

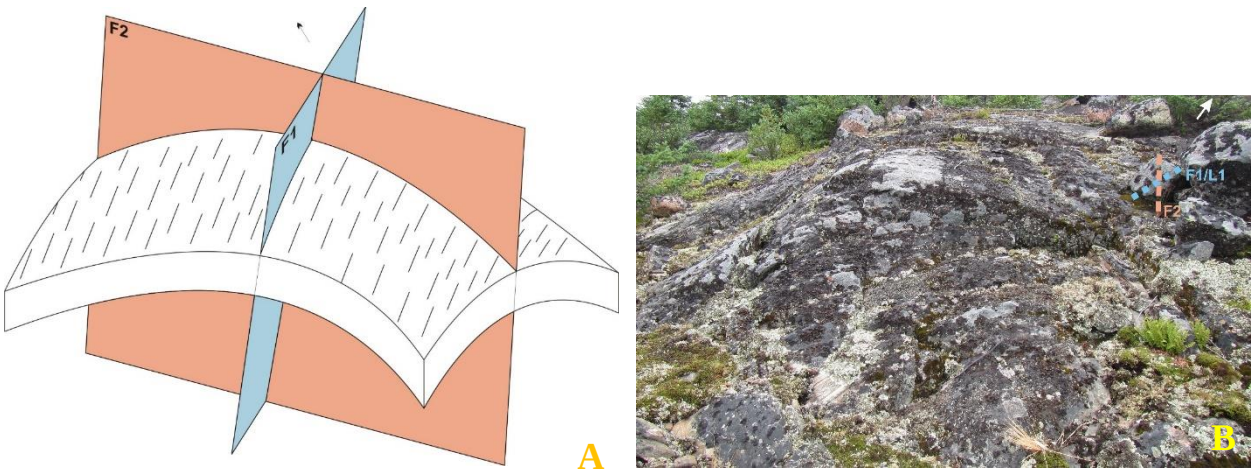

Figure 4-47. (A) Diagram showing a F1 fold refolded by a F2 fold, producing a canoe fold with a porpoising F2 fold hinge. L1 lineations are observed to trend parallel to the F1 fold hinge. (B) Outcrop photo of the fold. Heavy lichen cover and weathering obscure the majority of the fabrics.

Dymond Lake in similar NW-SE-trending planar fabrics, steep, SW-trending lineations were recorded rather than NW-trending lineations as expected.

4.4.4 D3

D3 fabrics are found preserved throughout the Dymond Lake region, with fabric styles similar to the S3 fabric observed in the Insula-Labyrinth Lakes and the Tazin River areas. S3 is a NE-SW-trending, moderately west-dipping fabric that overprints the S2 and S1 fabrics (Figure 4-48). S3 is primarily a more mylonitic fabric. North of Dymond Lake, S3 is also found as an overprinting foliation and occasional gneissosity.

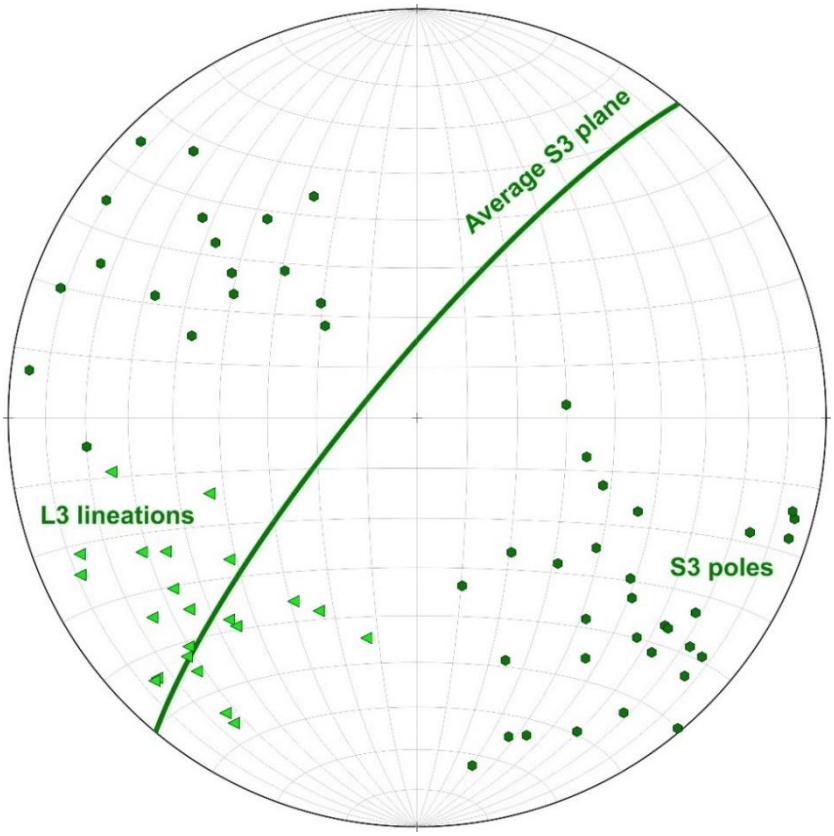

Figure 4-48. Equal-area lower hemisphere plot of the S3 planes and L3 lineations. Lineations form a tight shallow to moderately SW plunging cluster.

In outcrops where S1 and S3 fabrics are present, S3 is found to clockwise overprint S1 (Figure 4-49 A). Where S3 is found to overprint S2, transposition of S2 by S3 shows dextral shearing of S2 (Figure 4-49 B). Other dextral kinematic indicators are commonly observed in the S3 fabric, including dextral sigma clast, z-folds, pull apart and C-C' fabrics (Figure 4-51). As observed in most of the fabrics associated with the Black Bay Fault, there is some variance in dip direction of S3, and this is likely due to the impact of larger regional scale folding which is not easily

Figure 4-49. Fabrics from an outcrop north of Dymond Lake which contains S1 through S3 fabrics. (A) A tonalitic portion of the outcrop contains S1 compositional layering with an overprinting S3 foliation defined by alignment of the mafic minerals. (B) Megacrystic granite portion with a NW-SW S2 fabric which is cut by numerous S3 shears.

observed with our outcrop spacing. However, compared to the earlier fabrics, S3 is far more consistent and the observations of S3 in the Dymond Lake area align closely with the observations from the other study areas.

Shallow to moderate southwest-plunging L3 lineations are readily found around Dymond Lake and produce a tighter cluster (Figure 4-48) compared to the other study areas and other lineation generations. One felsic ultramylonitic outcrop on Dymond Lake contains a well-developed ductile slickenside striations that plunge shallowly to the southwest (Figure 4-50 B). The ductile striations provide the direction of shear (Lin et al., 2007), here indicating west-side up to the northeast. For a west-dipping fault this would be produced through dextral transpression. This

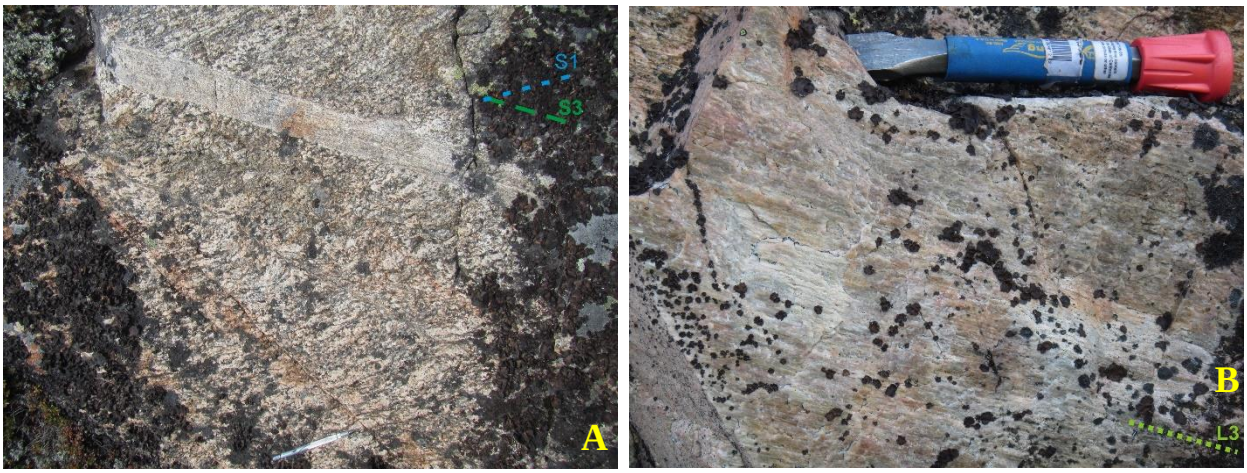

Figure 4-50. S3 shear crosscutting S1 foliated megacrystic granite. (A) A weak overprinting S3 fabric is observed in the quartz of the megacrystic granite, trending parallel to the shear band. (B) Well-developed shallowly southwest-plunging lineation found in a felsic ultramylonite.

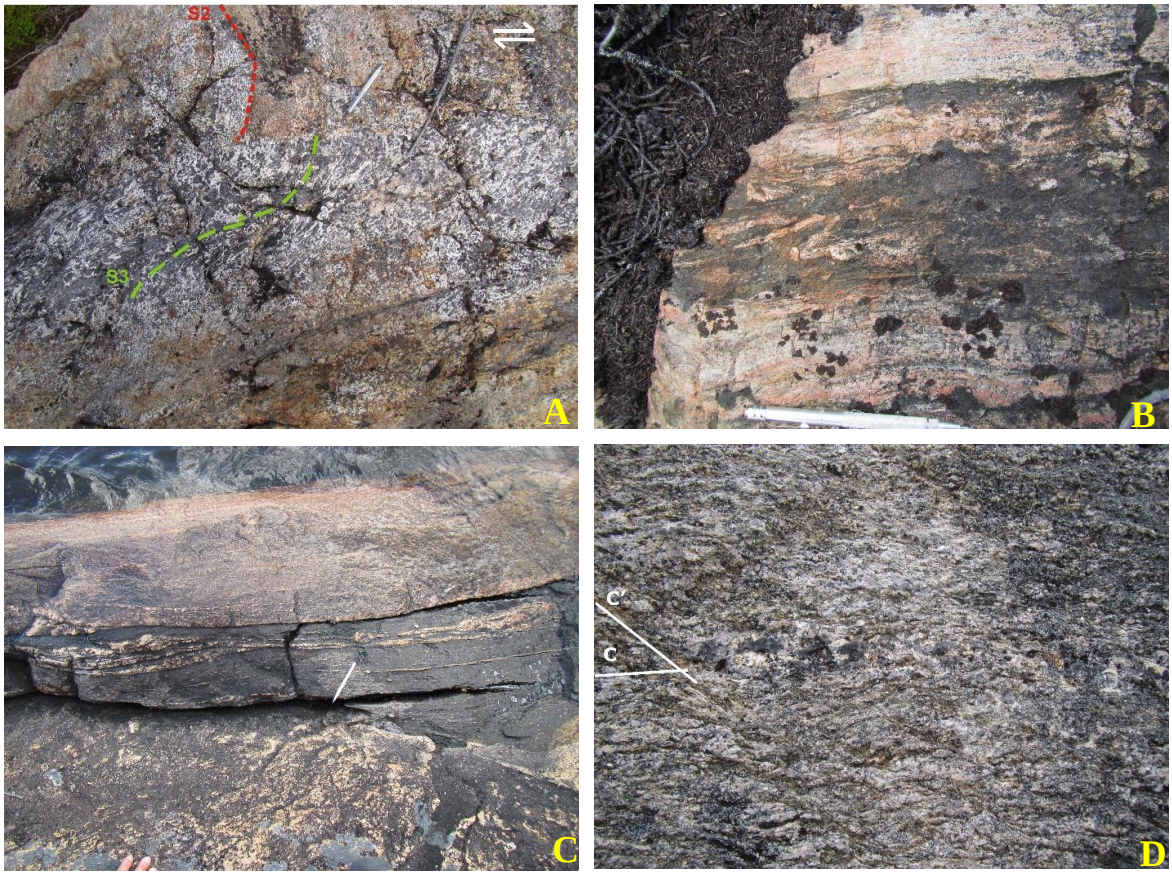

Figure 4-51. Various dextral kinematic indicators observed in the S3 fabric. (A) Leucotonalite intrusion along which NE-SW-trending dextral shearing has developed. (B) Small Z-fold of a more felsic layer. (C) Dextral pull-apart also containing dextral sigma clast. (D) C-C' fabric indicating dextral motion.

movement is consistent with the abundant dextral kinematics and the SW-plunging stretching lineations.

Moving westward, away from the Black Bay Fault around Dymond Lake, the impact of D3 decreases. There is also a shift from S3 fabrics that are penetrative at outcrop scale towards more discrete, dextral shear bands crosscutting the older fabrics (primarily S2) moving away from the fault. In the regions further away from the Black Bay Fault, development of S3 predominately occurred in zones of decreased competency, such as in cross-cutting leucotonalitic intrusions (Figure 4-51 A). The orientation of the blue quartz near the contact with the garnet-pyroxene tonalite host rock is parallel to the S2 foliation in the surrounding host rock, suggesting that the intrusion of the leucotonalite occurred during D2. Later deformation during D3 resulted in the development of an S3 shear band in the less competent intrusion and the quartz can be observed rotating into alignment approaching the shear. The presence of S3 isolated to the less competent areas is observed in multiple outcrops ~10 to 15 km west of the Black Bay Fault and may

represent the outer limit of the impact that D3 had on the area as closer to the fault S3 is less compositionally constrained.

4.4.5 D4

In the Dymond Lake area, a later brittle-ductile deformational event is also present, although it is unclear whether this deformation is associated with the Black Bay Fault. E-W-trending kink bands are observed along the southern portion of Dymond Lake in dioritic to gabbroic rocks (Figure 4-53). Additionally, small sinistral shear bands, up to a few centimeters wide and primarily E-W to NW-SE-trending, are found at Dymond Lake and surrounding areas (Figure 4-52 A). A dextral conjugate set of discrete to brittle-ductile shears (NE-SW-trending) is also present (Figure 4-52 B). The offset-orientation pattern of these brittle-ductile features indicates roughly E-W contraction. Due to the increase in heterogeneity of D3 moving westward from the Black Bay Fault into the McCann domain, separating the smaller scale S3 shear bands from the S4 brittle-ductile and discrete shears becomes more difficult.

Figure 4-53. Brittle-ductile to brittle fabrics observed in the Dymond Lake area with the development of E-W-trending kink banding.

In addition to the brittle-ductile shears and deformational fabrics, sets of small, late brittle fractures are found surrounding the larger faults at the south end of Dymond Lake (Figure 4-54). These brittle fractures show only small offset (< 5cm), and their orientation-offset pattern (sinistral movement along the NE-SW-trending component and dextral along the NW-SE-trending component) indicate E-W extension in late or post D4 time.

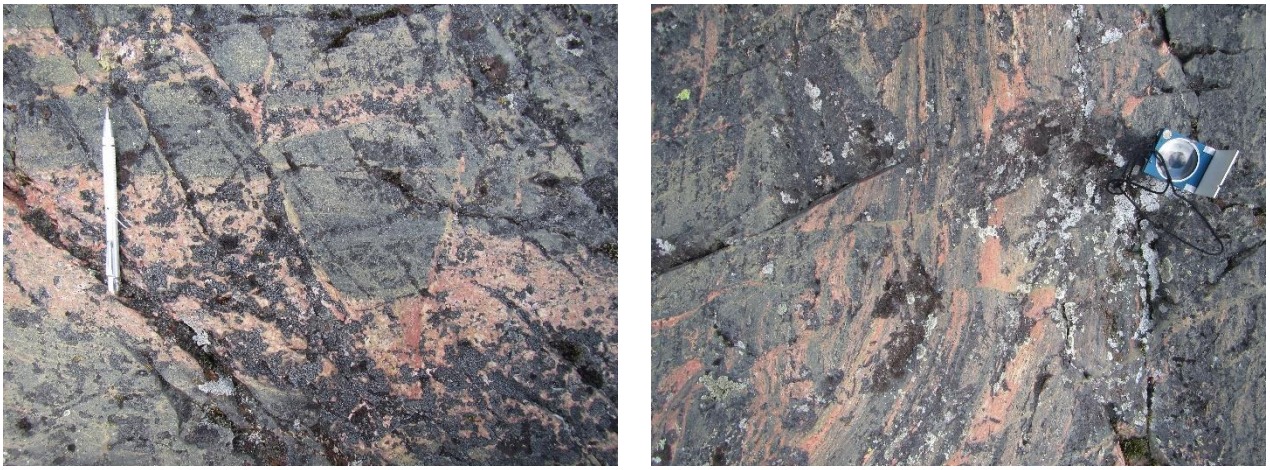

Figure 4-54. Late brittle fracture sets suggesting E-W extension. Potassic alteration along with epidote and chlorite infill in the fractures.

4.5 Summary and Deformation Sequence

4.5.1 Fault Geometry

Within our study area in the NWT, the Black Bay Fault marks the boundary between the Firedrake domain (to the east) and the McCann & Ena domains (to the west). Exposure of the fault itself has never been observed in the field. It is generally traced based on geophysical data, surface morphology and strain distribution, as well as identification of lithological characteristics unique to each domain. McCann domain rocks have abundant blue-qtz and Ena domain rocks contain numerous hyalophane-bearing pegmatites whereas rocks that belong to the Firedrake domain have abundant granodiorite migmatite and mafic xenoliths. Reliability of the geophysical and surface morphology decreases around Labyrinth Lake where the magnetic signature of the fault decreases, and the fault trend becomes complicated.

From our mapping we have established that the trace of the Black Bay Fault has an average NE-SW trend (~ 218°) for over 110km from the Saskatchewan-Northwest Territories border to the north end of Labyrinth Lake, at which point it turns to the NW for a distance of 8km, before returning to the NE. The fault then continues another 60km to the NE before making a larger (65km long) bend to the NW with a return to a NE-SW trend around Dymond Lake. Along the larger NW-SE-trending offset extending up to the Dymond Lake area, the boundary undulates rather than being a linear offset as what is found around Labyrinth Lake.

The orientation of structural fabrics associated with movement of the Black Bay Fault provides an estimate of the dip direction and dip magnitude of the fault. The most consistent data for the fault dip estimate comes from the Labyrinth and Insula Lake area where the fault was transected multiple times over a broad area. Here the S1 and S3 fabrics indicate a 60^{o} to 85^{o} westward dip for the SW striking section of the Black Bay Fault and the S2 fabrics suggest a sub-vertical to SW fault dip for the NW-trending segment of the fault. The work further to the north around Dymond Lake supports these conclusions, with the S1 and S3 fabrics in this area also indicating a steeply west-dipping fault orientation while S2 and remains steeply SW-dipping.

The dip direction of the S1 and S3 fabrics around the Tazin fly camp are variable but mostly east-dipping, which suggests a steep eastward dip direction of the Black Bay Fault in the Tazin region. This discrepancy in the fault dip direction may be due, in part, to the spatial distribution of the stations and structural measurements collected between the two areas. Around the Tazin

River area, the majority of structural fabrics were collected during the one land-locked fly camp resulting in a relatively dense (100's of meter spacing) distribution of measurements restricted primarily to the western side of the Black Bay Fault. Many of these outcrops contain folds of different scales ranging from meter, to outcrop and up to regional scale (the latter folds are roughly visibly in aeromagnetic survey near Tazin River proper). The influence of folding may render the S1 and S3 fabrics here unsuitable as indicators of the Black Bay Fault dip direction. However, a similar inconsistency or ambiguity of fault dip direction exists in the studies of the Black Bay Fault to the south, in northern Saskatchewan, with some describing the fault as east-dipping (ie. Bergeron, 2001) while other have described the fault as west-dipping or sub-vertical (ie. Normand et al., 2009) (discussed in section 3.2).

In addition to the main Black Bay Fault, fault splays related to the main fault are present in the Ena domain. These secondary faults were originally noted from the aeromagnetic survey, which shows multiple magnetic lows extending outwards from the Black Bay Fault into the Ena domain. These curve to become more E-W-trending moving southwestwards away from the fault, resembling a set of sympathetic shears. As with the Black Bay Fault itself, the fault splays were not observed on surface; they primarily are located in topographic lows. However, rare high strain zones, approaching mylonitic, were found adjacent to some of the magnetics lows during the regional mapping of the Ena domain. The location of these fault splays may be lithologically controlled, as they occur around the paragneisses and orthogneiss contact.

Apart from the fault splays found in the Ena domain, a large, E-W-trending secondary fault transects the southern end of Dymond Lake (Figure 4-40). This feature has been traced from air photos over 100 kilometers to the west (Martel et al., 2018), and other similarly oriented features are visible in the topography of the McCann domain west of Dymond Lake. These E-W-trending faults do not show up as clearly in the aeromagnetic survey compared the fault splays found in the Ena domain. Only the aeromagnetic pattern from the immediate area surrounding Dymond contains much evidence of the E-W-trending structure. Additionally, the aeromagnetic pattern north of the fault appears to curve like a large sinistral fold into the E-W-trending structure (Figure 4-37). This same pattern is observed in the lithologies around Dymond Lake (Figure 4-40). However, the topographic expression of the structures is very pronounced, with linear lakes and rivers and steep cliffs running adjacent to them. The relationship of the structures or

faults in the Dymond Lake area with the Black Bay Fault is not as clear as compared to the fault splays in the Ena domain, but these faults do not cut the fault itself and are believed to be secondary faults related to the deformation of the Black Bay Fault. These secondary faults appear to have played an important role in controlling emplacement of some of the younger intrusions in the area.

4.5.2 Deformation Sequence

Pre-D1

A background deformational fabric, pre-S1, is present in all three study areas, and on both sides of the Black Bay Fault. It appears unrelated to the deformation of the Black Bay Fault and is assumed to be related to deformational events (pre-D1) that impacted the southern Rae craton prior to the development of the Black Bay Fault. Pre-D1 is not a depositional fabric, even within the metasedimentary rocks that crop out in the Ena domain in the Tazin River area.

The orientation of the pre-S1 fabrics varies depending on which side of the fault the fabric is preserved (Figure 4-55). On the east side of the fault, in the Firedrake domain, pre-S1 was found to be NE-SW to ENE-SWS-trending in both study areas. In contrast, on the western side of the fault in both the Ena and McCann domains, pre-S1 trends NW-SE to WNW-SES. Preservation and recognition of the pre-D1 fabrics improves moving away from the fault and into the interior of the domains. Near to the fault, pre-S1 is commonly overprinted and transposed into the later deformational fabrics, primarily S1. Moving northward on the western side of the fault, the deformation zone associated with the Black Bay Fault and where the later overprinting fabrics are found increases in size, and consequently the preservation of pre-S1 decreases. In comparison, on the eastern side of the fault, the extent of the Black Bay Fault deformation zone remains smaller and more consistent in size in all three study areas resulting in better preservation of the pre-S1 fabrics.

The difference in orientations of pre-S1 across the fault is not unexpected as the different domains show evidence of having different tectonometamorphic histories (Pehrsson et al., 2015) and the pre-S1 fabrics on either side of the fault may not even be related to the same deformation events. Additionally, the subsequent movements along the Black Bay Fault would have produced significant offset of pre-S1 compared to the pre-fault positions.

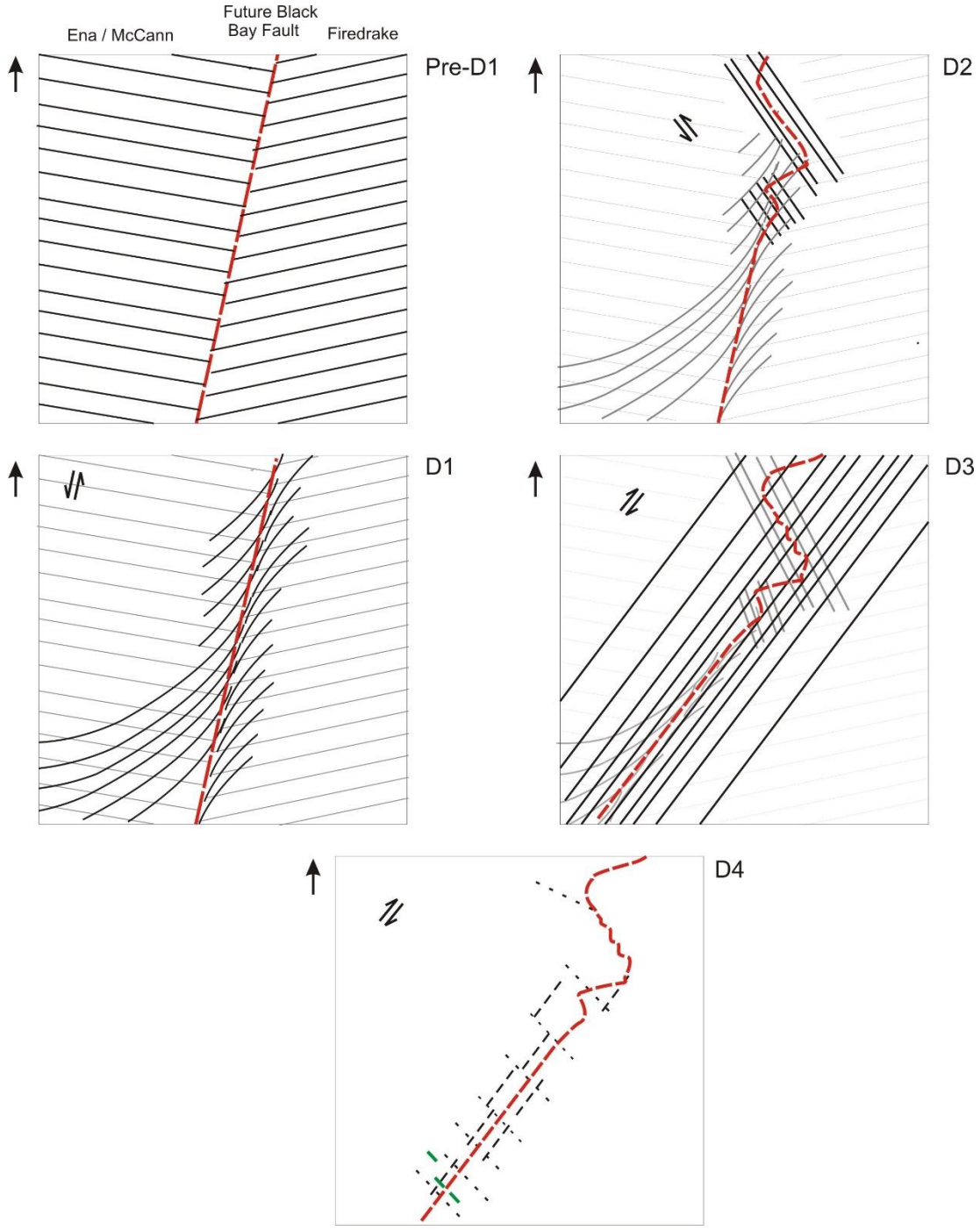

Figure 4-55. Interpreted deformation sequence of the Black Bay Fault and fabric generation. Pre-existing background gneissosity, pre-D1, varies in trend between the two sides of the fault. The Black Bay Fault develop during D1, a sinistral transpression event which produced a NNE-SSW-trending fabric with sympathetic shears becoming more eastward in the SW portion of the study area. Sinistral NW-SE shearing produced the folding and offset observed around Labyrinth Lake. A shift to dextral transpression produced an overprinting NE-SW-trending fabric during D3. D4 marks a shift to brittle-ductile deformation with a NE-SW-trending dextral component and a NW-SE-trending sinistral component along the fault and emplacement of mafic dykes in the NW-SE-trending component.

D1

The S1 fabric observed in all the study areas increases in intensity moving towards that Black Bay Fault on both the east and west sides. It is the earliest recognized deformational fabric that is clearly associated with the Black Bay Fault, and the associated event, D1, is assumed to mark the inception of the Black Bay Fault and associated deformation (Figure 4-55). D1 produced a steeply dipping, NNE-SSW-trending S1 foliation to well-developed gneissosity (Figure 4-56).

Sinistral kinematic indicators are recognized at many locations within the S1 fabric, and they become increasingly more common moving northward along the fault from the Tazin River area into the Insula-Labyrinth Lakes area. These kinematic indicators include folds transposing pre-S1 into S1 sinistrally, large sinistral δ-type porphyroclast and s-fold asymmetry.

L1 lineations and sheath folds associated with D1 provide additional information regarding the kinematics and strain of D1. L1 lineations comprise the majority of the measured lineations in the Tazin River area, and L1 lineations are better preserved in the Tazin River area compared to the other study areas. In the Insula-Labyrinth Lake area, L1 only comprises a minor amount of the lineations measured in the area while in the Dymond Lake area, L1 lineations are predominately found north of the lake. The preservation difference is probably due to overprinting by the subsequent D2 deformation event, which had negligible impact in the Tazin River area and north of the Dymond Lake area while both the Insula-Labyrinth Lakes area and Dymond Lake proper were more directly impacted by the later D2 deformation event. Nonetheless, all the areas contain a clustering of shallow NE-plunging L1 lineations along with a subordinate occurrence of shallowly SE-plunging lineations. Minor occurrences of steeply plunging L1 lineations are also present in all three study areas. NE-plunging L1 lineation observed in the S1 fabric in the Insula-Labyrinth Lakes and Dymond Lake areas should represent the elongation direction of D1 (Sullivan, 2013) and the fault movement direction.

The sheath folds observed in the S1 fabric around the Tazin River area (Figure 4-10) indicate the D1 deformation must have been a high strain event (Alsop and Holdsworth, 2004). To produce the observed fabrics and kinematics, D1 is inferred to be a sinistral transpressional event that produced west side up movement along the Black Bay Fault. The presence of sheath folds along with rare, steeply plunging lineations may indicate D1 contained a significant dip slip component. The shape of the sheath folds have a z-axis that is significantly smaller than the y-

axis, as evidenced by “cat-eye” sheath fold shapes in outcrop (Figure 4-10). This shape indicates the folds must have formed under general shear conditions (Alsop and Holdsworth, 2006), which supports the transpression interpretation. Additionally, the presence of the sheath folds helps explain the presence of the doubly plunging lineations observed in both areas with the lineations being expected to be aligned with the curving sheath fold axes.

The fault splays associated with the Black Bay Fault in the Ena domain are interpreted to have developed with the D1 event. While exposure is poor, one mylonitic sample contains a C-C’ fabric indicating sinistral motion. Furthermore, the trend of the S1 foliation in the Tazin River area was found to rotate clockwise going westward through the region of these splays. This is in contrast to the other two study areas where no significant shift in the S1 trend is observed moving away from the Black Bay Fault. The average S1 plane distal from the Black Bay Fault in the Tazin River area closely aligns with an average trend of the fault splays inferred from the aeromagnetic survey (Figure 4-8). Based upon their geometry and kinematics, the fault splays fit with the A1 horsetail type fault splay model described by Chinnery (1966). These fault splays also match the “synthetic branch fault” classification in more recent fault classification work by Kim and Sanderson (2006), which predict the development of fault splays which deviate around 30° or less from the main fault trend. In a broadly compressional setting they would have developed from sinistral transpression.

D2

Evidence of D2 is found only in the Insula-Labyrinth Lakes and Dymond Lake areas. Here, NW-SE-trending gneissosity, foliations and shears are developed, often containing sinistral kinematic indicators and moderate to shallowly NW-plunging L2 lineations. No D2 features were recognized in the Tazin River area nor in the northern portion of the Dymond Lake area around Damant Lake. In contrast, features associated with the other deformational events were at least partially observed in both in all three areas.

The D2 event is the most poorly understood of the various deformational events that impacted the Black Bay Fault. The D2 event appears to be associated with the major bend in the Black Bay Fault that occurs between the Insula-Labyrinth Lakes area and the Dymond Lake area. This event is also associated with the smaller, but similar bend found at the northern end of Labyrinth Lake and, possibly, with the less pronounced, left-stepping bends in the Black Bay Fault near

Insula Lake. The impact that the D2 event had on the Black Bay Fault was different than the other events and modified the structure of the Black Bay Fault rather than produced deformation along its length. However, for simplicity, D2 is still considered a deformation event in this thesis.

Due to the relative lack of L1 lineations observed around the Insula-Labyrinth Lakes area compared to the Tazin River area, the L2 lineations from around the Insula-Labyrinth Lakes area were rotated to see if they were originally L1 lineations. Treating the S1 and S2 planes as the fold limbs, the average S2 and the L2 lineations were rotated 55 clockwise around a steeply NW-plunging (302/73) axis. This rotation brings the average S2 fabric parallel to S1 in this area. The rotated L2 lineations fall into a NE-plunging cluster resembling the NE-plunging cluster of L1 (Figure 4-56). However, even after rotations, many of the lineations still plunge to the NW. These likely do not represent original L1 lineations and, instead, developed during the D2

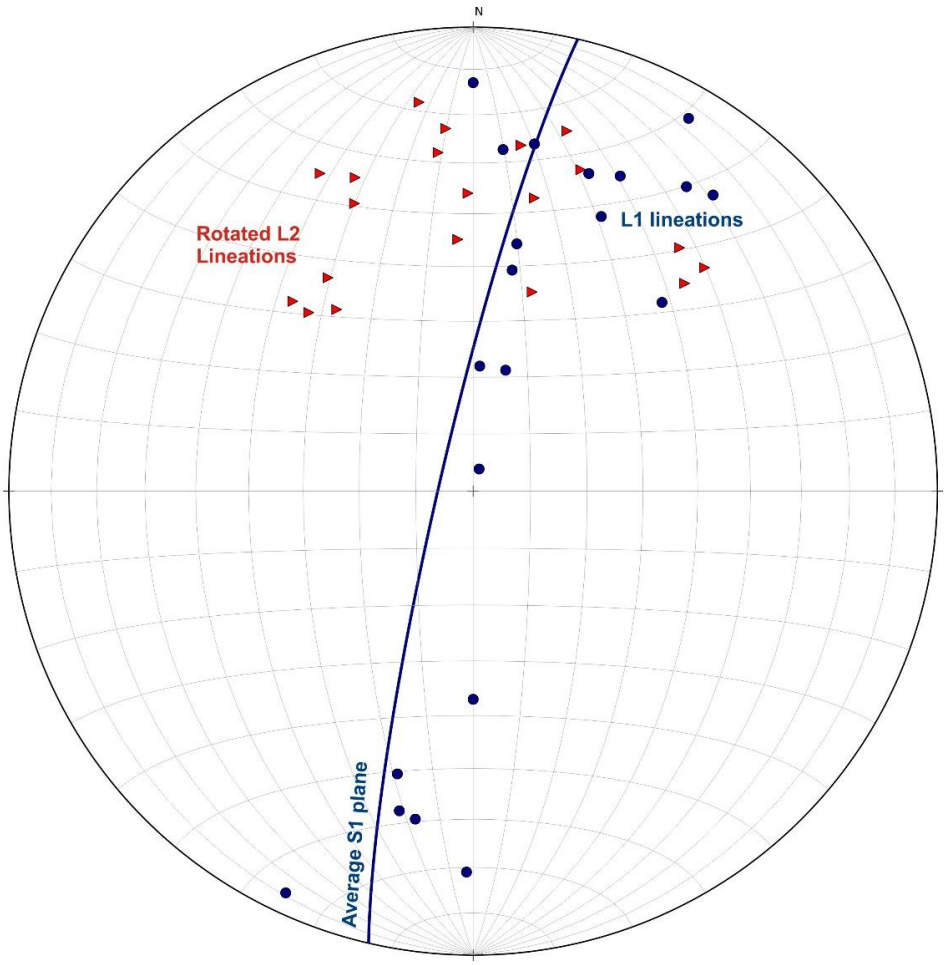

Figure 4-56. Equal-area lower hemisphere plot of all the L1 lineations measured in the study areas along with the average S1 plane close to the fault of both areas. When the L2 lineations are rotated based upon the geometry fault bend found around Labyrinth Lake, the majority appear to cluster similarly to the NE plunging component of L1.

deformation event. Therefore, the L2 lineation which developed during D2 appears to trend more towards the WNW with a moderate plunge compared to the rotated L1 lineations. However, the amount of the rotated L1 lineations composing the L2 lineations may be overestimated based from our work in the Dymond Lake area which found some doubly plunging F2 folds that contains L1 lineations on the enveloping surface. The lack of L1 lineations being rotated by the F2 folding as observed with the doubly plunging fold suggest that the rotation of L1 by D2 may be smaller than what the data from the Insula-Labyrinth Lakes area initially suggested.

The abrupt and significant change in trend of the boundary between the Firedrake and McCann domains at the northern end of Labyrinth Lake is a very perplexing fault configuration. Possible explanations for this pattern include (1) offset of the original (D1) trace of the Black Bay Fault by a D2, NW-SE-trending fault, (2) folding of the D1 fault trace around a steeply NW-plunging axis, and (3) closing of a region of D1 transtension created at a major left-step of the D1 Black Bay Fault trace. All of these possibilities are contentious and suffer from contradictory evidence.

On the simplified lithology/ deformation level map of Labyrinth Lake (Figure 4-25), it can be seen that the lithological units on both sides of the Black Bay Fault, as well as the fault zone itself, deflect to the NW for several kilometers before resuming a NE trend, resembling a large S-fold of the fault. However, the NW-trending section contains sinistral, ductile shears which are observed to crosscut or transpose the preexisting S1, sinistral fabric. It would be difficult to produce this bend simply by folding of the shear zone during the sinistral transpressional D1 event, as that should not produce sinistral shear on both the NE- and NW-trending sections (i.e., both “fold limbs”). Furthermore, in the Dymond Lake area, the S2 fabric and shears are found to extend 10’s km into the McCann domain which would be expected to be produced through shearing rather than folding.

In order to produce the bend in the fault, it seems, by default, that a sinistral NW-SE shearing event must have occurred, D2. Therefore, the fault bend appears to have been produced through the development of a sinistral NW-SE-trending transverse fault which offset the Black Bay Fault to NW and produced shear induced folding of the surrounding lithologies. Based upon the non-rotated lineations, which plunge moderately to the WNW and south dipping fabric, a compressional component appears to have been present and D2 was a sinistral transpressional

event which produced south-side up motion, continuing the uplift of the McCann and Ena domains relative to the Firedrake domain.

The large E-W-trending structure observed around Dymond Lake appears to be a large secondary fault which developed during the D2 event with apparent sinistral strike-slip motion as indicated by the deflection of the aeromagnetic and lithological patterns.

D3

D3 produced the most widely distributed and clearly identifiable fabric, S3, in all the study areas. In general, S3 is found to be aligned closely with the aeromagnetic trace of the Black Bay Fault, trending NE/SW and, primarily, moderately to steeply west-dipping. Similar to S1, there is some discrepancy with the dip direction of S3, with the S3 fabric found to be steeply east dipping around the Tazin River fly camp. Dextral kinematic indicators were readily found within S3 in all the areas, including Z-folded dykes, dextral-porphyroclast and dextral shears. L3 lineations were more readily observed in the Insula-Labyrinth Lake and Dymond Lake areas than in the Tazin River area. However, in all three regions, L3 is found to be moderately SW-plunging, with the clustering of the L3 lineations becoming tighter moving northward. The L3 lineations are preserved better in the more northern areas, possibly due to the rotation of L1 during L2 and the transposition of S1 into S2 during D2. With the destruction or alteration of the pre-existing fabric during D2, fabrics developed during D3 are more discernable in the northern areas than in the Tazin River area. Taken together, the (1) NE-SW-trending, west-dipping S3 fabric, (2) dextral kinematics and (3) SW-plunging L3 lineations, indicate D3 was a dextral-transpressional event which produced west-side up movement (Figure 4-57). West-side up movement is further supported with the ductile slickensides observed around Dymond Lake which confirmed the shear direction. Quartz-filled tension gashes at high angle to the hosting S3 fabric and found adjacent to a D3 shear are present in the Tazin River, which are similar to features described by Sanderson and Marchini (1984) in their transpression model, further support the interpretation of transpression during D3 deformation.

The D3 deformational event is not believed to be responsible for the formation of the fault splays in the Ena domain and it is unsure if they were re-activated during D3. The S3 fabric does not show the same rotation moving away from the fault (Figure 4-11), rather maintaining a more consistent orientation, oblique to the orientation of the splays. A lack of fault splay reactivation

or development is also observed in the Dymond Lake area with the large E-W-trending structure and associated folding of lithologies overprinted by the S3 fabrics

During D3 dextral transpression of the Black Bay Fault, the fault bend around Labyrinth Lake, which developed during D2, would have acted as a restraining bend, producing increased uplift of the McCann over the Firedrake around Labyrinth Lake in order to accommodate the increased compression into the bend (Figure 4-57). Evidence for re-activation of the S2 fabric in the bend around Labyrinth Lake was observed close to the bend, where blastomylonites aligned with the NW-SE-trending S2 fabric appear to have undergone later deformation. Lineations measured in the blastomylonites were found to plunge to the SW instead of the NW and a well-developed C-C' fabric in the blastomylonites shows SW side up movement (Figure 4-58). Also, the blastomylonites shows evidence of greater hydrothermal alteration than the majority of the S2

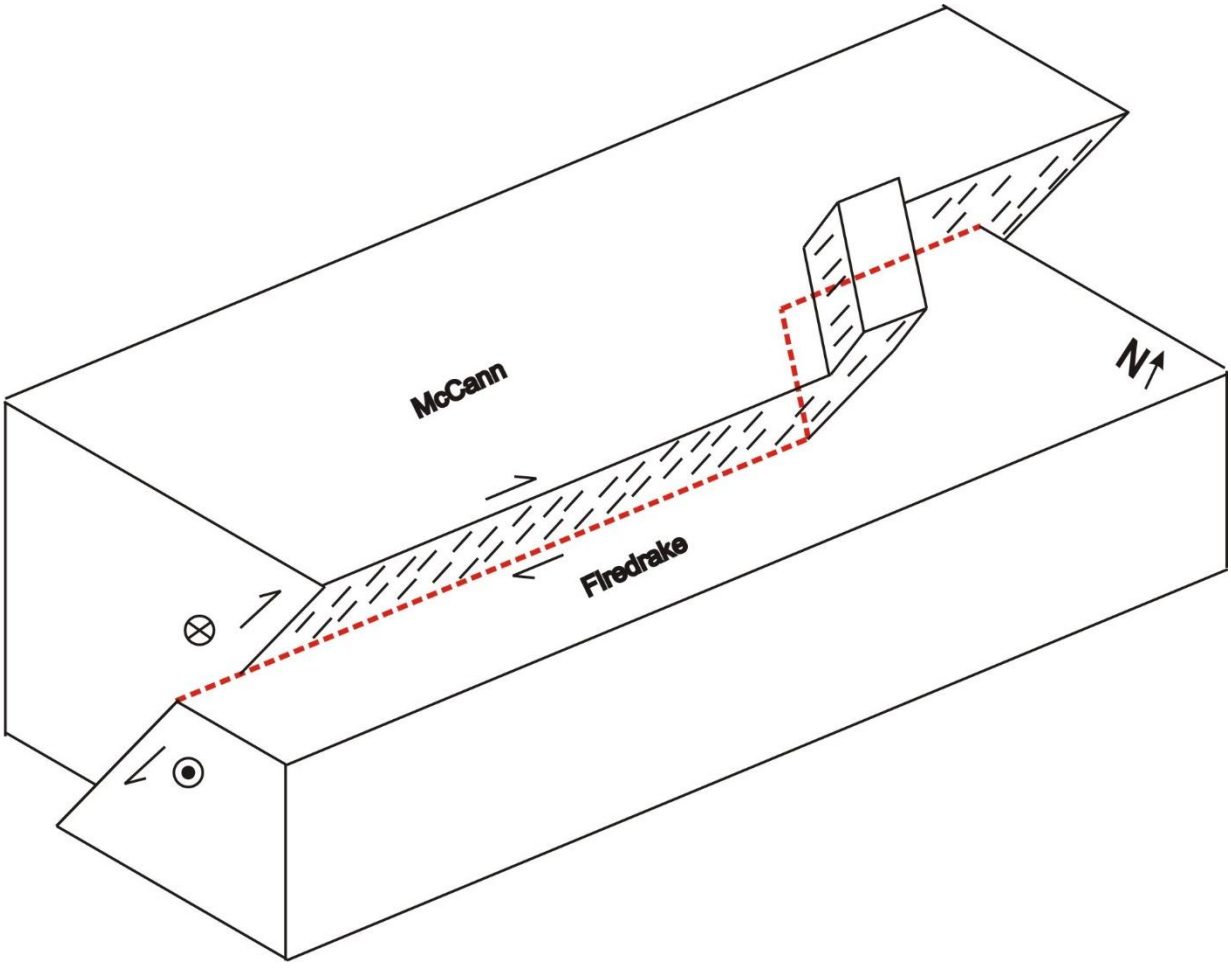

Figure 4-57. Model of the D3 transpressional event. The bend in the fault trace produced during D2 would have acted as a restraining bend during D3, producing greater thrusting and uplift around Labyrinth Lake.

fabrics, with epidotization and potassic alteration present in the fabric. The presence of the alteration in the S3 fabrics suggest that the hydrothermal alteration may have initiated during D3

The undulating pattern in the NW-SE offset of the Black Bay Fault in the Dymond Lake area is assumed to be a result of the D3 event. While this larger offset likely acted as a restraining bend like the offset around Labyrinth Lake, some of the strain appears to have been accommodated through the development of the smaller NE jogs in the offset.

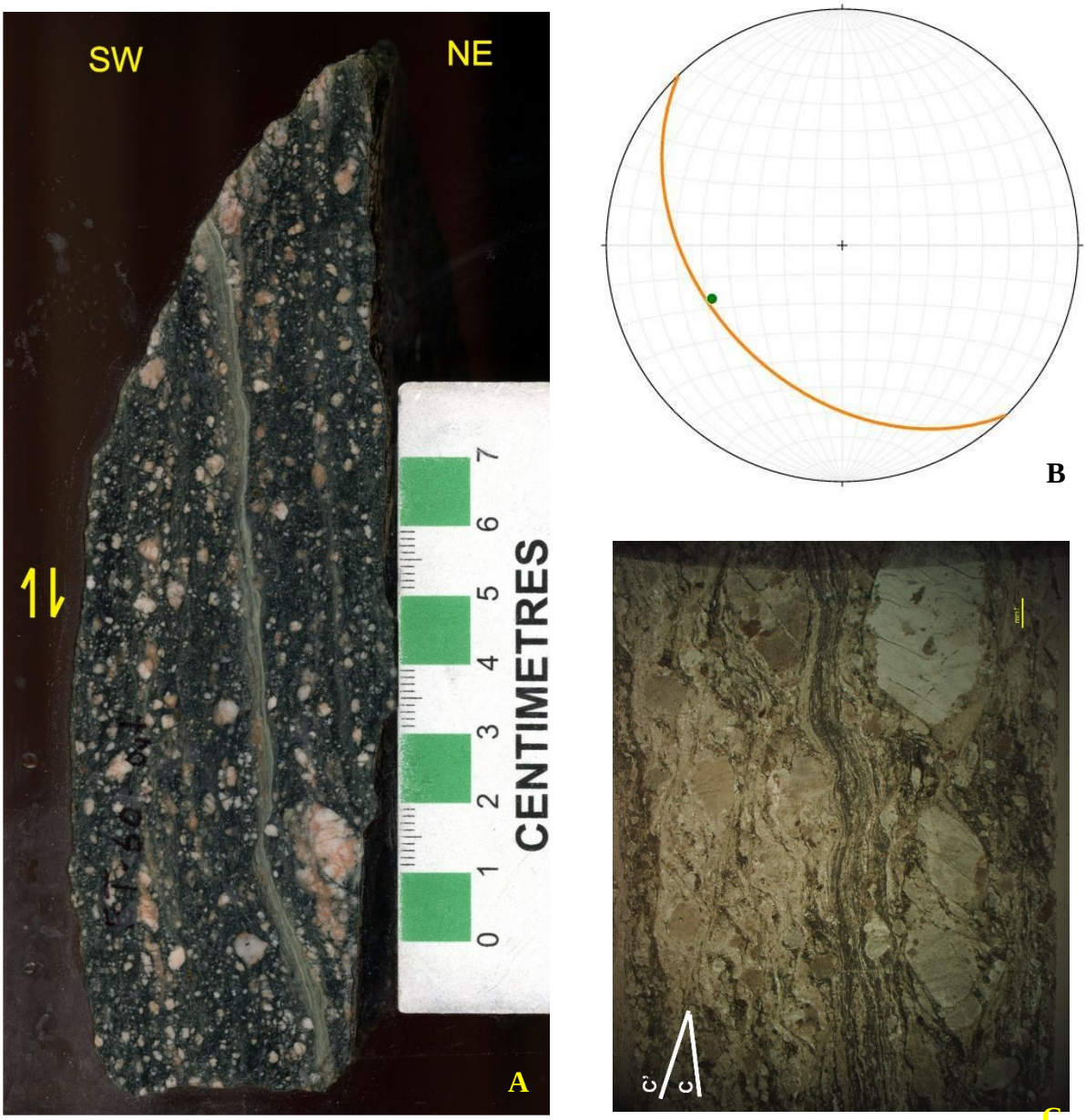

Figure 4-58. Evidence of reactivation of the S2 plane during D3 around Labyrinth Lake. (A) Hand sample of a blastomylonite with a C' shear in an epidote rich zone showing SW side up. (B) Stereonet of the outcrop from were the sample was collected. Plane is similar in orientation to the surrounding S2 planes, but lineation measured is similar in orientation to L3, indicating reactivation of S2 during D3. (C) Thin section with multiple C' shear showing the same SW side up movement.

A change in deformational character of the Black Bay Fault and adjacent region is observed between the Tazin River versus the Insula-Labyrinth Lakes areas for the D3 event. Though it is predominately ductile in both regions, the D3 fabric (S3) commonly occurs as mylonitic bands in the Tazin River area, while in the Insula-Labyrinth Lakes area S3 is found as broader mylonitic to gneissic sections. Additionally, whereas kinematic indicators around the Tazin River area were predominately crosscutting fabrics and pull-apart shears, the S3 fabrics around Labyrinth Lake contain more ductile indicators and well-developed C-C' fabric. The change in deformation style between areas, while remaining on the same side of the fault, is supportive of differential uplift having occurred along the Black Bay Fault during D3. With the development of the fault bend during D2, the increased uplift from the resulting restraining band (Mann and Gordon, 1996) during D3 could be the driver behind the observed differential uplift. Between the Insula-Labyrinth Lakes and Dymond Lakes areas, there is less of a difference in the style of the D3 deformation. However, surrounding Dymond Lake proper, there is a partial return towards the fabrics observed in the Tazin River area.

D4

A shift to brittle-ductile from purely ductile conditions occurred with the onset of D4. Dextral, brittle-ductile shears that trend parallel to the more well-defined S3 fabric are found close to the fault in all the study areas. Visible offset varies along these faults but offset over 1 meter are rarely noted. A conjugate, NW-SE-trending sinistral set of brittle-ductile faults is also present. Both shear sets decrease in frequency moving towards Labyrinth Lake from the Tazin River area. Around Dymond Lake, the amount of brittle-ductile to brittle ductile deformation increases significantly, with these structures becoming almost as pervasive as similar ones around Uranium City have been reported. The orientation of the D4 sinistral shears is similar to the D2 orientation, the D4 shears occur as discrete surfaces or zones whereas S2 fabrics occur as broadly deformed gneisses.

Some of the sinistral brittle-ductile shears appear to have acted as a conduit for a mafic dyke swarm in the Tazin River area (Figure 4-18). As the mafic dykes are found to be metamorphosed and foliated, it is possible that the shift from ductile to brittle-ductile deformation may have been gradual.

A clear brittle-ductile overprinting fabric is observed bounding the E-W-trending secondary fault at the southern end of Dymond Lake (Figure 4-40). Reactivation of this splay appears to have occurred during a D4 or later deformational event, possibly in association with late-stage uplift of the McCann domain or regional exhumation, and the E-W-trending structure was able to propagate further west. In addition to the sinistral movement along the fault, there is evidence of normal, southside down brittle-ductile movement in an associated mylonite that has been heavily hematized (Figure 4-59). A south side down component along the E-W-trending fault fits with the observed decrease in metamorphic grade on the southside of the fault.

Figure 4-59. vertical face of a hematized mylonitic fabric from Dymond Lake which is showing top to the left movement, indicating south-side down

Beyond the brittle-ductile faults, evidence of a final shift to a brittle regime, is indicated by two sets of faults containing breccias that trend E-W and N-S, respectively. The brittle fault sets intersect at a larger angle than the brittle-ductile system and is believed to be conjugate, which while contrary to what is expected with a shift from a ductile to brittle regime, is supported with the corresponding kinematics. In the Tazin River area and further south, the brittle faulting is quite pervasive and can be detected in aeromagnetic surveys. However, as with the brittle-ductile shearing, evidence of brittle deformation diminishes moving northward into the Insula-Labyrinth Lakes area and, also, disappears from the aeromagnetic signature.

The brittle-ductile to brittle faults/shears are commonly surrounded by alteration minerals (see 6. Mineralization), and suggest hydrothermal alteration was still on-going during D4.

5. Geochronology

5.1 Overview

In this section, new geochronological data is presented from samples collected during our field work. In addition to the new data presented, the results from a cpx-syenite which was dated by other GEM2 South Rae members are briefly discussed with a focus on the structural fabrics found within the syenite and which deformation event the syenite is associated with. In addition, a synthesis of the various published geochronological ages available in the surrounding region was compiled in order to better constrain the timing of the different deformation events associated with the Black Bay Fault.

5.2 Analytical methods

Two samples (15-DJ-468B and 15-DJ-476C) were collected in the Insula-Labyrinth Lakes area for U-Pb geochronological analysis during the 2015 field season in an attempt to constrain the timing of deformation and the development of the structural fabrics associated with the Black Bay Fault. Both samples were sent to Overburden Drilling Management in Ottawa for zircon separation via Electric Pulse Disaggregation. Following disaggregation of the sample, a heavy liquid separation was used to obtain a non-magnetic heavy mineral concentrate from which ~100 zircon from each sample were picked. The zircons were then sent to the Geological Survey of Canada in Ottawa where they were mounted on a 2.5 cm diameter epoxy puck along with zircon standards. Primary standard Z6266 with an $^{206}Pb/^{238}U$ age of 559 Ma and secondary standard Z1242 with a $^{207}Pb/^{206}Pb$ age of 2679.7 Ma were used. Mounts were polished down to the midpoint using 9, 6 and 1µm sized diamond compound and back-scattered electron detector images were taken of the zircons using a MIRA3 TESCAN scanning Electron Microscope. Uranium- lead geochronology of the zircons was done at the Geological Survey of Canada using the Sensitive High-Resolution Ion Microprobe (SHRIMP) situated in the J.C Roddick Ion Microprobe facility in Ottawa and was done using the procedures described by Stern (1997) and Stern and Amelin (2003) . Zircons were analyzed using a $^{16}O^-$ primary beam which produced a 20µm spot size with a primary and secondary standard analyzed after every five analyses of the unknown. A common lead correction of 1.003 was applied to the result based on Stern (1997). Analytical data are given in Table A-1,Table A-2. Concordia plots and weighted average ages were calculated using Isoplot version 4.15 (Ludwig, 2009). Weighted average mean plots were

calculated using the $^{207}Pb/^{206}Pb$ system to the older age of the zircons (Ludwig, 1998). The Th/U and Hf/Yb ratios are provided for reference in the Appendix

5.3 Sample 15-DJ-468B

Sample 15-DJ-468B was collected from a non-magnetic, aplitic granitic dyke (biotite, quartz, K-feldspar) to the south of Labyrinth Lake by Labyrinth Rapids on the western side of the fault in the McCann domain. The outcrop was within 250 m of the inferred trace of the Black Bay Fault and domain boundary. The dyke contains a weak S3 foliation and crosscuts a highly deformed blue-quartz monzonitic to granodioritic gneiss that contains an older S1 gneissosity. The dyke shows boudinage necking and has been Z-folded (Figure 5-1). It is interpreted to have been emplaced during the dextral D3 event and the sample was collected in order to produce an age for the D3 event.

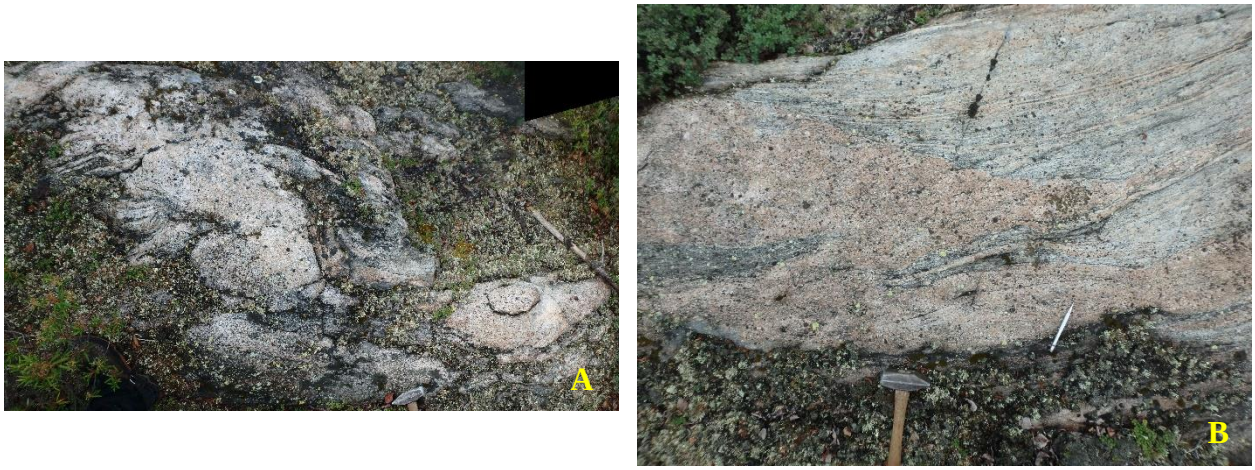

Figure 5-1. (A) Granitic dyke from which sample 468B was collected for geochronological dating. (B) Continuation of the granitic dyke elsewhere in the outcrop which shows the dyke having been Z-folded and boudinaged, indicating syn-tectonic emplacement with D3

Over 500 zircons, ranging in size between 75 and 750 µm, were recovered from the sample. Two distinct zircon populations are observed through the backscatter images, a larger, more rounded zircon population (Figure 5-2, #113) and another population containing smaller, more prismatic zircons (Figure 5-2, #112). The older, rounded zircons occasionally contain rims. However, these rims were too small to be analysed.

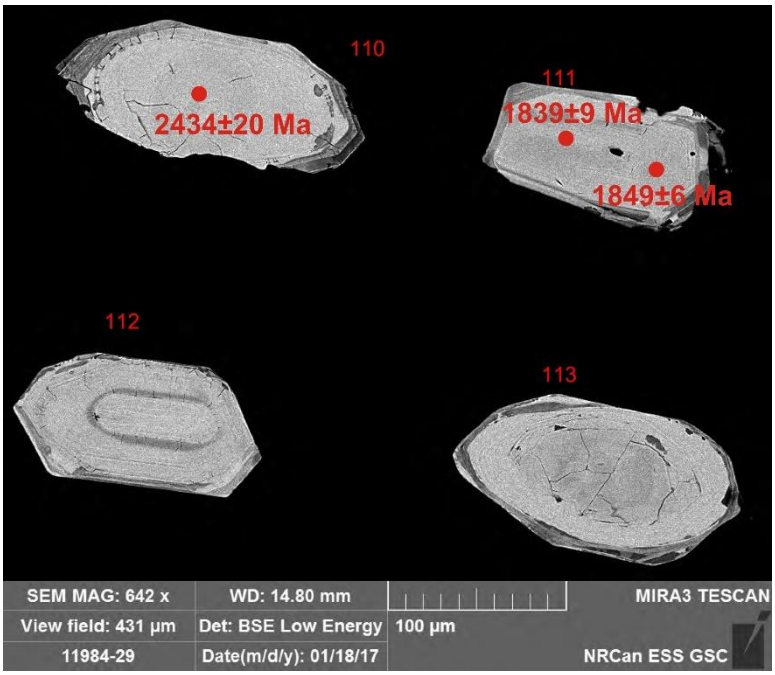

Figure 5-2. Examples of the zircon grains collected from sample 468B. Zircons 111 and 112 are more prismatic and are interpreted to have grown during crystallization of the dyke. Zircon 110 is more rounded and older and represents inherited zircons from the host rock

115 zircons were mounted, and 34 spots were analysed on 33 zircons. 7 spots were excluded in our analysis due to those having a larger % discordance compared to the rest of the spots. The analytical results roughly define a Discordia line with an upper intercept at 2581± 56 Ma and a lower intercept at 1881± 96 Ma (Figure 5-4). The concordia diagram shows two distinct zircon populations, a younger tightly clustered population at ~1850 Ma from 6 spots and an older, more disperse population ranging from ~2300 to ~2700 Ma from the remaining spots. The younger zircon population (a total of 6 analyses) yields a weighted mean age of 1844.4 ± 2.1 Ma (Figure 5-3). The older zircon population was too spread out to provide a distinct age. The two age populations are found to correlate well with the two morphological zircon groupings observed. The smaller, more prismatic zircons, (i.e. zircons # 111; Figure 5-2) are found to contain younger ages while, larger and more rounder population correlate with the older age group (i.e. zircon #110 Figure 5-2). Based upon the shapes and ages of the zircons, the younger age of 1844.4 ± 2.1 Ma is interpreted to represent the crystallization age of the dyke whereas the older zircons are likely inherited from the surrounding host rock and record earlier igneous and potentially metamorphic events.

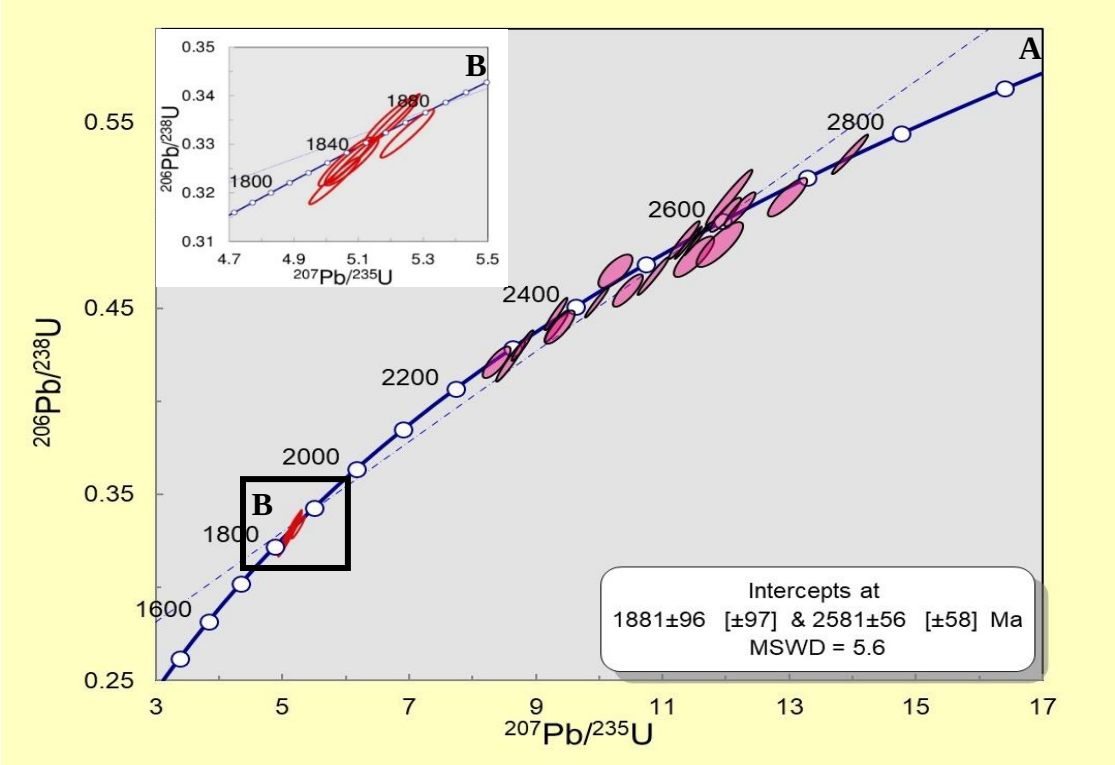

Figure 5-4. (A) Concordia diagram for sample 468. Two separate zircon populations are present, with a younger tight cluster at ~1850 Ma (red) and an older more disperse population ranging from ~2300 to ~2700 Ma (pink). (B) Blown-up concordia diagram of the younger age population.

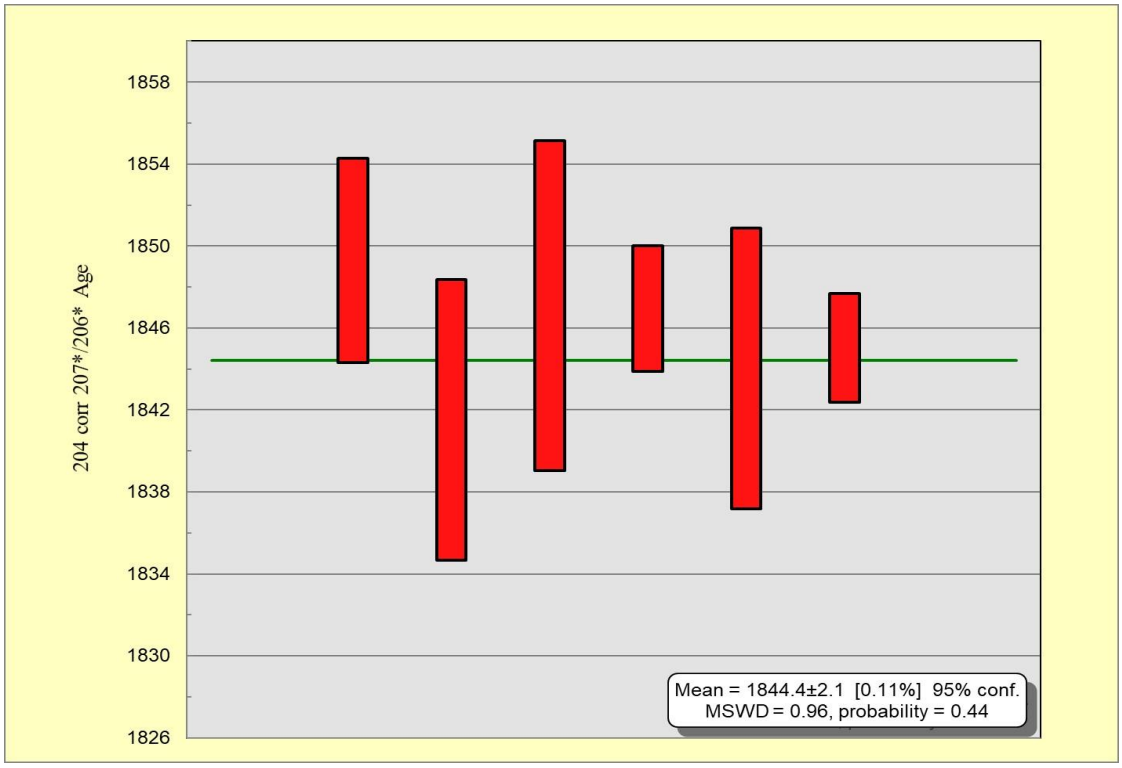

Figure 5-3. Weighted average mean plot of the younger zircon population representing the age of crystallization of the dyke

5.4 Sample 15-DJ-476C

Sample 15-DJ-476C was collected from a strongly deformed augen granodioritic gneiss (biotite, hornblende, quartz, plagioclase, K-feldspar) with well developed gneissosity and strong lineation (Figure 5-5). The sample was collected in the McCann domain, from the southern end of Insula Lake, but to the east of a more highly deformed straight gneiss to mylonitized rock. Due to the less severe deformation at the sample location, older fabrics are possibly preserved in this sample. A weak sinistral C-S fabric was observed in the granodioritic gneiss at an outcrop slightly further to the south. The fabric of the gneiss here appears to be an S1 fabric which has been transposed into an S2 orientation. The gneiss was cut by a very weakly foliated aplitic granite, similar in composition to the dyke sampled for geochronological analysis (sample 15-DJ-468 described above). The host rock of the dated dyke is also similar in composition and fabric to the 15-DJ-476C sample and is likely from the same lithological unit. This sample was collected in the hopes of producing better time constraints on the D1 deformation event.

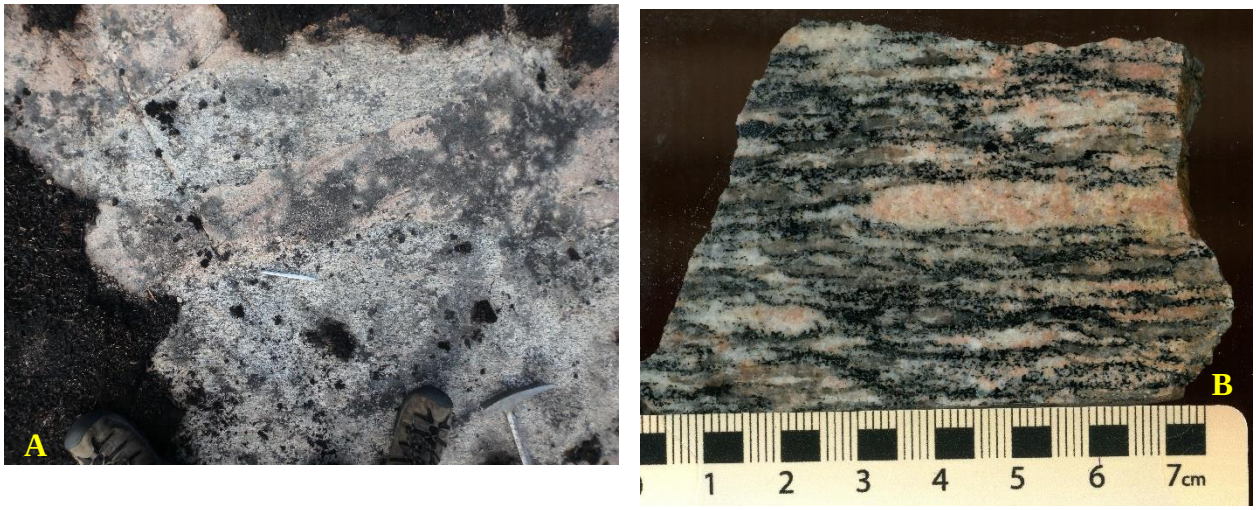

Figure 5-5. Outcrop from which sample 476C was collected for geochronological dating. (A) Orthogneiss is cut by weakly deformed granitic intrusions. (B) Hand sample of the dated orthogneiss showing the well-developed fabric and elongated to augen feldspar (B).

Sample 15-DJ-476C was rich in zircons with over 1000 grains recovered during separation, ranging in size from 50 to 250 µm. Morphologically, all of the zircons are very similar and quite rounded. In many of the zircons, the back-scattered electron images show prismatic cores which are surrounded by rounded rims (Figure 5-6 A).

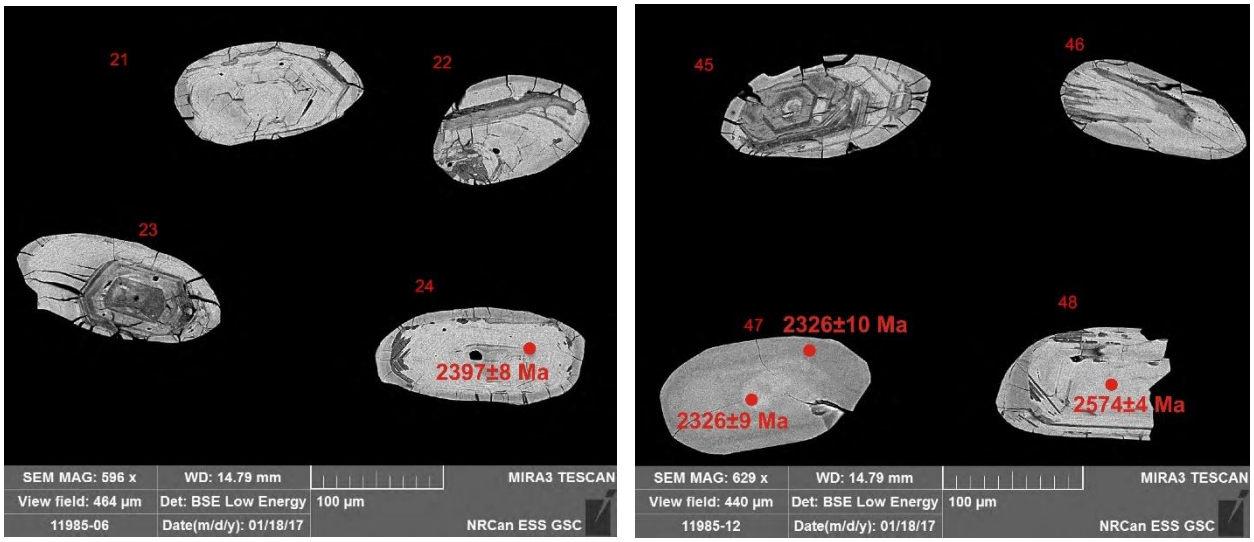

Figure 5-6. Back-scattered images of representative zircons from sample 476C. Zircons are morphologically similar, with rounded rims and prismatic cores.

119 zircons were mounted and imaged from which 36 spots were analysed from 32 zircons with the SHRIMP. 4 spots were excluded from our calculations due to an elevated % discordance. A loosely defined Discordia line for the data has an upper intercept age of 2615 ± 57 Ma and a lower intercept age of 1866 ± 170 Ma (Figure 5-7)

Two separate age populations lie on the concordia line, an older population at ~2550 Ma and a younger population at ~2350 Ma with a spread of ages beneath the concordia line in-between the two groupings (Figure 5-7). The three most concordant data from the younger population give a weighted mean age of 2330.4 ± 5 Ma, but the probability of fit is quite low and this age is only used as reference. The ages of the older zircon population is more variable, with a larger spread. A weighted mean age of 2588.9 ±8.6 Ma is obtained when rejecting the ages with larger absolute age errors, but the probability of fit remains very low.

Both the cores and rims were analysed, with the cores producing the older ~2589 Ma ages (Figure 5-6 B) while the rims produced the ~2330 Ma ages (Figure 5-6 B), as is expected. While the younger intercept age (1866 ± 170 Ma) does loosely correlate with the known Snowbird and Trans-Hudson orogenies (discussed in Chapter 2), the large age uncertainty and the large range where the zircons plot likely negate the usefulness of this age.

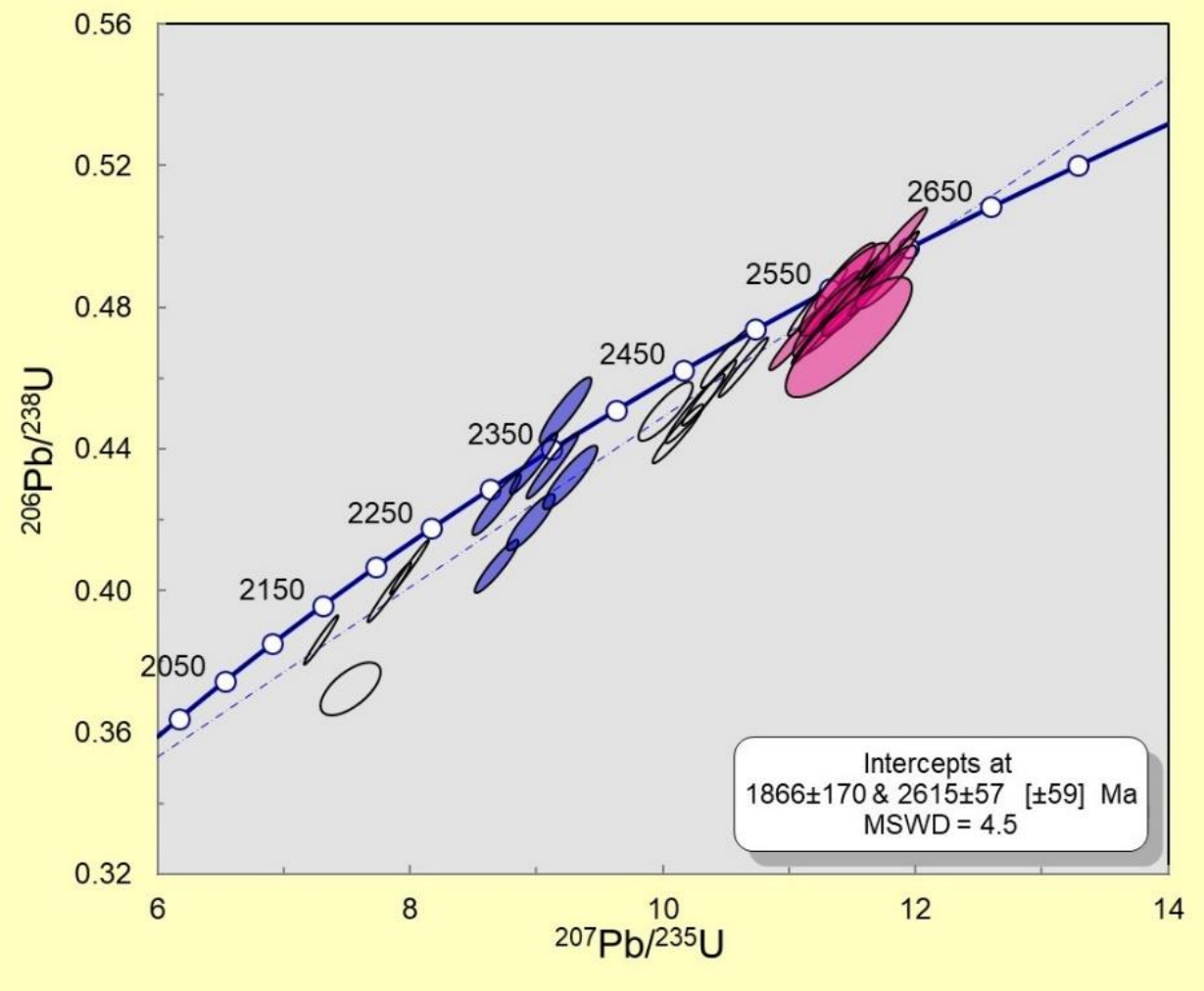

Figure 5-7. Concordia plot of the zircon U-Pb data for sample 476C. Two zircon populations can be observed to fall along the concordia line with an older cluster at ~2550 Ma (magenta) and a younger cluster at ~2350 Ma (blue)

5.5 Gemelo Rare-Earth Element Showing

A large cpx-rich syenitic intrusion is present along the eastern arm of Labyrinth Lake in the Firedrake domain (Figure 4-1). This area is of interest because of its economic potential, the syenite contains rare-earth element mineralization (Acosta-Góngora et al., 2017). (see 6.3 Insula-Labyrinth Lakes). Deformation of the syenite varies, but overall the intrusion contains a weak to moderate NE-SW striking foliation (055/80) (Figure 5-8). While no kinematic indicators were noted in the outcrop, the orientation of the fabric resembled the S3 fabric observed further to the west and closer to the Black Bay Fault. Surrounding the syenite are more strongly deformed migmatitic Firedrake gneisses that contain gneissic fabrics orientated NW-SE, possibly belonging to S2.

In an attempt to constrain the timing of mineralization, a sample of the Gemelo syenite (15-PA-390) was collected for U-Pb dating. Pehrsson et al. (2016) reported a crystallization age of 1829 ± 4 Ma for this sample. Based on the relatively weak deformational fabric in the syenite, the Gemelo syenite is inferred to have been emplaced syn-tectonically during D3. This is further supported with the mineralization which is aligned with the S3 foliation (Figure 5-8), and believed to be magmatic in origin (Acosta-Góngora et al., 2017).

Figure 5-8. Outcrop photos of the Gemelo syenite. The syenite contains a weak to moderate NE-SW foliation along which mineralization is also orientated.

5.6 Available Geochronological data from the surrounding area

In addition to the specific samples collected for geochronology during the structural investigation of the Black Bay Fault, samples for geochronology from the broader GEM2 South Rae project area were collected during 2015 and 2016 and analysed by Regis et al. (2017) at the GSC. In addition, Davis et al. (2015) analysed geochronology samples collected from a 2012 transect of the South Rae area, and Berman et al. (2013) analysed archival metasedimentary rocks collected during the 1950's mapping projects of the southern Rae. Beyond the GEM2 South Rae project area in the Northwest Territories, limited geochronology studies from regions bordering the Black Bay Fault have been completed on rocks in the Uranium City area in Saskatchewan, with a significant number of results from both the Zemlak and Beaverlodge domains. The ages reported in the region are a mix of SHRIMP, TIMS and some Laser Ablation from zircon, monazite and baddeleyite and are primarily used to provide a general regional picture of the ages present in the different domains to further the discussion on the various the deformations events which impacted the Black Bay Fault. The compilation is comprised from the reported $^{207}Pb/^{206}Pb$ ages.

Although these geochronological data are not correlated with any specific Black Bay Fault fabrics, they do offer broad insight into the timing of the different deformation and metamorphic events which impacted the southern Rae. Furthermore, because we did not collect any geochronological samples from Ena domain during our field seasons, the data from the corresponding Zemlack domain offers the best proxy for understanding the history of the correlative Ena domain.

Through all the domains that border the Black Bay Fault, except the Beaverlodge domain just north of Lake Athabasca, Neoarchean crystallization ages ranging from ~2550 Ma up to ~2700

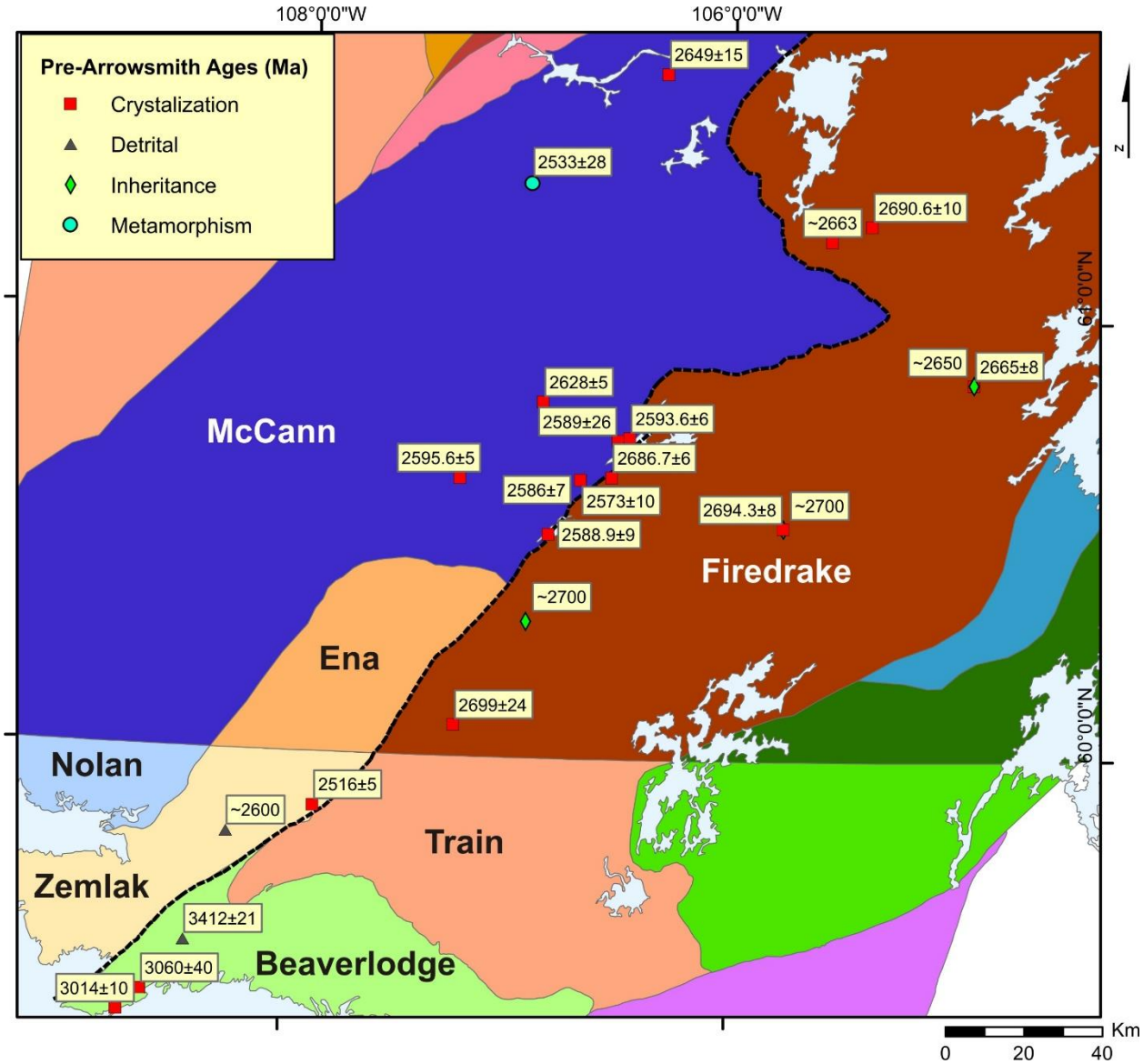

Figure 5-9. Domain map of the Black Bay Fault area showing the various Pre-Arrowsmith, Archean U-Pb ages and their types reported in the area. Archean ages are found in all domains adjacent to the Black Bay Fault. See Table A-3 for age data sources.

Ma are found (Figure 5-9). The age range remains valid across the Black Bay Fault for the McCann and Firedrake domains which both contain similar crystallization ages, although the ages found in the Firedrake domain are slightly older than those reported for the McCann domain. The sampled rocks comprise the majority of the basement rock of the South Rae, providing a representative suite of the area. Differentiating itself from the other domains, the Beaverlodge domain contains ~3000 Ma crystallization ages and detrital ages older than ~3400 Ma.

Evidence of the 2.5 to 2.3 Ga Arrowsmith orogeny was previously identified in the Beaverlodge domain (Hartlaub et al., 2007), but in the other domains bounding the Black Bay Fault, signs of the Arrowsmith orogeny was previously poorly constrained (Figure 5-10). Arrowsmith ages have been noted in the McCann domain (Berman et al., 2013; Davis et al., 2015), but these studies do not give clear evidence whether or not the Firedrake domain also contains evidence of the Arrowsmith event. This is due, in part, to the fact that position of the Black Bay Fault relied predominately on the aeromagnetic surveys prior to this study. Consequently archival samples and those collected via the 2012 traverse close to the fault could not be confidently placed into their respective domains. However, with a more refined fault location, in particular around Labyrinth Lake, a compilation of the Arrowsmith ages in the region confirms a lack of 2.5-2.3 Ma ages in the Firedrake domain samples (Figure 5-10). In particular, the augen granodioritic gneiss collected for this study just west of the fault in the McCann Domain and discussed earlier (Sample 15-DJ-476C), provides additional support that while evidence of the Arrowsmith Orogeny is found near to the Black Bay Fault, it does not cross over into the Firedrake domain.

Evidence of post-Arrowsmith magmatism and metamorphism is abundant throughout all the domains, as shown in Figure 5-11. The majority of the ages reported in the South Rae study area range from 1850-1830 Ma (Figure 5-11), including the Z-folded dyke dated in this study (section 5.3). However, there is a significant difference in the post-Arrowsmith ages found around Uranium City (Figure 5-12) compared to the NWT data. Specifically, samples producing ages in the 1850-1830 Ma range (Figure 5-11) are rare in Saskatchewan. Instead an older age range, 1930-1910 Ma, is reported from numerous samples around Uranium City from both sides of the Black Bay Fault.

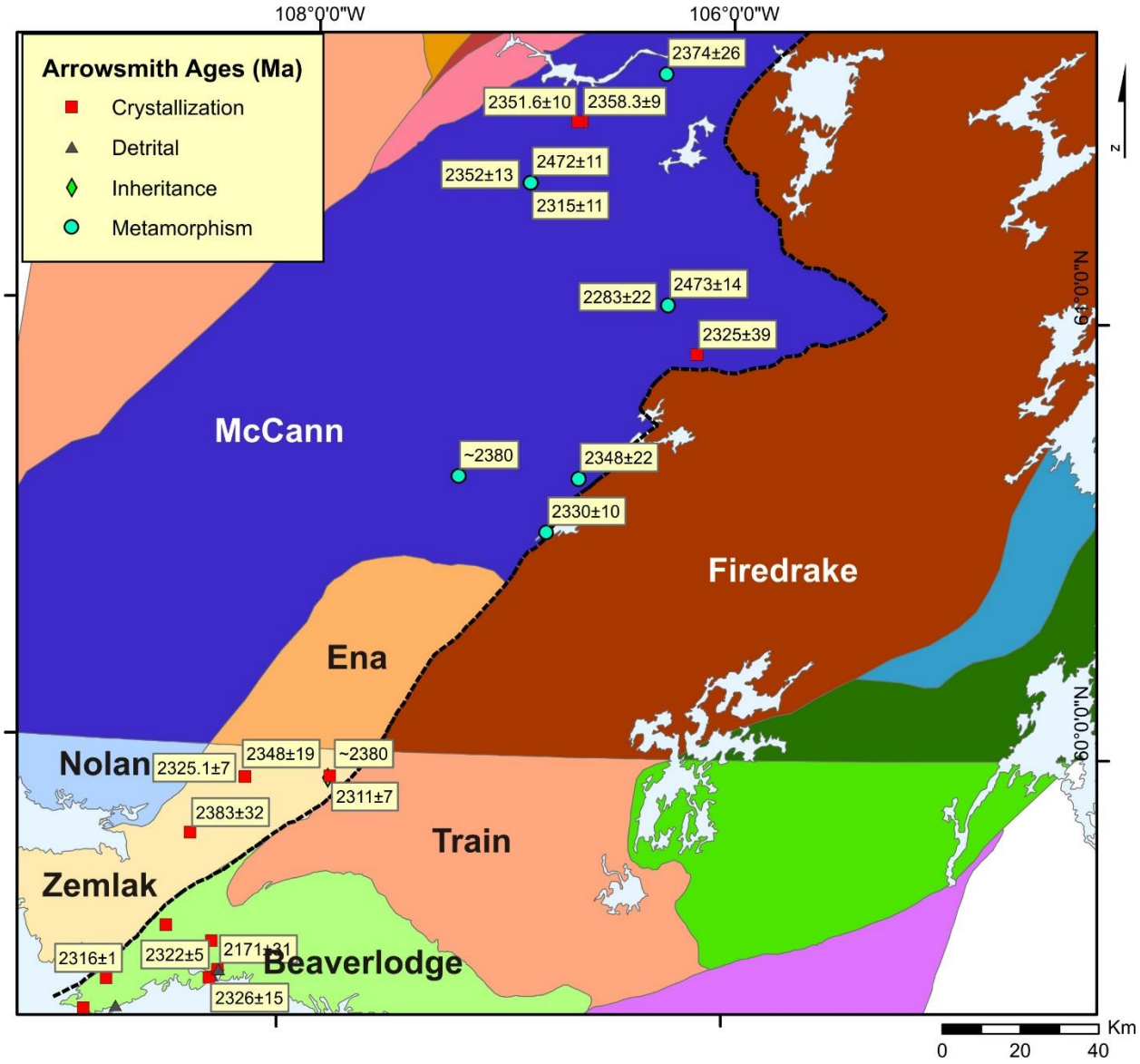

Figure 5-10. Domain Map of the Black Bay Fault area with the various Arrowsmith ages reported in the area. Note that the Firedrake/Train domain does not contain any Arrowsmith ages. See Table A-4 for age data sources.

The older ages in the Beaverlodge domain may not be comparable, as this domain had a different metamorphic history than the other domains. The majority of the Beaverlodge domain underwent retrogression to greenschist grade facies including in the region adjacent to the fault while the Black Bay Fault was active (Ashton et al., 2001) This lower grade metamorphism may not have recorded the age of the later deformation events which would have not been conducive towards the growth of garnet and the corresponding monazite inclusions which was the mineral dated for many of the Beaverlodge domain ages ((Bethune et al., 2013) .

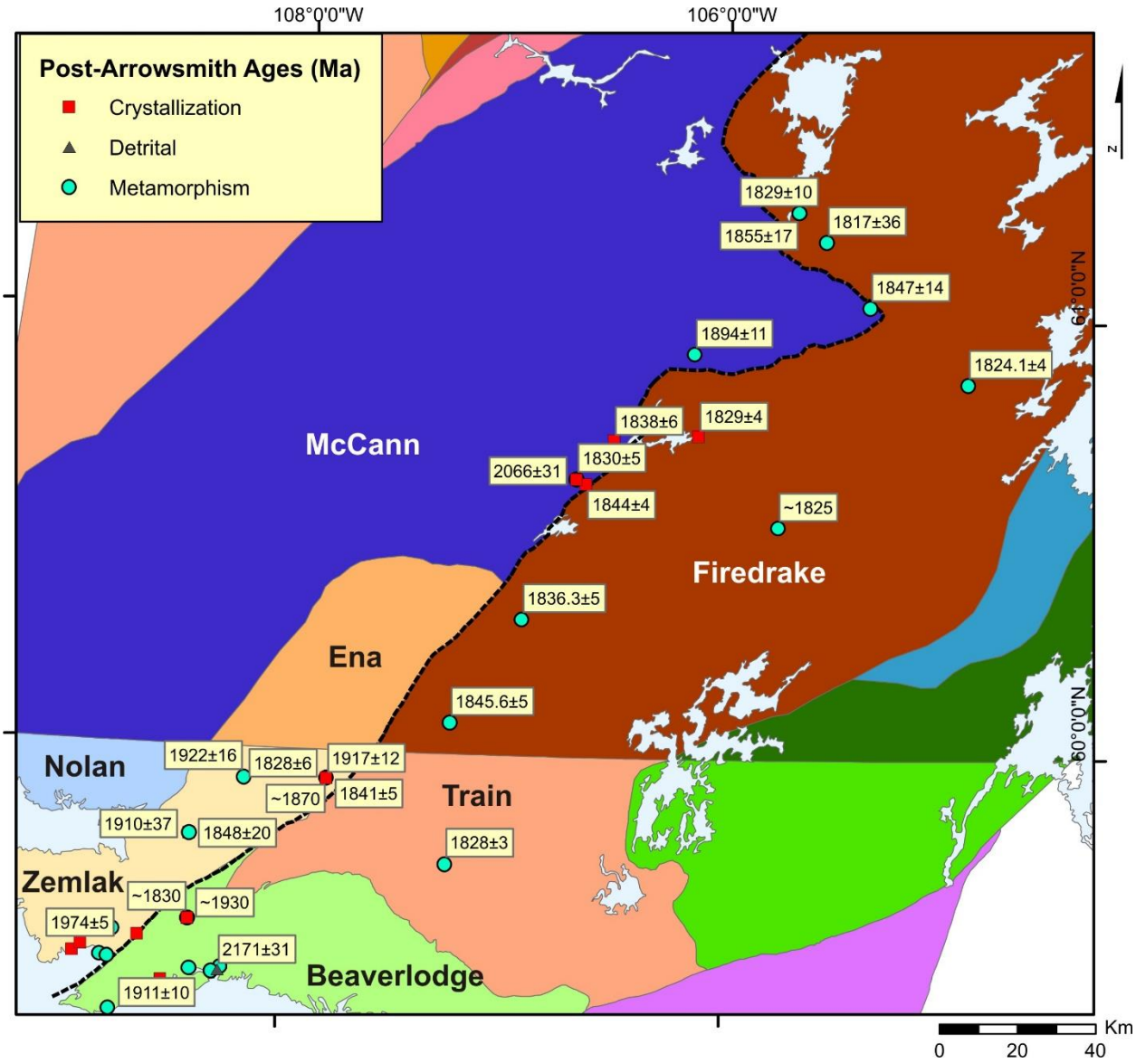

Figure 5-11. Domain map of the Black Bay Fault area showing the reported Post-Arrowsmith U-Pb ages. See enlarged area of the Uranium City area (Red) in Figure 5-12 for a complete view of the ages reported there. Data source of ages in Table A-5

The reason for the age discrepancy in the Zemlak domain is less clear. It should be noted that several of the younger ages in the Zemlak domain are predominately from the Hoidas and Bear Lake rare-earth element deposits, using monazite, titanite and apatite rather than zircon (Table A-5), and they may be recording hydrothermal fluid activity in the area (Normand, 2014). By comparison, the younger ages from the south Rae study area are predominately from zircon.

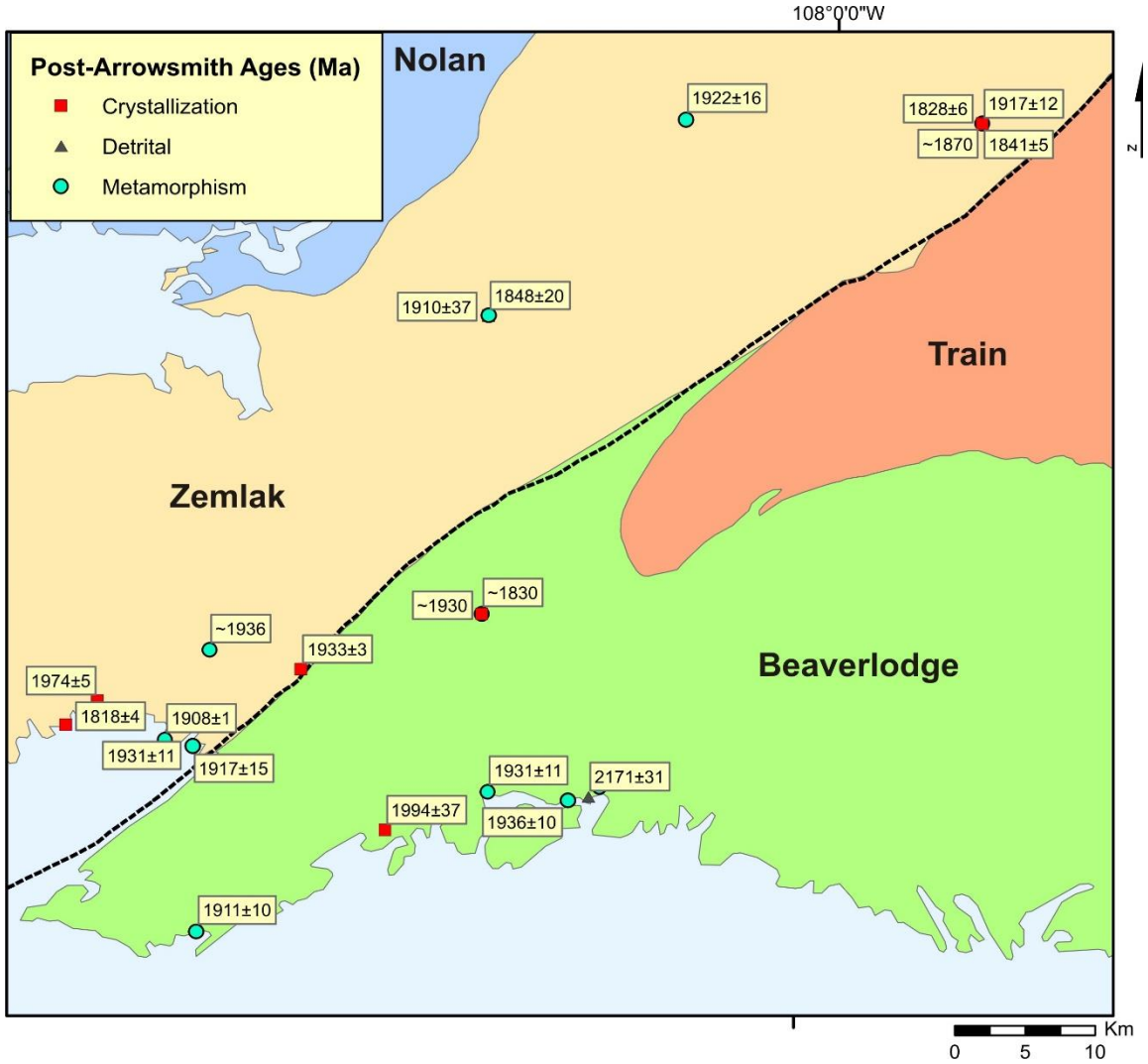

Figure 5-12. Enlarged area of the Uranium City area showing the post-Arrowsmith ages reported in the area. See Table A-5 for age data sources.

Some attempts to correlate the Saskatchewan geochronology results with the development of the various Black Bay Fault deformational fabrics have been attempted in previous studies (i.e. Bethune et al., 2013; Morelli et al., 2009; Shiels et al., 2016). In northern Saskatchewan, a persistent east-west regional fabric is observed outside of the shear zone on both sides of the fault (Zemlak and Beaverlodge) which is then overprinted by the NE-SW fabric within the shear zone (Ashton et al., 2001). Towards the western edge of the Zemlak, outside of the area impacted by the Black Bay Fault, a leucogranite dated at 1.93 Ga is crosscut by the east-west fabric, which has been assumed to indicate that fabrics associated with the Black Bay Fault did not develop until later (Ashton et al., 2009). More recently, work done in the middle of the Beaverlodge domain by Bethune et al. (2013) with in-situ dating of monazite grains which co-crystallized

with garnets indicates that peak metamorphism in that domain occurred at 1.94-1.93 Ga with the development of an east-west fabric and that the development of the Black Bay Fault and onset of dextral transpression occurred at 1.91-1.90 Ga. Similar 1.93 Ga and 1.91 Ga monazite ages were found in a psammite collected from Bushell Inlet, which is adjacent to the Black Bay Fault in the Zemlak domain (Shiels et al., 2016). These studies appear to indicate that the Snowbird orogeny is likely the primary tectonic driver behind the Black Bay Fault (Ashton et al., 2009) while the east-west fabric occurred during the Taltson-Thelon orogeny (Bethune et al., 2013)

One study by Dieng et al. (2013) who examined the uranium mineralization at the Cinch Lake deposit, situated south of Uranium City adjacent to the Black Bay Fault on the west side of the fault, attempted to build a genetic model for the mineralization. The study attempted to tie fault movement and timing of deformation to uraninite ages present, producing a complicated and lengthy fault history. Their model has the Black Bay Fault and the other surrounding fault developing and undergoing deformation as early as 2.33 Ga (Dieng et al., 2013). These fault systems are shown to be east-dipping and listric, and they suggest the region initially experienced brittle-ductile dextral transtension followed by ductile folding and thrusting, then brittle-ductile thrusting and then a return to extensional brittle movement (Dieng et al., 2013). However, very little structural evidence or discussion is presented. Their model is primarily based upon work from the 1960's and 1970's and is contradicted by the more modern studies of the area (i.e. Ashton et al., 2013, 2001; Bethune et al., 2010) as well as our observations further north. Furthermore, at Cinch Lake, a well-developed NW-dipping mylonitic fabric with a SW-plunging stretch lineation, consistent with D3, was observed during our re-visit of the Uranium City area; this does not fit with their model.

5.7 Timing Implications

Although numerous samples yielding Arrowsmith ages (~2.3 Ga) are found in all domains west of the Black Bay Fault and, also, east of the fault in the Beaverlodge domain, this age range is conspicuously absent in the Firedrake domain (Figure 5-10). Due to this lack of Arrowsmith ages in the Firedrake domain, it is assumed that D1 and the development of the S1 fabric is not associated with the Arrowsmith orogeny and, further, that development of the Black Bay Fault post-dates this event.

The broadly distributed “pre-S1” fabrics observed in all domains provides a tentative older age limit for the Black Bay Fault development. The pre-S1 fabrics that we identified in the Ena domain in our study area (based upon orientations and overprinting fabrics) are similar in distribution and orientation to the E-W fabric observed in the Zemlak and Beaverlodge domains in Saskatchewan. Due to the similarities in orientation, the pre-S1 fabric observed in the McCann domain is likely the same. If we assume they are, in fact, the same fabric, then the 1.94-1.93 Ga age (Taltson-Thelon orogeny) established for these fabrics in Saskatchewan (Bethune et al., 2013) could be considered to be an older age limit for initiation of the Black Bay Fault.

Explaining the post-Taltson-Thelon age differences between Saskatchewan and our study area in the Northwest Territory is complicated (Figure 5-11), although the change in deformation style encountered between our two focus areas, and the continuing style change into Uranium City may provide insight into the discrepancy. Our D1 and D2 deformation events have not been identified in the prior structural investigations of the Black Bay Fault around Uranium City. Instead, our D3 dextral transpressional event seems to correlate with the primary event noted there. One possible exception come from the work done by Normand et al. (2009) around Hoidas Lake, who noted a change in fold vergence and lineations from NE to SW, although no sinistral kinematic indicators were noted.

The ages associated with a NE-SW-trending ductile fabric in the Uranium City area have been assumed to correlate solely with dextral transpression along the Black Bay Fault. Though reasonable, this may be an incorrect assumption, as noted in some of the Saskatchewan studies (ie. Bethune et al., 2010; Normand, 2014). The current timing interpretation of ductile dextral motion in Saskatchewan stems primarily from an assumed lack of younger metamorphic ages in the Train domain in conjunction with the older ages from the Uranium City area (Ashton et al., 2009). However, the new ages found in the South Rae as part of the larger mapping project clearly show an abundance of ~1.83 Ga metamorphic and crystallization ages in both the McCann domain and in the Firedrake (Train) domain (Figure 5-11), thus invalidating one of the noted assumptions.

Based upon the age from our Z-folded dyke (15-DJ-468) along with the Gemelo age and other similar ages in the surrounding area, our D3 deformation event appears to have had commenced by 1844 Ma and have lasted until at least 1830 Ma. However, it seems unlikely that the D3 event

begun at 1910 Ma, as has been suggested from the Saskatchewan studies, due to the time length and given the lack of more ages in between. Instead, the later D3 age appears to have not been as well recorded in the Uranium City area due to a change in deformational styles.

In particular, the outcrop from which the meta-psammite dated at 1.93 Ga and 1.91 Ga and associated with dextral movement by Shiels et al. (2016) was visited during our brief re-examination of the Uranium City area. While dextral kinematics are clearly visible within the sheared and boudinaged felsic layers, a significant amount of quartz is present (Figure 5-13) and the deformation style appears to be more brittle-ductile than the clearly ductile deformation observed in our Northwest Territories study areas. Consequently, while the dextral fabrics are clearly visible in the outcrop, the metamorphic grade of this deformation may not have been high enough to promote the monazite growth in garnet and record the event. The older ages found around Uranium City may instead be correlated with our D1 event and development of the older NNE-SSW S1 fabric, with the older fabric masked by the younger D3 event.

Figure 5-13. Meta-psammite with dextral shear bands. Outcrop is located in the Bushell Inlet in the Zemlak domain. Significant amount of quartz-infilling present. This same outcrop was dated (1.93 & 1.91 Ga) by Shiels et al., (2016).

6. Mineralization

6.1 Introduction

While not a primary aspect of our study of the Black Bay Fault, the spatial association of mineralization with the Black Bay Fault and whether any structural controls appeared to be present was investigated as a minor portion of the study. Around the Black Bay Fault in the Uranium City area, multiple vein type uranium deposits and showings are present and the Black Bay Fault is believed to have acted as channel for hydrothermal fluids and controlled uranium mineralization (Bergeron, 2001). Beyond uranium mineralization, the Hoidas Lake and Bear Lake rare-earth element deposits are found in the Zemlak domain and associated with secondary faults off the Black Bay Fault (Halpin, 2010). The Hoidas Lake deposit in particular has a resource estimate of 2 560 835 tons with a grade of 2.027% of total rare-earth oxides (Normand, 2014), and veins enriched up to 32.9% total rare-earth oxides are present (Pandur et al., 2014). The mineralization is primarily contained in allanite veins and apatite breccias and believed to hydrothermal in origin from a magmatic source (Halpin, 2010). While a number of deposits are present in Saskatchewan, whether the fault-associated mineralization continues along the Black Bay Fault into NWT has never been examined prior to the GEM2 South Rae project.

6.2 Tazin River

In the Tazin River area, particularly around our fly camp, significant hydrothermal alteration is present, with potassic alteration and epidotization frequently observed. While no apatite breccias like those found in the Hoidas area were discovered during our transects of the Tazin River area, similar hydrothermal alteration and other mineralization similar to the Hoidas deposit are present in the Ena domain. Mylonitic to brittle-ductile shears oriented parallel to the S3/S4 fabric with indications of containing allanite (dark red staining surrounding black crystals) were found (Figure 6-1 A) though never sampled or measured with a scintillometer. Elsewhere small 4cm-wide diopside-allanite veins trending sub-parallel to the Black Bay Fault (Figure 6-1 B) surrounded by altered mafic xenoliths were observed, possibly indicating the presence of a rare-earth element occurrence in the vicinity.

Beyond hints of rare-earth element mineralization, multiple radiometric anomalies were recorded within the Ena domain (informally named Sarita, Hidden and Triple-X), with scintillometer readings ranging from 1800 counts per second at some of the anomalies up to 11000 counts per

second in one location for the combined K, Th and U band (Figure 6-1 C). In comparison, the background readings in the area range from 150 counts per second up to 800 counts per second in locations with syenite intrusions and pegmatites. The anomalies are generally heavily weathered and buried beneath vegetation, though the 11000 counts per second anomaly could be loosely traced for around 300 meters (Figure 6-1 D, E). In general, the anomalies appear to follow the S4 brittle-ductile to brittle fractures (Figure 6-1 F) and were primarily found within 100 meters of the Tazin River and the Black Bay Fault trace. Some elevated readings were found further back from the river along what appear to be smaller D3 fault splays, trending sub-parallel to the Black Bay Fault. As part of the larger mapping project, samples for geochemistry were collected from the anomalies, but they did not contain statistically significant elevation concentrations of uranium, thorium, potassium nor in rare-earth elements (Acosta-Góngora et al., 2018). However, the anomalies were difficult to sample, and only very weathered samples were collected, and it is likely that we were unable to collect proper samples of the mineralization.

Figure 6-1. Examples of the different mineralization anomality observed in the Tazin River area. The majority of the alteration and mineralized veins are found to trend sub-parallel to S3 and the Black Bay Fault. (A) Small mineralized fracture with dark red staining, found to be an indicator for allanite in the Ena domain. (B) Vein comprised of diopside-allanite striking NE-SW. (C, D and E) Sarita anomaly trending NE-SW and extending over 200m with cps of over 11000 recorded, found within close proximity to the Black Bay Fault. (F) Triple-X anomaly also containing mineralization-oriented NE-SW.

6.3 Insula-Labyrinth Lakes

Compared to the Tazin River area, hydrothermal alteration was less prevalent in the Insula-Labyrinth Lakes area, with the difference especially pronounced in the McCann domain versus the Ena domain to the south. Alterations were primarily found where reactivation of the S2 fabric during D3 occurred with epidotization along with the presence of some oxides (**Error! R eference source not found.**). One exception was the pyroxenite unit found in the McCann domain, close to the Black Bay Fault. Rusty coloured patches, possibly indicative of sulphides, were prevalent throughout the unit, with an increase where sheared leucosome were found adjacent (Figure 6-2 A). The increased shearing surrounding the leucosome may have provided a conduit or a source for the mineralization fluid. Data from the lake sediment survey of the 75B NTS map sheet completed during the 2015 field season as part of the GEM2 South Rae project show elevated Ag and Zn in two lakes found down ice from a larger outcrop of the pyroxenite (McCurdy et al., 2016), supporting our assumption of possible sulphides in the pyroxenite.

Beyond possible sulphides and minor hydrothermal alteration, the Insula and Labyrinth Lake area contains the largest rare-earth element showing that we discovered in the South Rae mapping area. Near the eastern arm of Labyrinth Lake in the Firedrake domain, a large moderately to weakly deformed clinopyroxene-syenite intrusion was discovered, referred to as the Gemelo syenite ("Twin" in reference to Hoidas) (Figure 4-1). The syenite body is around 10 km east of the Black Bay Fault. Bands and veins rich in clinopyroxene accompanied by dark-red staining, indicating the presence of allanite, were initially noted. Additionally scintillometer reading of up to 1362 counts per second are reported (Acosta-Góngora et al., 2018). While the radiation anomaly with the Gemelo syenite is not as large compared to those found in the Tazin River area or around Hoidas, these readings were still elevated compared to the surrounding migmatitic gneiss of the Firedrake domain which produced readings of around 200 counts per second. Initially discovered at the end of the 2015 field season, the Gemelo syenite was revisited during the 2016 field season to better delineate the size of the intrusion and further investigate its rare-earth element potential.

Further investigation revealed that the clinopyroxene in the Gemelo syenite is primarily diopside, with magnetite and some hyalophane alteration (Figure 6-2). The Gemelo syenite also contains hyalophane-rich layers and band. Crosscutting hyalophane-bearing quartz-syenite pegmatite

dykes ae also present. In areas where the intrusion is more of a quartz-syenite, the quartz is dark smoky grey, indicating radiation damage.

Samples for assay were collected from the Gemelo region from locations with visible mineralization and elevated counts per second. A 2015 sample of clinopyroxene-magnetite-hyalophane-allanite segregations and veins produced rare-earth element concentrations of >0.97% (Ce = 4750 ppm + La = 2270ppm + Nd = 2230 ppm) (Figure 6-2 B) (Acosta-Góngora et al., 2017). Resampling of the syenite during the 2016 field season produced similar results over multiple samples, although slightly lower (Acosta-Góngora et al., 2018). Based on the assay results and mineralization textures, it is suggested that the Gemelo system may represent a magmatic version of the hydrothermally dominated Hoidas deposit (Acosta-Góngora et al., 2017).

The layering and mineral alignment of the clinopyroxenes in the Gemelo syenite shows evidence of either syn-tectonic emplacement or the development of a post-emplacement foliation. Where mineralization was less prominent, a foliation is visible in the syenite primarily defined by alignment of the mafic minerals with a strike and dip of (055/80). Based on this orientation, the foliation appears to be a weak S3 fabric, possibly due to development towards the tail end of the deformation event. Heavily mineralized locations in the syenite are often aligned similarly to the foliation. Compared to the surrounding migmatitic gneiss, the foliation of the syenite was stronger and more consistent in strike. Surrounding locations which could be measured appear to have a gneissic fabric aligned with S2, but due to the variably in the strike and dip, the gneissosity may be part of S0 instead. As discussed in section 5.5, a crystallization age of 1829 ± 4 Ma was obtained for the syenite (Pehrsson et al., 2016).

Emplacement of the Gemelo syenite and the associated rare-earth element mineralization appears to be at least partially structurally controlled and related to the D3 event. Where the Gemelo syenite is located, at the eastern arm of Labyrinth Lake, is directly east of the bend in the Black Bay Fault. The D2 may have developed a weakness in this region which may have facilitated emplacement of the syenite during D3. The crystallization age of Gemelo is very similar to some of the Hoidas ages reported by Pandur et al. (2013) who reported ages of 1.84 to 1.83 Ga for some of the later stages of mineralization. The similar ages and proximity to the Black Bay Fault

Figure 6-2. Example of mineralization found in the Insula-Labyrinth Lakes area. (A) Pyroxenite unit often contained rusty section indication potential sulphides. Sheared leucosome was often adjacent. (B) Gemelo syenite with large cpx crystals. Note dark red staining, indicating the presence of allanite.

suggest a larger rare-earth element system (Acosta-Góngora et al., 2018) in which emplacement and mineralization was facilitated through deformation along the Black Bay Fault.

6.4 Dymond Lake

In the Dymond Lake area there is a return to the mineralization and hydrothermal alteration style found in the Uranium City area. A large amount of epidote, chlorite, hematite and potassic alteration is observed surrounding the E-W-trending fault at Dymond Lake, and presumably related to this fault. The gabbro bounding the E-W-trending fault (Figure 4-40) contains quartz veins and evidence of sulphides, primarily rusty weathering and some pyrite (Figure 6-4). A weathered sample collected from the rusty coloured area produced Au results of 0.38 ppm (Acosta-Góngora et al., 2018). The gabbro appears to be structurally linked to the E-W-trending fault found at Dymond Lake. A NE-SW-trending fabric present in the gabbroic unit suggests emplacement predated D3 and may have occurred with D2.

Northwest of Dymond Lake, yellow staining found around brittle structures is potential evidence of uranium mineralization. The quartz surrounding the yellow staining is very smoky, suggesting radiation damage and the presence of radioactive material nearby. No sample could be collected for assay. The orientation of the brittle structures matches the orientation of the larger E-W-trending and N-S-trending faults found at Dymond Lake.

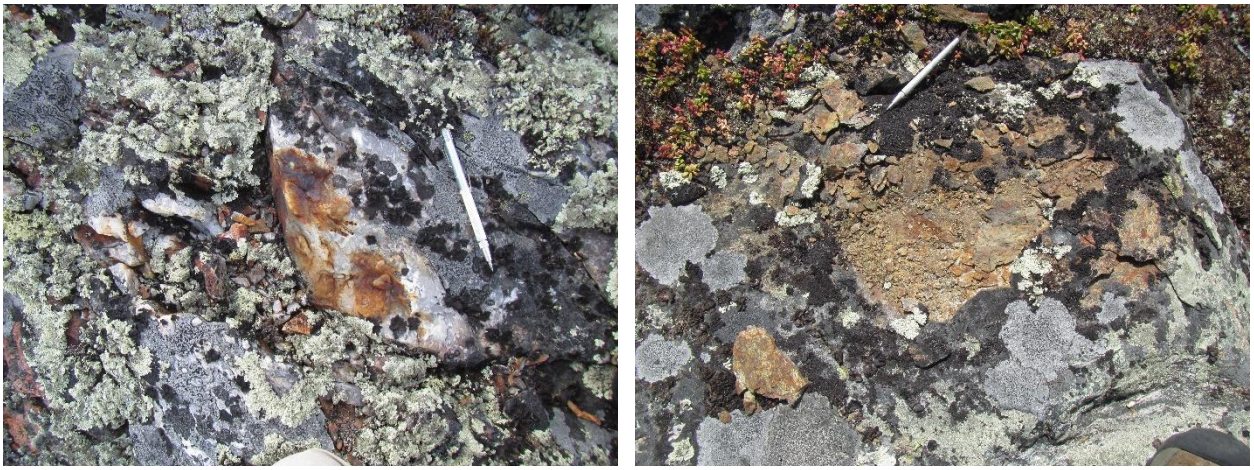

Figure 6-4. Rusty weather and quartz veins associated with sulphides observed in the gabbroic unit found at Dymond Lake.

Only a few hints of rare-earth element mineralization is found in the Dymond Lake area. A cpx-syenite at Dymond Lake appears to have been emplaced along the E-W-trending structure (Figure 4-40), with only a weak NE-SW-trending foliation, similar to the foliation seen in the Gemelo syenite at Labyrinth Lake. South of Dymond Lake, another cpx-syenite shows similar structural controls, with this intrusion reported to intrude along a NE-SW-trending structure (Martel et al., 2018). However, while both of these intrusions were similar in composition to that of the Gemelo syenite, no evidence of rare-earth element mineralization was found in either intrusion. Approximately 200 meters away from where possible uranium mineralization was noted, a pyroxenite dyke is present that is surrounded by dark red staining, possibly indicative of the presence of allanite (Figure 6-3). The pyroxenite dyke is oriented 250/80, similar in orientation as the S3 fabric observed in the surrounding area.

Figure 6-3. Pyroxenite dyke which intrudes into metasediments. Dark red staining surrounding the dyke may indicate the presence of allanite, based upon observations from Hoidas Lake and Gemelo. Dyke orientation is similar to the S3 fabric in region.

7. Regional Tectonic Framework

7.1 Introduction

The primary objective of this chapter is to place the different Black Bay Fault deformational events identified in this study in the context of the larger scale tectonic events in the area using the structural characteristics of the different deformational events and the available geochronological data in the area. As will be evident, many of the age constraints are tenuous, and alternative scenarios are offered in several instances. This discussion is offered as a step toward a more thorough understanding of the Black Bay Fault history rather than a definitive answer.

7.2 D1

D1 is a deformational event that produced sinistral shear, and probably transpression, along the Black Bay Fault in NWT that occurred in a regime of transpression (Figure 7-1). It has been identified in this study on the basis of sinistral kinematic indicators associated with the earliest foliations (S1) identified in the Black Bay Fault deformation zone in all the study areas. The S1 fabrics and sinistral kinematics are observed clearly on both side of the Black Bay Fault and pre-existing fabrics, pre-S1, are observed to be transposed into the NNE-SSW-trending fabric. This event has not been clearly identified in the Saskatchewan section of the Black Bay Fault.

The granodioritic gneiss sample, 15-DJ-476C, was collected for age dating in the hope of establishing constraints on the timing of the D1 and/or D2 events. Unfortunately, the lack of any metamorphic ages younger than 2.33 Ga (Figure 5-7) makes the sample too old to put a very useful age constraint on the deformation. Alternatively, the abundance of ~1.91 to 1.90 Ga ages in Saskatchewan, including in-situ ages from garnet rims trending parallel to the Black Bay Fault (Bethune et al., 2013), may reflect the timing of D1 sinistral transpression. While these ages have previously been assigned to the D3 dextral transpression, as discussed in section 5.6, the later deformational events may not have been well recorded in the metamorphic history in Saskatchewan.

Based on field observations between the western domains and the Firedrake domain in both the Tazin River area and the Insula-Labyrinth Lakes, there exists a difference in the metamorphic grade between the two sides, with granulite grade facies on the western side compared to upper

amphibolite grade facies in the Firedrake domain. The difference is not as great in the Dymond Lake area due to the Firedrake being a higher grade, although the western side is still at a higher metamorphic grade than the eastern side. Furthermore, the lack of Arrowsmith ages only in the Firedrake domain indicates the McCann and Firedrake domains had different tectonometamorphic histories prior to the development of the Black Bay Fault. As such,

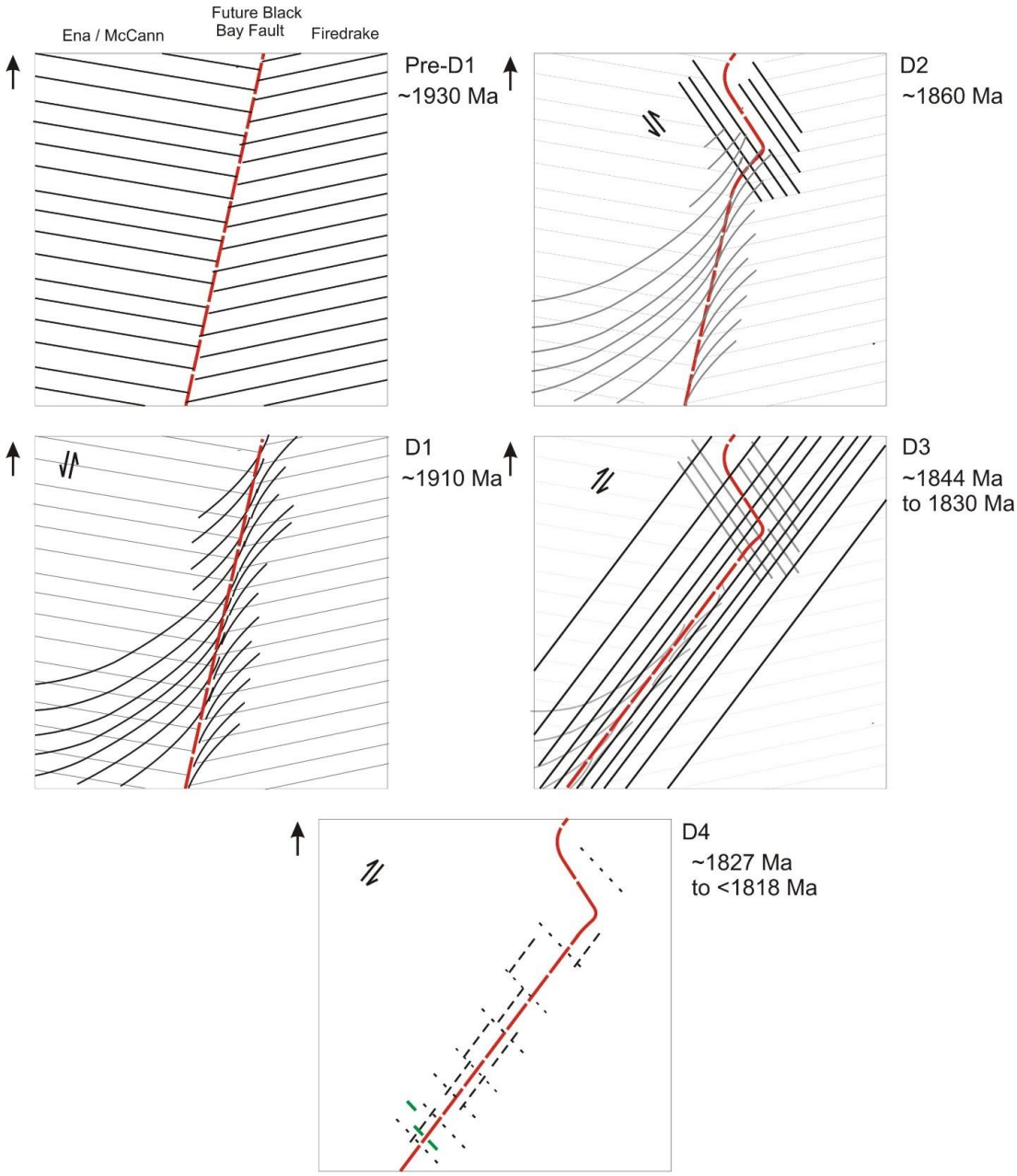

Figure 7-1. Simplified deformation sequence of the Black Bay Fault with the estimated timing constraints on each event. Prior to development of the Black Bay Fault, a pre-S1 E-W fabric was formed ~1930 ma. D1 produced sinistral transpression and the development of the Black Bay Fault at ~1910 Ma. A fault bend developed with D2 possibly around 1860 Ma. A shift to D3 dextral transpression occurred by 1844 Ma which continued at least until 1830. A shift towards more brittle-ductile deformation occurred by ~1827 Ma and lasted until at least 1818 Ma.

significant uplift of the western-side of the Black Bay Fault relative to the east side (i.e. reverse fault movement) must have occurred to produce the higher metamorphic grade observed in the McCann.

However, preservation of dip-slip fabrics in our study area appears poor with the majority of the stretching lineations found in the different fabrics indicating the simple-shear component is mostly strike-slip. However, our S1 fabric with rare steeply plunging lineations along with the sheath folds indicating high strain provides the best evidence that D1 was the main event on the Black Bay Fault producing large scale uplift of the western domains.

Preliminary results from P-T-t work that is currently on-going as part of the larger GEM2 South Rae mapping project appear to support that relative uplift of the McCann domain occurred around the assumed time of D1. Northwest of Labyrinth Lake, a sample in the McCann domain, in the vicinity of the fault, from a garnet-clinopyroxene-orthopyroxene-amphibole-plagioclase metagabbro of the Orpheus dyke swarm which intruded post-Arrowsmith at 2.27 Ga, contains a peak metamorphic age of ~1.90 Ga at 12-14 kbars and 850 °C (Martel et al., 2018)). Furthermore, in the surrounding area ~ 15 km north of Labyrinth Lake, again in the McCann domain and near to the Black Bay Fault, a sample collected in 2012 from a foliated quartz diorite produced a metamorphic age of 1894 ± 11 Ma (Davis et al., 2015), which is one of the only ages in our area that matches the older ages found in Saskatchewan. This area is north of the fault offset at Labyrinth Lake and may have provided better preservation through the subsequent deformation events of the Black Bay Fault. Unfortunately, it was not examined during our field seasons.

Beyond these loose P-T-t constraints in our area, other structures in the larger South Rae area show evidence of movement and uplift around this time. To the southeast, outside of project area, the east-verging Leg Lake shear zone (within the Snowbird tectonic zone) records evidence of rapid exhumation from similar high pressure metamorphism around the same time at ca. 1896.7 ± 0.8 Ma (Mahan et al., 2006).

The proposed ~1.90 Ga timing constraint for D1 sinistral transpression points to the Snowbird orogeny as the probable driver for this initial activity along the Black Bay Fault. Accretion of the Hearne craton on to the Rae craton during the Snowbird orogeny would have produced a NW-SE compressional regime in the South Rae (Kraus and Ashton, 2000), which would have been

conducive towards producing the proposed reverse fault zone in the overall D1 sinistral transpression along the Black Bay Fault.

In order to better constrain the timing of D1, the edge of the deformation zone in the Firedrake around Labyrinth Lake, which contains many sinistral indicators and transposition of pre-S1 gneissosity, may provide a possible location for geochronology samples.

7.3 D2

The D2 event created a NW-SE-trending S2 fabric with sinistral shear sense (Figure 7-1). This trend is roughly orthogonal to both the preceding S1 fabric and the subsequent S3 fabric. The S2 fabric is best developed around Labyrinth Lake and Dymond Lake and appears to be spatially associated with the sharp bend of the Black Bay Fault in those areas. The S2 fabric is also observed in the Insula Lake region, to the SW, but not in the Tazin River area, nor in northern Saskatchewan.

Understanding and constraining the D2 event is difficult and D2 remains the most poorly understood deformation event on the Black Bay Fault. D2 modified the shape of the fault rather than producing significant displacement along the length of the fault like the other events, but it is classified in this study as another deformation event on the Black Bay Fault for simplicity. It is plausible that the S2 fabric could have developed as a sinistral shear system that is conjugate to the dextral S3 fabric (which is consistently developed along the Black Bay Fault zone). However, this possibility appears to be in conflict with several noted overprinting relationship between the D2 and D3 deformational fabrics. Specifically, S2 is observed on the enveloping surface of F3 folds and there are numerous locations where the S3 fabric is observed to overprint the S2 fabric around Dymond Lake. However, some form of kinematic relationship between S2 and S3 cannot be completely ruled out.

There are currently no ages that specifically relate to the D2 event. Hence, the age constraints inferred for D1 and D3 serve as loose timing brackets for D2 1.90 Ga > D2 > 1.85Ga. A possible tectonic driver behind the D2 event is the “indentation” of the Slave craton into the Rae craton, initially proposed by Gibb (1978). He suggested the Slave craton acted as a rigid wedge that pushed in into a more rigid-plastic Rae craton during the continued amalgamation of the western cratons of Nuna following the initial accretion of the Slave craton onto the Rae craton during the

Thelon Orogeny. The primary candidate for this process is the Wopmay orogeny, which began at around 1.88 Ga and involved the accretion of the Hottah terrane onto the Slave craton (Hildebrand et al., 2010), thus producing indentation of the Slave craton into the Rae craton. Therefore, D2 and the shearing which produced the bend in the Black Bay Fault around Labyrinth Lake may have developed as an escape structure to accommodate the indentation of the Slave craton.

However, due to many unknowns surrounding the D2 event, the deformation may also be associated with late effects from the Snowbird Orogeny or early Trans-Hudson orogeny. The Wholdaia Lake shear zone, another NE/SW-trending structure (although SE-dipping) located east of the Black Bay Fault and separating the Firedrake domain from the Snowbird Domain (Figure 1-2) has a minimum age of shearing of ca. 1864 Ma (Thiessen et al., 2017). Therefore, our D2 event on the Black Bay Fault may be syntectonic with the later shearing along the Wholdaia Lake shear zone although the tectonic driver behind this event has not been discussed.

7.4 D3

D3 produced dextral transpressional shear along the Black Bay Fault, as indicated by dextral kinematic indicators in the S3 fabric (Figure 7-1). The S3 fabric has a similar trend to the S1 fabric, and it can be difficult to distinguish these fabrics in the Tazin River area. In the Insula Lake and Labyrinth Lake and Dymond Lake areas, the S2 fabric is highly oblique to both S1 and S3. Evidence of S2 crosscutting S1 and S3 cutting S2 is used to establish the relative timing of these three deformational events with the outcrop from the Dymond Lake area described in Figure 4-49 providing a key example were all three fabrics are observed.

Geochronology sample 15-DJ-468B, which comes from an aplitic granitic dyke, yields an age of 1844 ± 2.1 Ma. The dyke displays a weak S3 foliation and is Z-folded, reflecting syn-tectonic emplacement with the dextral D3 event. Based on this age constraint, the primary tectonic driver appears to be the on-going Trans-Hudson orogeny. While primary stress regime from the whole Trans-Hudson orogeny has been hypothesized to be NW directed compression driven by the collision of the Superior craton into the Hearne-Rae cratons (Hoffman, 1988b) which would not be conducive in producing dextral motion along the Black Bay Fault, there may have been some variance in the south portion of the Trans-Hudson orogeny.

Along the southern margin of the Hearne craton, the poorly exposed Sask craton is believed to have collided with the Hearn craton during the Trans-Hudson orogeny around 1.84 Ga (Ansdell, 2005) (Figure 2-2). Ashton et al. (2013) suggest this collision shifted the compressional environment to a more E-W direction. However, timing on the start of collision for the Sask craton onto the Hearne craton remains poorly constrained and may have initiated earlier (Ansdell, 2005). Under west-directed collision, dextral motion would be able to occur along the NE-SW-trending structures in the southern Rae. Ductile, west-side up dextral transpression along the Legs Lake shear zone, located to the east in the Snowbird Tectonic zone, is known to have occurred at ca. 1.85 Ga (Mahan et al., 2006). While Ashton et al. (2009) believes that the onset of brittle-ductile deformation occurred at this time, our new data supports ductile deformation along the Black Bay Fault was still on going at this time.

There is a lack of Trans-Hudsonian ages in the domains east of the Beaverlodge domain (Tantato and Dodge (Figure 1-2), similar to the lack from the Uranium City area. In the Tantato and Dodge domains, this lack of Trans-Hudsonian ages has been attributed to a lack of volatiles present during this event, preventing the metamorphic event from being recorded (Ashton et al., 2009). However, as shown in Figure 5-13, significant amount of quartz is present in the dextral shears, indicating the presence of volatiles at this location. Instead it appears that the metamorphic grade in the rocks currently exposed in Uranium City area was not high enough during D3 to readily promote the growth of monazite or zircon. This is supported with the grade of metamorphism observed in the sediments from the Thluicho Lake group west of the Black Bay Fault in the central Zemlak domain. These sediments have a maximum age of deposition currently of ca. 1.92 Ga (Bethune et al., 2010), and only record greenschist facies metamorphism during the subsequent events (Hunter, 2007). This is in contrast to the surrounding basement rocks in the southern Zemlak which is predominately composed of upper amphibolite facies metamorphism rocks (Bethune et al., 2010).

Therefore, it appears that there is an increase in metamorphic grade and change in deformational style during D3 moving northward from Uranium City to the Tazin River area in the Ena/Zemlak domain. The same pattern is also observed moving further northward towards the Insula-Labyrinth Lakes area, though with a smaller amount of change. The increase in metamorphic grade may in part be due to the change in domains on the western side of the Black Bay Fault,

shifting from the Ena domain to the McCann domain and can partially explain the rather abrupt shift from amphibolite to granulite grade facies. While through the regional mapping of the GEM2 South Rae project, the Ena and McCann domain were assumed to be genetically similar, with the change in magnetic signature between the Ena and McCann domains assumed to be representing a change in metamorphic grade rather than another shear zone, this assumption may be incorrect. Instead, in northern Saskatchewan the boundary between the Zemlak and Nolan has been interpreted to have formed during the Arrowsmith orogeny (Bethune, 2017) which then acted as a tectonic front at ca. 1.93 Ga (Ashton et al., 2005). Therefore, while the metamorphic grade and deformation style continues to increase moving further northward between the Ena and McCann domains, this change may be unrelated to the Black Bay Fault.

However, the change observed within the Ena/Zemlak domain does support that differential uplift occurred along the Black Bay Fault. While there is no significant variance in topography, the change in deformational fabrics suggest differential uplift occur, producing increased erosion moving northward and resulting in the exposure of the more ductile fabrics. Timing of the differential uplift is constrained to D3 or later in order to produce the observed change in S3 fabrics. Therefore, the differential uplift is not a product of the D1 event which produced the larger overall uplift of the western side. The restraining bend created by the change in fault trend at Labyrinth Lake could have produced increased uplift of the western side of the fault during D3, but it is not clear that this would have produced differential uplift extending down to the Tazin River area.

7.5 D4

D4 resulted from continued dextral transpression but records a shift from ductile towards more brittle-ductile deformation. Development of a sinistral NW-SE-trending S4 fabric occurred during D4. The prevalence of S4 fabrics decreases moving northward from the Tazin River area into the Insula-Labyrinth Lakes area (Figure 7-1).

While timing of D4 was not directly investigated in our study, the emplacement of the syn-tectonic mafic dykes in the S4 shears in the Tazin River area provide possible insight into the timing. Due to the relative dearth of mafic intrusions in the South Rae mapping area, a reasonable correlation of the mafic dykes with those from a dyke swarm in the larger surrounding area can be made, offering timing constraints and insight into the stress regime of

the region at the time. Based on the observed orientation of the mafic dykes in the Tazin River area (trending ~335-155) along with emplacement along brittle-ductile shears, the mafic dykes in our area may belong to the Sparrow diabase dyke swarm.

The Sparrow diabase dykes form a large (50 000 km^2) dyke swarm centred around the Nonacho basin near the Great Slave Lake Shear Zone in the Northwest Territories (Bostock and van Breemen, 1992), around 200 km to the northwest of the Tazin River Area. Although the Sparrow dykes are primarily found around the Nonacho basin area, the full extent of their distribution is unknown (Bostock and van Breemen, 1992).

The emplacement characteristics of the Sparrow dykes in the Nonacho basin are broadly similar to those of the mafic dykes found in the Tazin River area. The majority of the Sparrow dykes are oriented 320 ± 15 ° and have been emplaced along sinistral brittle-ductile shears (Bostock and van Breemen, 1992). Rarely are they greater than 2 meters wide and some of the dykes in the Nonacho basin show sinistral slip following emplacement (Bostock and van Breemen, 1992), all characteristics which our Tazin River dykes share.

The unmetamorphosed composition of the Sparrow dikes is primarily clinopyroxenes and plagioclase, but the clinopyroxenes can be altered to hornblende (Mcglynn et al., 1974). Unfortunately, all of the mafic dykes observed in our area have been metamorphosed to an amphibolite facies (Figure 4-17 C), thus preventing a direct comparison through compositional comparisons with Sparrow dykes from their core area. However, the altered Sparrow dykes do share similar composition with our Tazin River dykes. Work by Bostock and van Breemen (1992) produced a baddelyite ages for the Sparrow dykes of 1827 ± 4 Ma, which fits with our assumption of post-D3 emplacement of the dykes in our area.

To the south around Uranium City, a similar mafic dyke swarm is present, known as the Uranium City dykes. These are found on either side of the Black Bay Fault, extending up to 30 km into the Beaverlodge domain and 45 km into the Zemlack domain (Ashton et al., 2005). Unlike our mafic dykes and the Sparrow dykes, the Uranium City dykes are primarily E-W-trending, although there is some variability near to the Black Bay Fault, where some dykes trend NE-SW, parallel to the fault (Morelli et al., 2009). On the east-side of the Black Bay Fault, in the Beaverlodge domain, the Uranium City dykes have been hypothesised to be the feeder dykes for the mafic volcanic rocks found in the Martin Group (Ashton et al., 2001). The Uranium City

dykes are also believed to be structurally controlled (emplacement along observed along pre-existing fractures), and the dykes are observed to fork when conjugate fracture sets are encountered (Ashton et al., 2009). The majority of the Uranium City dykes have been found to be un-metamorphosed although some have been reported to have undergone weak metamorphism to green-schist facies (Ashton et al., 2009). A slightly younger baddeleyite age of 1818 ± 4 Ma has been found for the Uranium City dykes (Morelli et al., 2009), but they have been considered to be coeval with the Sparrow dykes due to similar petrology (Ashton et al., 2009).

One of Uranium City dykes observed during our revisit of the Uranium City area contained sinistral drag folds along the margins (Figure 7-2 A) while another one contained a brecciated zone along the northern margin (Figure 7-2 B). Neither example display a foliation or metamorphism to amphibolite grade facies like the dykes in our Tazin River area, with chilled margins still visible and only brittle fractures present in the Uranium City dykes.

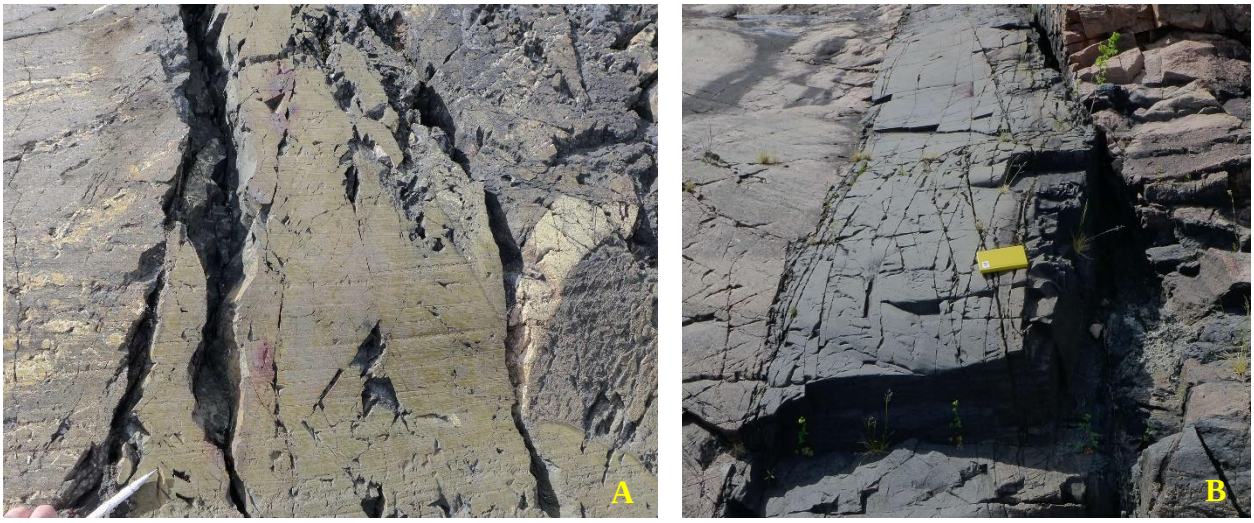

Figure 7-2. Uranium City dykes showing varying levels of deformation. (A) Dyke appears to be situated in a pre-existing sinistral shear though cooling rims can be seen. (B) Elsewhere the vicinity, a relatively undeformed Uranium City dyke which contains a brecciated zone along the northern margin.

The shears that the NW-SE-trending Sparrow dykes are emplaced along are parallel to the Bathurst Fault, which is the sinistral conjugate component to the large dextral, NE-SW-trending McDonald Fault which offset sedimentary rocks of the East Arm basin and mylonites of the Great Slave Lake shear zone (Bostock and van Breemen, 1992). Development of this large fault system is believed to have initially occurred during the Taltson-Thelon orogeny (Hoffman, 1987), with ductile shearing along the Bathurst fault at 1933 Ma and 1895 Ma (Ma et al., 2018).

Re-activation of this fault system which produced more brittle-ductile deformation occurred after ~1.84 Ga during the accretion of the Nahanni-Fort Simpson Terrane on to the Hottah Terrane which produced continued re-indentation of the Slave craton in to the Rae craton (Hoffman, 1987). Emplacement of the Sparrow dykes is believed to be related to the Nahanni-Fort Simpson collision which fits with the corresponding east-west compressional environment that would be produced during this event (Ashton et al., 2009). The difference in dyke orientation and the slightly younger ages of the Uranium City dykes has been suggested to be due to the accretion of the southern extent of the Nahanni-Fort Simpson collision towards the end of the orogeny (Ashton et al., 2009).

Based upon the similarities in emplacement, it appears that the Tazin River dykes likely belong to the Sparrow dyke swarm, indicating that a shift towards more brittle-ductile D4 deformation was underway by ca. 1827 Ma with D4 on-going until at least 1818 Ma based upon the Uranium City dykes.

Both the Uranium City dykes and our Tazin River dykes were examined on the same side of the Black Bay Fault (west) and in the same domain (Ena/Zemlak). If these dykes are part of the same system, they provide some support for the presumption of differential uplift northward along the Black Bay Fault indicated in the S3 fabrics. The fact that the Tazin River dykes have been amphibolitized and the Uranium City dykes have not been metamorphosed, suggests that differential uplift of the Ena domain was still ongoing or initiated during D4. This fits with the observed decrease in the prevalence of brittle-ductile and brittle structures further north.

8. Summary

The Black Bay Fault has been known in northern Saskatchewan since the 1950's, and its extension well into the NWT has been postulated on the basis of the aeromagnetic signature of the region. However, the current study, which was conducted as part of the GEM2 South Rae mapping project, is the first systematic investigation of the Black Bay Fault in NWT. This mapping program has provided better constraints to delineate and characterize the Black Bay Fault and the bounding zone of deformation. Detailed evaluation of deformational fabrics and kinematic indicators has elucidated a more complicated deformation history of the Black Bay Fault than had been identified from prior work in northern Saskatchewan. In particular, previously unrecognized deformational events with sinistral kinematics have been identified. Furthermore, it was discovered that the style of deformation changes moving northward along the fault, transitioning from the brittle-ductile fabrics and mylonites found around the Uranium City area, to a straight gneiss regime in the Northwest Territories focus study area. Overall, the data collected, and observations made during this study indicate that the Black Bay Fault has experienced four main deformational events, D1 to D4 which are summarized as follows:

D1- Produced a steeply west-dipping, NNE-SSW-trending gneissosity, sinistral kinematic indicators, shallowly NE-plunging lineations and rare, steeply plunging lineations through sinistral transpression with west-side up movement. D1 also produced the sheath folds and L-tectonites found in the fabrics surrounding the Black Bay Fault. This event produced uplift of the western domains (Ena and McCann) relative to the eastern (Firedrake) and is inferred to have occurred ca. 1910 Ma. This appears to be coeval with the Snowbird Orogeny and the collision of the Hearne craton into the eastern margin of the Rae craton. D1 is a newly discovered deformation event and the fabric has not been clearly identified in previous work in northern Saskatchewan, although it appears to be preserved in the geochronology record.

D2- Is a deformational event that is regionally limited along the Black Bay Fault which modified the geometry of the fault rather than producing movement along the length of the fault like the other events. It produced the left stepping bend of the fault and the development of a NW-SE-trending fabric with sinistral shear kinematic indicators and shallowly NW-plunging lineations through shear driven folding. The majority of evidence for this event is best preserved around Labyrinth Lake and Dymond Lake, where the bends are located, as well in between these lakes..

D2 is hypothesized to be related to the indentation of the Slave craton into the Rae craton during the Wopmay orogeny, to the west, at ca. 1860 Ma; however, timing around this deformation event remains very poorly constrained. The D2 event does not appear to have impacted the Tazin River area or the northern Saskatchewan sections of the Black Bay Fault, further to the south.

D3- Produced a steeply west-dipping, NE-SW-trending ductile fabric with moderately SW-plunging lineations as a result of dextral transpression, producing west-side up movement. This ductile event was previously recognized as the first deformation event related to the Black Bay Fault in studies from Saskatchewan. An increase in intensity and wider distribution of D3 fabrics is observed moving northward along the fault. The fault bend that developed during D2 would have acted as a restraining band during the subsequent D3 event and likely produced some of the increase in deformation fabrics and differential uplift, particularly in the McCann domain. Our data indicates D3 began by 1844.4 ± 2.1 Ma and continued until at least 1830 Ma. It is believed to be driven from far-field tectonic effects associated with Trans-Hudson Orogeny. Previous studies in Saskatchewan concluded this event occurred earlier, but lower grade deformation around Uranium City during the D3 event could explain the lack of D3 ages in northern Saskatchewan.

D4- Marked a shift to brittle-ductile deformation associated with dextral movement along the fault and the development a sinistral NW-SE-trending, small-offset, conjugate faults. Some of the NW-SE-trending faults contain syn-tectonically emplaced mafic dykes. The shift to brittle-ductile conditions appears to have occurred by ca. 1827 Ma and continued past ca. 1818 Ma based upon the mafic dyke emplacement. Continuation of the Trans-Hudson Orogeny along with the termination of the Wopmay Orogeny is believed to be the tectonic driver of the brittle-ductile deformation (Ashton et al., 2009). While exhumation of the overall area occurred, differential uplift, particularly of the Ena domain occurred with this event based upon the presence of the metamorphosed Tazin River mafic dykes compared to the primarily un-metamorphosed Uranium City dykes in Saskatchewan.

Additionally, our work on the Black Bay Fault found that fault-associated rare-earth element mineralization and hydrothermal alteration present in northern Saskatchewan extends northward into the Northwest Territories with the presence of multiple structurally controlled radiometric anomalies and hydrothermal alteration. This mineralization is primarily restricted to S3 and S4

fabrics, and could, thus, be related to the shift from a ductile regime towards a more brittle-ductile environment. A new rare-earth element occurrence, Gemelo, was discovered close to the Black Bay Fault around Labyrinth Lake where the host rock contains evidence of syn-tectonic emplacement during D3. The Black Bay Fault appears to have been an important structure facilitating the emplacement of rare-earth elements in the southern Rae, and further exploration for rare-earth mineralization around the Black Bay Fault is warranted. Furthermore, the large secondary faults present around Dymond Lake appear to indicate a return to the style of mineralization observed further to the south and may host economically important metals.

9. References

Acosta-Góngora, P., Martel, E., Pehrsson, S.J., 2018. Geochemistry results from the south Rae mapping project , Northwest Territories , 2015 and 2016 field seasons. Geol. Surv. Canada Open File, 1 .zip file. https://doi.org/https://doi.org/10.4095/306501

Acosta-Góngora, P., Pehrsson, S.J., Martel, E., Lauzon, G., Jamison, D., 2017. South Rae Project: preliminary field observations (2015) and lake sediment analysis, Northwest Territories and Saskatchewan. Geol. Surv. Canada 1 ppt file. https://doi.org/https://doi.org/10.4095/302765

Alsop, G.., Holdsworth, R.., 2004. The geometry and topology of natural sheath folds: a new tool for structural analysis. J. Struct. Geol. 26, 1561–1589. https://doi.org/10.1016/J.JSG.2004.01.009

Alsop, G.I., Holdsworth, R.E., 2006. Sheath folds as discriminators of bulk strain type. J. Struct. Geol. 28, 1588–1606. https://doi.org/10.1016/J.JSG.2006.05.005

Ansdell, K.M., 2005. Tectonic evolution of the Manitoba–Saskatchewan segment of the Paleoproterozoic Trans-Hudson Orogen, Canada. Can. J. Earth Sci. 42, 741–759. https://doi.org/10.1139/E05-035

Ashton, K.E., Boivin, D., Heggie, G., 2001. Geology of the Southern Black Bay Belt, West of Uranium City, Rae Province. Saskatchewan Geol. Surv. Sask. Energy Mines 2, 14.

Ashton, K.E., Card, C.D., Davis, W., Heaman, L.M., 2007. New U-Pb Zircon Age Dates from the Tazin Lake Map Area (NTS 74N). Saskatchewan Geol. Surv. Saskatchewan Minist. Energy Resour. 2, 8.

Ashton, K.E., Card, C.D., Modeland, S., Parts, I., Province, R., 2005. Geological Reconnaissance of the Northern Tazin Lake Map Area (NTS 74N), Including Parts of the Ena, Nolan, Zemlak, and Taltson Domains, Rae Province. Saskatchewan Geol. Surv. Saskatchewan Ind. Resour. Misc. Rep 2, 1–24.

Ashton, K.E., Hartlaub, R.P., Bethune, K.M., Heaman, L.M., Rayner, N., Niebergall, G.R., 2013. New depositional age constraints for the Murmac Bay group of the southern Rae craton, Canada. Precambrian Res. 232, 70–88. https://doi.org/10.1016/j.precamres.2012.05.008

Ashton, K.E., Hartlaub, R.P., Heaman, L.M., Morelli, R.M., Card, C.D., Bethune, K., Hunter, R.C., 2009. Post-Taltson sedimentary and intrusive history of the southern Rae Province along the northern margin of the Athabasca Basin, Western Canadian Shield. Precambrian Res. 175, 16–34. https://doi.org/10.1016/j.precamres.2009.09.004

Ashton, K.E., Kraus, J., Hartlaub, R.P., Morelli, R.M., 2000. Uranium City Revisited: A New Look at the Rocks of the Beaverlodge Mining Camp, Saskatchewan Geological Survey. Sask. Energy Mines.

Bergeron, J., 2001. The deformational history of the Black Bay structure near Uranium City, Northern Saskatchewan. University of Saskatchewan.

Berman, R.G., Davis, W.J., Pehrsson, S., 2007. Collisional Snowbird tectonic zone resurrected: Growth of Laurentia during the 1.9 accretionary phase of the Hudsonian orogeny. Geology 35, 911–914. https://doi.org/10.1130/G23771A.1

Berman, R.G., Pehrsson, S., Davis, W.J., Ryan, J.J., Qui, H., Ashton, K.E., 2013. The Arrowsmith orogeny: Geochronological and thermobarometric constraints on its extent and tectonic setting in the Rae craton, with implications for pre-Nuna supercontinent reconstruction. Precambrian Res. 232, 44–69. https://doi.org/10.1016/j.precamres.2012.10.015

Berman, R.G., Sanborn-barrie, M., Stern, R.A., Carson, C.J., 2005. Tectonometamorphism at ca. 2.35 and 1.85 Ga in the Rae domain, western Churchill Province, Nunavut, Canada: insights from structural, metamorphic and in situ geochronological analysis of the southwestern Committee Bay belt. Can. Mineral. 43, 409–442.

Bethune, K.M., 2017. Crustal dynamics and tectonic assembly of the west-southwest Rae craton – What are key relationships in the Athabasca region telling us? Geological Association of Canada, Kingston.

Bethune, K.M., Berman, R.G., Rayner, N., Ashton, K.E., 2013. Structural, petrological and U-Pb SHRIMP geochronological study of the western Beaverlodge domain: Implications for crustal architecture, multi-stage orogenesis and the extent of the Taltson orogen in the SW Rae craton, Canadian Shield. Precambrian Res. 232, 89–118. https://doi.org/10.1016/j.precamres.2013.01.001

Bethune, K.M., Hunter, R.C., Ashton, K.E., 2010. Age and provenance of the Paleoproterozoic Thluicho Lake Group based on detrital zircon U-Pb SHRIMP geochronology: New insights into the protracted tectonic evolution of the southwestern Rae Province, Canadian Shield. Precambrian Res. 182, 83–100. https://doi.org/10.1016/j.precamres.2010.07.003

Bickford, M.E., Collerson, K.D., Lewry, J.F., Schmus, W.R. Van, Chiarenzelli, J.R., 1990. Proterozoic collisional tectonism in the Trans-Hudson orogen, Saskatchewan. Geology 18, 14–18.

Bostock, H.H., van Breemen, O., 1992. The timing of emplacement, and distribution of the Sparrow diabase dyke swarm, District of Mackenzie, Northwest Territories. Geol. Surv. Canada Radiogenic, 49–55.

Chacko, T., De, S.K., Creaser, R.A., Muehlenbachs, K., 2000. Tectonic setting of the Taltson magmatic zone at 1.9–2.0 Ga: a granitoid-based perspective. Can. J. Earth Sci. 37, 1597–1609. https://doi.org/10.1139/e00-029

Chinnery, M.A., 1966. SECONDARY FAULTING II. GEOLOGICAL ASPECTS. Can. J. Earth Sci. 3, 175–190.

Condie, K.C., O'Neill, C., Aster, R.C., 2009. Evidence and implications for a widespread magmatic shutdown for 250 My on Earth. Earth Planet. Sci. Lett. 282, 294–298. https://doi.org/10.1016/J.EPSL.2009.03.033

Corrigan, D., Pehrsson, S., Wodicka, N., de Kemp, E., 2009. The Palaeoproterozoic Trans-Hudson Orogen: a prototype of modern accretionary processes. Geol. Soc. London, Spec. Publ. 327, 457–479. https://doi.org/10.1144/SP327.19

Davis, W.J., Pehrsson, S.J., Percival, J. a, 2015. Results of a U-Pb zircon geochronology transect across the southern Rae craton, Northwest Territories, Canada. Geol. Surv. Canada Open File, 1–67. https://doi.org/10.4095/295610

De, S.K., Chacko, T., Creaser, R.A., Muehlenbachs, K., 2000. Geochemical and Nd-Pb-O isotope systematics of granites from the Taltson Magmatic Zone, NE Alberta: Implications for early Proterozoic tectonics in western Laurentia. Precambrian Res. 102, 221–249. https://doi.org/10.1016/S0301-9268(00)00068-1

Dieng, S., Kyser, K., Godin, L., 2013. Tectonic history of the North American shield recorded in uranium deposits in the Beaverlodge area, northern Saskatchewan, Canada. Precambrian Res. 224, 316–340. https://doi.org/10.1016/j.precamres.2012.09.011

Economy, S.M. of the, 2010. Precambrian Domain Map of Saskatchewan.

Flowers, R.M., Bowring, S.A., Williams, M.L., 2006. Timescales and significance of high-pressure, high-temperature metamorphism and mafic dike anatexis, Snowbird tectonic zone, Canada. Contrib. to Mineral. Petrol. 151, 558–581. https://doi.org/10.1007/s00410-006-0066-7

Gibb, R.A., 1978. Slave-Churchill collision tectonics. Nature 271, 50–52. https://doi.org/10.1038/271050a0

Gibb, R.A., Walcott, R.I., 1971. A precambrian suture in the Canadian shield. Earth Planet. Sci. Lett. 10, 417–422. https://doi.org/10.1016/0012-821X(71)90090-2

Gunning, M.H., Card, C.D., 2005. Transects across the Black Bay Shear Zone and Trend , Northwest Saskatchewan Transects across the Black Bay Shear Zone and Hoidas-Nisikkatch Rare-element Trend , Northwest Saskatchewan. Sask. Ind. Resour. Open File, 47.

Hale, W.E., 1954. Black Bay Map-Area, Saskatchewan (Preliminary Account). Geol. Surv. CANADA 59.

Halpin, K.M., 2010. The Characteristics and Origin of the Hoidas Lake REE Deposit. University of Saskatchewan.

Hanmer, S., Bowring, S., van Breemen, O., Parrish, R., 1992. Great Slave Lake shear zone , N W Canada : mylonitic record o f Early Proterozoic continental convergence , collision and indentation. J. Struct. Geol. 14, 757 to

773.

Hanmer, S., Williams, M., Kopf, C., 1995. Striding-Athabasca mylonite zone: implications for the Archean and Early Proterozoic tectonics of the western Canadian Shield. Can. J. Earth Sci. 32, 178–196. https://doi.org/10.1139/e95-015

Hartlaub, R.P., Chacko, T., Heaman, L.M., Creaser, R.A., Ashton, K.E., Simonetti, A., 2005. Ancient (Meso- to Paleoarchean) crust in the Rae Province, Canada: Evidence from Sm-Nd and U-Pb constraints. Precambrian Res. 141, 137–153. https://doi.org/10.1016/j.precamres.2005.09.001

Hartlaub, R.P., Heaman, L.M., Chacko, T., Ashton, K.E., 2007. Circa 2.3-Ga Magmatism of the Arrowsmith Orogeny, Uranium City Region, Western Churchill Craton, Canada. J. Geol. 115, 181–195. https://doi.org/10.1086/510641

Hildebrand, R.S., Hoffman, P.F., Bowring, S.A., 2010. The Calderian orogeny in Wopmay orogen (1.9 Ga), northwestern Canadian Shield. GSA Bull. 122, 794–814. https://doi.org/10.1130/B26521.1

Hoadley, J.W., 1955. Abitau Lake, Northwest Territories Sheet 75B. https://doi.org/https://doi.org/10.4095/108289

Hoffman, P.F., 2014. The origin of Laurentia: Rae craton as the backstop for proto-Laurentian amalgamation by slab suction. Geosci. Canada 41, 313–320. https://doi.org/10.12789/geocanj.2014.41.049

Hoffman, P.F., 1988a. UNITED PLATES OF AMERICA, THE BIRTH OF A CRATON: Early Proterozoic Assembly and Growth of Laurentia. Ann. Rev. Earth Planet. Sci 16, 543–603.

Hoffman, P.F., 1988b. UNITED PLATES OF AMERICA , and Growth of Laurentia.

Hoffman, P.F., 1987. Continental transform tectonics: Great Slave Lake shear zone (ca. 1.9 Ga), northwest Canada. Geology 15, 785–788. https://doi.org/10.1130/0091-7613(1987)15<785:CTTGSL>2.0.CO;2

Hunter, R.C., 2007. A geological investigation of the Thluicho Lake Group, southwestern Rae Province, Saskatchewan, Canada. University of Regina.

Kim, Y.S., Sanderson, D.J., 2006. Structural similarity and variety at the tips in a wide range of strike-slip faults: A review. Terra Nov. 18, 330–344. https://doi.org/10.1111/j.1365-3121.2006.00697.x

Kraus, J., Ashton, K.E., 2000. New insights into the structural geology and tectonic setting of the Uranium City area, Northwestern Saskatchewan. Sasktachewan Geol. Surv. Sask Energy Mines 2, 16–25.

Lin, S., Jiang, D., Williams, P.F., 2007. Importance of differentiating ductile slickenside striations from stretching lineations and variation of shear direction across a high-strain zone. J. Struct. Geol. 29, 850–862. https://doi.org/10.1016/j.jsg.2006.12.006

Ludwig, K.R., 2009. Isoplot 4.1, A geochronological toolkit for Microsoft Excel. Berkeley Geochronol. Cent. 76.

Ludwig, K.R., 1998. On the Treatment of Concordant Uranium-Lead Ages. Geochim. Cosmochim. Acta 62, 665–676. https://doi.org/10.1016/S0016-7037(98)00059-3

Ma, S., Kellet, D.A., Godin, L., 2018. Structural style and timing of deformation on the Bathurst Fault (eastern Slave craton): Implications for basement fault-controlled fluid pathways. Target. Geosci. Initiat. 2017 Rep. Act. 1, 79–87. https://doi.org/http://doi.org/10.4095/306391

Macdonald, R., 1984. Bedrock Compilation, Greater Beaverlodge Area {NTS 74N-6 to -11). Saskatchewan Geol. Surv. Saskatchewan Energy Mines Miscellane, 42–45.

Mahan, K.H., Williams, M.L., 2005. Reconstruction of a large deep-crustal terrane: Implications for the Snowbird tectonic zone and early growth of Laurentia. Geology 33, 385–388. https://doi.org/10.1130/G21273.1

Mahan, K.H., Williams, M.L., Flowers, R.M., Jercinovic, M.J., Baldwin, J.A., Bowring, S.A., 2006. Geochronological constraints on the Legs Lake shear zone with implications for regional exhumation of lower continental crust, western Churchill Province, Canadian Shield. Contrib. to Mineral. Petrol. 152, 223–242. https://doi.org/10.1007/s00410-006-0106-3

Mann, P., Gordon, M.B., 1996. Tectonic Uplift and Exhumation of Blueschist Belts Along Transpressional Strike-Slip Fault Zones. Geophys. Monogr. 96, 143–154.

Martel, E., Pehrsson, S., Berman, R., Regis, D., Davis, W., Thiessen, E., Percival, J., 2018. A 1.9 to 1.84 Ga continent-scale high pressure terrane in the Churchill Province, Rae Craton, Canada: extent, timing and relationship to Nuna assembly, in: RFG 2018. Vancover.

Martel, E., Pehrsson, S.J., Percival, J., Acosta-Góngora, P., Thiessen, E., Regis, D., Jamison, D., Neil, B., Knox, B., 2018. Geology and mineral potential of the southern Rae Craton, Northwest Territories, NTS 75-G and H, Geological Survey of Canada. https://doi.org/10.4095/306542

Martel, E., van Breemen, O., Berman, R.G., Pehrsson, S., 2008. Geochronology and tectonometamorphic history of the Snowbird Lake area, Northwest Territories, Canada: New insights into the architecture and significance of the Snowbird tectonic zone. Precambrian Res. 161, 201–230. https://doi.org/10.1016/j.precamres.2007.07.007

McCurdy, M.W., Pehrsson, S.J., Falck, H., Day, S.J.A., Campbell, J.E., 2016. Geochemical data for lake sediments and surface waters, Abitau Lake area, Northwest Territories (NTS 75-B), Geological Survey of Canada. https://doi.org/10.4095/299389

Mcglynn, J.C., Hanson, G.N., Irving, E., Park, J.K., 1974. Paleomagnetism and Age of Nonacho Group Sandstones and Associated Sparrow Dikes, District of Mackenziel. Can. J. Earth Sci. 11, 30–42.

Morelli, R.M., Hartlaub, R.P., Ashton, K.E., Ansdell, K.M., 2009. Evidence for enrichment of subcontinental lithospheric mantle from Paleoproterozoic intracratonic magmas: Geochemistry and U-Pb geochronology of Martin Group igneous rocks, western Rae Craton, Canada. Precambrian Res. 175, 1–15. https://doi.org/10.1016/j.precamres.2009.04.005

Normand, C., 2014. Rare Earths in Saskatchewan: Mineralization Types, Settings, and Distributions. Saskatchewan Minist. Econ. Sask. Geol. Surv. 105.

Normand, C., Mcewan, B., Ashton, K.E., 2009. Geology and REE Mineralization of the Hoidas Lake – Nisikkatch Lake Area Revisited m ain No l an Zemlak 2, 1–17.

Pandur, K., Ansdell, K.M., Pearson, J., Harper, C., Halpin, K.M., Creighton, S., Kontak, D.J., McFarlane, C., 2013. The Hoidas Lake Vein-Type Rare Earth Element Deposit: Zonation, Alteration, Fluid Evolution and Age Constraints, in: Saskatchewan Geological Survey Open House. p. 28.

Pandur, K., Kontak, D.J., Ansdell, K.M., 2014. Hydrothermal evolution in the Hoidas Lake vein-type REE deposit, Saskatchewan, Canada: Constraints from fluid inclusion microthermometry and evaporate mound analysis. Can. Mineral. 52, 717–744. https://doi.org/10.3749/canmin.140005

Partin, C.A., Bekker, A., Sylvester, P.J., Wodicka, N., Stern, R.A., Chacko, T., Heaman, L.M., 2014. Filling in the juvenile magmatic gap: Evidence for uninterrupted Paleoproterozoic plate tectonics. Earth Planet. Sci. Lett. 388, 123–133. https://doi.org/10.1016/J.EPSL.2013.11.041

Passchier, C.W., 2001. Flanking structures. J. Struct. Geol. 23, 951–962. https://doi.org/10.1016/S0191-8141(00)00166-8

Pehrsson, S., Martel, E., Percival, J., Campbell, J., Acosta-gongora, P., Thiessen, E., Jamison, D., Regis, D., Neil, B., Lauzon, G., Gibson, D., Lin, S., 2016. New regional geology and mineral occurrences of the South Rae in Northwest Territories from GEM2: implications for continuation of the Boomerang, Black Bay and Axis-Thye Lake trends, in: Saskatchewan Open House. p. 26.

Pehrsson, S.J., Berman, R.G., Eglington, B., Rainbird, R., 2013. Two Neoarchean supercontinents revisited: The case for a Rae family of cratons. Precambrian Res. 232, 27–43. https://doi.org/10.1016/j.precamres.2013.02.005

Pehrsson, S.J., Campbell, J.E., Martel, E., McCurdy, M.W., Agosta-Gongora, P., Thiessen, E., Jamison, D., Lauzon, G., Buller, G., Falck, H., Dyke, A.S., 2015. Report of 2015 activities for the geologic and metallogenic framework of the South Rae Craton, southeast Northwest Territories: GEM 2 South Rae quaternary and

bedrock project. Geol. Surv. Canada 24. https://doi.org/10.4095/297387

Pehrsson, S.J., Currie, M., Ashton, K.E., Harper, C.T., Paul, D., Pana, D., Berman, R.G., Bostock, H., Corkery, T., Jefferson, C.W., Tella, S., 2014a. Bedrock geology compilation and regional synthesis of south Rae and parts of Hearne domains, Churchill Province, Northwest Territories, Saskatchewan, Nunavut, Manitoba and Alberta. https://doi.org/10.4095/292232

Pehrsson, S.J., Percival, J.A., Davis, W.J., McCurdy, M.W., Berman, R.G., Hillary, E.M., Kiss, F., MacKinnon, A., Jefferson, C.W., 2014b. Operation GEM South Rae: Reconnaissance geology of the most poorly known part of the Churchill Province, Northwest Territories and Nunavut. Geol. Surv. Canada 25. https://doi.org/10.4095/293762

Regan, S.P., Williams, M.L., Chiarenzelli, J.R., Grohn, L., Mahan, K.H., Gallagher, M., 2017. Isotopic evidence for Neoarchean continuity across the Snowbird Tectonic Zone, western Churchill Province, Canada. Precambrian Res. 300, 201–222. https://doi.org/10.1016/J.PRECAMRES.2017.07.022

Regis, D., Martel, E., Davis, W.J., Pehrsson, S.J., Regis, D., Martel, E., Davis, W.J., Pehrsson, S.J., 2017. U-Pb zircon geochronology of metaplutonic rocks across the southern Rae province, Northwest Territories. Geol. Surv. Canada Open File, 1–37. https://doi.org/doi.org/10.4095/302772

Sanderson, D.J., Marchini, W.R.D., 1984. Transpression. J. Struct. Geol. 6, 449–458. https://doi.org/10.1016/0191-8141(84)90058-0

Schneider, D.A., Heizler, M.T., Bickford, M.E., Wortman, G.L., Condie, K.C., Perilli, S., 2007. Timing constraints of orogeny to cratonization: Thermochronology of the Paleoproterozoic Trans-Hudson orogen, Manitoba and Saskatchewan, Canada. Precambrian Res. 153, 65–95. https://doi.org/10.1016/J.PRECAMRES.2006.11.007

Shiels, C., Partin, C.A., Eglington, B.M., 2016. Provenance approaches in polydeformed metasedimentary successions: Determining nearest neighboring cratons during the deposition of the Paleoproterozoic Murmac Bay Group. Lithosphere 8, 519–532. https://doi.org/10.1130/L537.1

Stern, R.A., 1997. The GSC Sensitive High Resolution Ion Microprobe (SHRIMP): analytical techniques of zircon U-Th-Pb age determinations and performance evaluation. https://doi.org/10.4095/209089

Stern, R.A., Amelin, Y., 2003. Assessment of errors in SIMS zircon U–Pb geochronology using a natural zircon standard and NIST SRM 610 glass. Chem. Geol. 197, 111–142. https://doi.org/10.1016/S0009-2541(02)00320-0

Stern, R.A., Card, C.D., Pana, D., Rayner, N., 2003. SHRIMP U-Pb ages of granitoid basement rocks of the southwestern part of the Athabasca Basin, Saskatchewan and Alberta. Geol. Surv. Canada Radiogenic, 20.

Taylor, F.C., 1959. Geology of Penylan Lake - Firedrake Lake.

Thiessen, E.J., Regis, D., Gibson, H.D., 2017. U-Pb zircon geochronology of the Paleoproterozoic Wholdaia Lake shear zone, south Rae craton, Northwest Territories. Geol. Surv. Canada Open File. https://doi.org/10.4095/300655

Tremblay, L.P., 1972. Memoir 367 Geology of the Beaverlodge Mining Area, Saskatchewan.

Tremblay, L.P., 1971a. Generalized geological map, Beaverlodge area, Saskatchewan.

Tremblay, L.P., 1971b. Beaverlodge Structure Sections.

Tremblay, L.P., 1968. GEOLOGY OF THE BEAVERLODGE MINING AREA , (Parts of 74 N / 9 and 74 N/10). Geol. Surv. Canada Memoir 367, 489.

Wheeler, J.O., Hoffman, P.F., Card, K.D., Davidson, A., Sanford, B. V, Okulitch, A. V, Roest, W.R., 1996. Geological map of Canada. https://doi.org/10.4095/208175

Appendix: Geochronological Data

Table A-1. SHRIMP U-Pb data for a granitic dyke from the Labyrinth River area (Sample 15-DJ-468B)

15DJ468B Granitic Dyke, IP843																											
NAD83 UTM zone 13 6722603N 409507E																							Apparent ages (Ma)				
Spot Name	U (ppm)	Th (ppm)	Th/U	Hf/Yb	1s abs err	Yb ppm	1s abs err	Hf ppm	1s abs err	204Pb/ 206Pb	err (%)	f(206) 204 %	206Pb * (ppm)	208Pb */ 206Pb	err (%)	207Pb* /235U	err (%)	206Pb* /238U	err (%)	Corr Coeff	207Pb* /206Pb *	err (%)	206Pb/ 238U	err (abs)	207Pb/ 206Pb	err (abs)	Disc (%)
11984-111.2	378	507	1.39	105	3	88	2	9183	112	6.3E-6	71	0.01	104.7	0.407	0.9	5.026	1.3	0.3225	1.2	0.962	0.1130	0.3	1802	19	1849	6	+3
11984-111.1	302	502	1.72	81	2	116	2	9395	116	6.3E-5	28	0.11	84.7	0.513	1.6	5.060	1.3	0.3264	1.3	0.935	0.1124	0.5	1821	20	1839	9	+1
11984-010.1	420	285	0.70	81	2	139	3	11298	148	5.4E-4	7	0.93	117.8	0.228	1.3	5.079	1.3	0.3264	1.2	0.909	0.1129	0.6	1821	19	1846	10	+2
11984-086.1	1243	343	0.29	60	1	265	5	15823	194	8.7E-6	35	0.02	349.1	0.083	1.2	5.085	1.2	0.3268	1.2	0.985	0.1128	0.2	1823	19	1846	4	+1
11984-042.1	890	642	0.75	20	1	489	11	9823	119	8.0E-4	4	1.39	255.9	0.229	2.4	5.200	1.3	0.3349	1.2	0.929	0.1126	0.5	1862	19	1842	9	-1
11984-002.1	1538	267	0.18	67	2	276	5	18388	222	7.3E-5	10	0.13	443.0	0.055	3.9	5.211	1.2	0.3354	1.2	0.989	0.1127	0.2	1864	20	1843	3	-1
11984-112.1	464	13	0.03	81	2	165	3	13421	164	8.6E-5	22	0.15	132.5	0.012	8.5	5.251	1.3	0.3322	1.2	0.952	0.1146	0.4	1849	20	1874	7	+2
11984-013.1	107	53	0.52	199	5	56	1	11068	134	3.2E-5	50	0.06	38.7	0.141	2.5	8.373	1.7	0.4214	1.3	0.789	0.1441	1.0	2267	25	2277	18	+1
11984-099.1	184	128	0.72	110	3	104	3	11423	162	5.2E-5	38	0.09	66.7	0.210	2.1	8.593	1.8	0.4219	1.7	0.957	0.1477	0.5	2269	32	2320	9	+3
11984-024.1	194	383	2.04	43	1	213	4	9148	111	4.0E-5	33	0.07	71.8	0.591	0.9	8.781	1.3	0.4303	1.3	0.957	0.1480	0.4	2307	25	2323	7	+1
11984-036.1	196	410	2.15	39	1	234	5	9115	110	8.9E-5	21	0.15	75.5	0.621	0.9	9.309	1.3	0.4474	1.3	0.956	0.1509	0.4	2384	25	2356	7	-1
11984-009.1	416	76	0.19	89	2	144	3	12820	154	9.2E-6	45	0.02	157.6	0.051	2.0	9.319	1.4	0.4408	1.3	0.931	0.1533	0.5	2354	25	2383	9	+1
11984-077.1	605	102	0.17	82	2	171	3	13968	171	5.2E-6	58	0.01	229.0	0.050	2.0	9.361	1.7	0.4405	1.3	0.799	0.1541	1.0	2353	26	2392	17	+2
11984-048.1	1611	745	0.48	21	1	570	12	11792	155	1.2E-4	7	0.21	628.0	0.152	1.9	9.956	1.2	0.4538	1.2	0.973	0.1591	0.3	2412	24	2446	5	+2
11984-110.1	1054	92	0.09	53	1	240	5	12677	164	1.0E-5	27	0.02	425.9	0.026	4.3	10.243	1.7	0.4704	1.2	0.715	0.1579	1.2	2485	25	2434	20	-3
11984-059.1	348	164	0.49	39	1	247	5	9681	118	4.8E-6	71	0.01	137.5	0.143	1.4	10.443	1.5	0.4599	1.2	0.822	0.1647	0.9	2439	25	2504	14	+3
11984-017.1	191	74	0.40	59	2	174	7	10313	164	5.9E-5	26	0.10	76.9	0.121	4.1	10.843	1.5	0.4677	1.4	0.971	0.1682	0.3	2473	29	2539	6	+3
11984-070.1	1235	619	0.52	32	1	387	8	12375	150	1.4E-5	20	0.02	517.0	0.151	0.6	11.325	1.4	0.4873	1.4	0.958	0.1686	0.4	2559	29	2543	7	-1
11984-045.1	732	713	1.01	14	0	585	11	8368	101	2.0E-5	22	0.03	305.5	0.288	0.6	11.401	1.2	0.4858	1.2	0.990	0.1702	0.2	2552	25	2560	3	+0
11984-095.1	474	145	0.32	60	2	213	5	12838	159	6.2E-4	6	1.07	194.9	0.102	3.9	11.480	1.8	0.4783	1.5	0.820	0.1741	1.0	2520	31	2597	17	+4
11984-115.1	907	729	0.83	24	1	403	9	9615	152	4.9E-5	15	0.09	380.0	0.239	0.6	11.535	1.2	0.4876	1.2	0.991	0.1716	0.2	2560	25	2573	3	+1
11984-091.1	328	168	0.53	65	2	161	4	10542	129	9.8E-5	20	0.17	136.5	0.156	3.0	11.898	2.0	0.4847	1.7	0.826	0.1780	1.1	2548	35	2635	19	+4
11984-033.1	427	161	0.39	54	1	197	4	10545	128	4.8E-6	58	0.01	183.8	0.109	1.3	11.981	1.3	0.5005	1.2	0.900	0.1736	0.6	2616	26	2593	10	-1
11984-035.1	917	56	0.06	86	2	163	3	13921	169	1.1E-5	29	0.02	401.5	0.017	2.5	12.039	2.0	0.5098	1.9	0.971	0.1713	0.5	2656	42	2570	8	-4
11984-043.1	814	179	0.23	37	1	367	7	13423	190	3.5E-6	50	0.01	352.0	0.062	4.4	12.217	1.3	0.5034	1.2	0.906	0.1760	0.6	2628	26	2616	9	-1
11984-082.1	113	41	0.37	34	1	259	5	8743	106	4.1E-5	41	0.07	49.7	0.101	2.8	12.963	1.6	0.5100	1.3	0.854	0.1843	0.8	2657	29	2692	13	+2
11984-006.1	765	751	1.01	23	1	379	7	8905	108	2.4E-6	58	0.00	350.4	0.296	0.9	13.955	1.4	0.5331	1.3	0.972	0.1898	0.3	2755	30	2741	5	-1

Table A-2. SHRIMP U-Pb Data for a granodioritic gneiss from the Insula Lake area (Sample 15-DJ-476C)

15DJ476C Granodioritic Gneiss, IP843																											
NAD83 UTM zone 13 6710073N 398809E																							Apparent ages (Ma)				
Spot Name	U (ppm)	Th (ppm)	Th/U	Hf/Yb	1s abs err	Yb ppm	1s abs err	Hf ppm	1s abs err	204Pb/ 206Pb	err (%)	f(206) 204 %	206Pb * (ppm)	208Pb */ 206Pb	err (%)	207Pb* /235U	err (%)	206Pb* /238U	err (%)	Corr Coeff	207Pb* /206Pb *	err (%)	206Pb/ 238U	err (abs)	207Pb/ 206Pb	err (abs)	Disc (%)
11985-025.1	494	213	0.45	34	1	297	7	10101	141	4.2E-5	21	0.07	163.8	0.130	2.3	7.297	1.2	0.3860	1.2	0.978	0.1371	0.3	2104	22	2191	4	+5
11985-044.1	331	116	0.36	71	2	167	4	11825	171	2.8E-5	32	0.05	113.6	0.105	3.0	7.836	1.4	0.3996	1.4	0.976	0.1422	0.3	2167	26	2254	5	+5
11985-058.1	604	267	0.46	39	1	293	6	11387	138	1.8E-5	28	0.03	211.1	0.134	1.1	7.995	1.3	0.4067	1.2	0.986	0.1426	0.2	2200	23	2259	4	+3
11985-093.1	115	19	0.17	109	3	116	2	12618	203	6.0E-4	13	1.05	36.8	0.047	8.0	7.530	2.1	0.3721	1.3	0.635	0.1468	1.6	2039	23	2309	28	+14
11985-047.2	114	153	1.38	73	2	168	3	12310	164	1.1E-4	29	0.20	44.2	0.401	1.7	9.224	1.5	0.4513	1.4	0.912	0.1483	0.6	2401	27	2326	10	-4
11985-047.1	110	161	1.51	73	2	175	4	12704	156	7.4E-5	33	0.13	40.1	0.435	1.5	8.683	1.5	0.4247	1.3	0.926	0.1483	0.5	2282	26	2326	9	+2
11985-089.1	119	20	0.18	147	4	86	2	12660	164	2.0E-5	58	0.03	44.4	0.054	3.7	8.974	1.4	0.4364	1.3	0.945	0.1491	0.5	2335	26	2336	8	+0
11985-056.1	584	132	0.23	108	3	129	3	13873	168	9.9E-6	38	0.02	218.4	0.065	1.6	9.121	1.5	0.4356	1.4	0.962	0.1518	0.4	2331	28	2367	7	+2
11985-024.1	520	160	0.32	40	1	287	8	11443	164	1.2E-4	12	0.22	181.9	0.099	3.4	8.681	1.3	0.4072	1.2	0.926	0.1546	0.5	2202	23	2397	8	+10
11985-007.1	181	115	0.65	50	1	191	4	9503	115	2.2E-4	15	0.39	65.4	0.177	1.8	8.949	1.4	0.4197	1.3	0.884	0.1547	0.7	2259	24	2398	11	+7
11985-040.1	474	222	0.48	37	1	269	5	9937	121	1.0E-4	14	0.18	176.0	0.138	1.3	9.261	1.5	0.4324	1.4	0.900	0.1553	0.7	2317	27	2405	11	+4
11985-018.1	385	227	0.61	31	1	319	15	9789	130	1.0E-4	15	0.17	149.1	0.176	1.8	10.020	1.4	0.4506	1.2	0.858	0.1613	0.7	2398	24	2469	12	+3
11985-014.1	672	170	0.26	43	1	265	5	11275	153	4.4E-6	50	0.01	268.8	0.075	1.3	10.512	1.3	0.4659	1.2	0.946	0.1636	0.4	2466	25	2494	7	+1
11985-038.2	271	182	0.69	35	1	257	6	8982	111	9.9E-5	21	0.17	105.2	0.189	1.7	10.258	1.5	0.4515	1.4	0.963	0.1648	0.4	2402	29	2506	7	+5
11985-029.1	444	220	0.51	35	1	281	6	9944	137	3.8E-4	8	0.66	173.9	0.141	1.5	10.366	1.4	0.4560	1.3	0.971	0.1649	0.3	2422	27	2506	6	+4
11985-055.1	247	123	0.52	52	2	177	6	9208	229	2.5E-4	12	0.43	94.1	0.148	3.4	10.123	1.3	0.4442	1.2	0.957	0.1653	0.4	2370	25	2510	6	+7
11985-032.1	541	231	0.44	38	1	299	6	11334	150	2.6E-4	8	0.46	215.3	0.129	1.2	10.636	1.2	0.4631	1.2	0.979	0.1666	0.3	2453	25	2524	4	+3
11985-038.1	530	447	0.87	25	1	348	8	8565	119	3.1E-5	59	0.05	219.2	0.248	0.8	11.226	1.4	0.4815	1.3	0.966	0.1691	0.4	2534	28	2549	6	+1
11985-085.1	176	132	0.78	31	1	275	5	8521	103	5.6E-5	28	0.10	73.8	0.221	1.5	11.438	1.4	0.4890	1.3	0.916	0.1696	0.6	2566	27	2554	9	-1
11985-033.1	183	106	0.60	53	1	185	4	9807	132	3.9E-5	33	0.07	74.3	0.171	1.7	11.062	1.3	0.4717	1.3	0.961	0.1701	0.4	2491	26	2559	6	+3
11985-064.1	422	273	0.67	30	1	309	6	9211	112	3.6E-5	22	0.06	174.6	0.189	1.0	11.338	1.3	0.4815	1.2	0.952	0.1708	0.4	2534	25	2565	7	+1
11985-075.1	354	286	0.83	22	1	407	14	8931	108	1.5E-5	38	0.03	147.8	0.232	1.0	11.432	2.0	0.4853	1.8	0.874	0.1708	1.0	2550	38	2566	17	+1
11985-048.1	477	337	0.73	25	1	394	8	9878	121	1.7E-4	10	0.29	198.7	0.208	0.9	11.475	1.3	0.4849	1.3	0.984	0.1716	0.2	2549	28	2574	4	+1
11985-001.1	177	80	0.47	64	2	155	3	9873	119	4.1E-6	100	0.01	72.6	0.136	1.8	11.323	1.8	0.4774	1.6	0.892	0.1720	0.8	2516	33	2577	13	+3
11985-006.1	351	197	0.58	47.4	1	216	5	10248	124	4.5E-5	22	0.08	142.6	0.165	1.2	11.230	1.3	0.4730	1.2	0.978	0.1722	0.3	2497	25	2579	4	+4
11985-085.2	257	135	0.54	27	1	308	6	8314	102	4.7E-5	29	0.08	109.8	0.153	2.8	11.816	1.5	0.4973	1.5	0.973	0.1723	0.3	2602	31	2580	6	-1
11985-077.1	150	85	0.58	48.5	1	180	4	8750	115	7.8E-5	27	0.13	62.0	0.163	2.0	11.498	1.4	0.4822	1.3	0.952	0.1729	0.4	2537	27	2586	7	+2
11985-028.1	421	128	0.31	57	2	207	4	11820	203	2.8E-4	13	0.48	174.4	0.089	2.1	11.505	1.4	0.4816	1.3	0.919	0.1733	0.6	2534	27	2589	9	+3
11985-060.2	494	392	0.82	19.2	1	476	12	9165	112	2.5E-5	28	0.04	209.0	0.229	1.0	11.797	1.2	0.4926	1.2	0.982	0.1737	0.2	2582	26	2594	4	+1
11985-036.1	374	162	0.45	42.7	1	256	5	10953	133	4.0E-5	22	0.07	156.2	0.120	1.4	11.685	1.2	0.4867	1.2	0.980	0.1741	0.2	2557	26	2598	4	+2
11985-026.1	546	204	0.39	53.8	1	214	4	11519	139	2.0E-4	9	0.34	229.4	0.110	1.3	11.761	1.4	0.4889	1.2	0.877	0.1745	0.7	2566	26	2601	11	+2
11985-060.1	522	440	0.87	18.4	1	508	21	9364	144	1.4E-4	74	0.24	211.5	0.254	5.1	11.469	2.9	0.4719	2.4	0.820	0.1763	1.6	2492	49	2618	27	+6

Table A-3. Compilation of available pre-Arrowsmith U-Pb ages around the Black Bay Fault

ID	Age (Ma)	Error (Ma)	Type	Side of Fault	Domain	Area	Rock Type	Lat	Lon	Reported By
4700-6106	3412	21	Detrital	East	Beaverlodge	Fookes Lake	Fookes Lake Quartzite	59.556	-108.440	Ashton et al., 2013
RH98-LBG	3060	40	Crystal	East	Beaverlodge	Lodge Bay	Lodge Bay Granite	59.439	-108.624	Hartlaub et al., 2004
HUD84-319	3014	10	Crystal	East	Beaverlodge	Elliot Bay	Elliot Bay Granite	59.390	-108.725	Persons, 1983
12PBA-S084	2700		Inheritance	East	Firedrake	Abitau	Grt-bt migmatitic paragneiss,	60.314	-106.937	Davis et al., 2015
15EM71A	2700		Inheritance	East	Firedrake	Gardiner Lake	Firedrake soup	60.534	-105.753	Regis et al., 2017
15EM81A	2699	24	Crystal	East	Firedrake	Dunvegan Lake	Tonalite	60.072	-107.254	Regis et al., 2017
15EM71B	2694	8	Crystal	East	Firedrake	Gardiner Lake	Older firedrake	60.534	-105.753	Regis et al., 2017
16EM1206C	2691	10	Crystal	East	Firedrake	Bull Lake	Cpx-syenite	61.227	-105.345	Regis et al., 2017
12PBA035	2687	6	Crystal	East	Firedrake	Labyrinth Lake	Hbl-tonalite orthogneiss	60.646	-106.554	Davis et al., 2015
15EM80A	2665	8	Crystal	East	Firedrake	Smalltree Lake	Older firedrake	60.864	-104.865	Regis et al., 2017
12PBA092	2663		Crystal	East	Firedrake	Gozdz Lake	Opx-tonalite	61.192	-105.535	Davis et al., 2015
15EM80B	2650		Inheritance	East	Firedrake	Smalltree Lake	Firedrake soup	60.864	-104.865	Regis et al., 2017
16EM1216A	2649	15	Crystal	West	McCann	Mcarthur	Cpx-qtz-monzodiorite	61.572	-106.327	Regis et al., 2017
12PBA-S090	2628	5	Crystal	West	McCann	Sylvan Lake	Opx-bt,mangerite	60.816	-106.883	Davis et al., 2015
4705-0121	2600		Detrital	West	Zemlak	Ena Lake	Ena Lake Psammopelitic Gneiss	59.809	-108.272	Ashton et al., 2013
15EM55C	2596	5	Crystal	West	McCann	Thoa River	Megacrystic monzogranite	60.637	-107.260	Regis et al., 2017
15EM83A	2594	8	Crystal	West	McCann	Labyrinth Lake	Tonalite	60.737	-106.474	Regis et al., 2017
12PBA-S014	2589	26	Crystal	West	McCann	Labyrinth Lake	Hbl-bt granodiorite orthogneiss	60.730	-106.528	Davis et al., 2015
15DJ476C	**2589**	**9**	**Crystal**	**West**	**McCann**	**Insula Lake**	**Granodioritic gneiss**	**60.514**	**-106.843**	**This thesis**
12PBA-S088B	2586	7	Crystal	West	McCann	Labyrinth Rapids	Labyrinth rapids megacrystic	60.639	-106.699	Davis et al., 2015
12PQB88C	2573	10	Crystal	West	McCann	Labyrinth Rapids	Augen Monzogranite	60.639	-106.699	Regis et al., 2017
C174	2533	28	Meta	West	McCann	Cronyn Lake	Granulite-facies diatexite migmatite	61.315	-106.966	Berman et al., 2013
0461-042	2516	5	Crystal	West	Zemlak	Nisikkatch Lake	Gneissic diorite	59.877	-107.883	Card et al., 2016

Table A-4. Compilation of available Arrowsmith U-Pb ages around the Black Bay Fault

ID	Age (Ma)	Error (Ma)	Type	Side of Fault	Domain	Area	Rock Type	Lat	Lon	Reported By
T703	2487	13	Meta	West	McCann	Stephenson Lake	Diatexite migmatite	61.720	-105.872	Berman et al., 2013
J419	2473	14	Meta	West	McCann	Conventry Lake	Granulite-facies metatexite migmatite	61.042	-106.297	Berman et al., 2013
C174	2472	11	Meta	West	McCann	Cronyn Lake	Granulite-facies diatexite migmatite	61.315	-106.966	Berman et al., 2013
10CN326-1	2383	32	Crystal	West	Zemlak	Bear Lake	Bear Lake REE Titanite	59.795	-108.427	Normand, C., 2014
	2380		Inheritance	West	Zemlak	Hoidas	Hoidas REE dykes	59.935	-107.812	Gunning and Card, 2005
15EM55C	2380		Meta	West	McCann	Thoa River	Megacrystic monzogranite	60.637	-107.260	Regis et al., 2017
16EM1216A	2374	26	Meta	West	McCann	Mcarthur	Cpx-qtz-monzodiorite	61.572	-106.327	Regis et al., 2017
T696	2372	16	Meta	West	McCann	Gardenia Lake	Metatexite migmatite	61.989	-105.682	Berman et al., 2013
12PBA-S080	2358	9	Crystal	West	McCann	Burpee Lake	Foliated blue quartz grt-opx diatexite	61.460	-106.727	Davis et al., 2015
C174	2352	13	Meta	West	McCann	Cronyn Lake	Granulite-facies diatexite migmatite	61.315	-106.966	Berman et al., 2013
12PBA-S078	2352	10	Crystal	West	McCann	Burpee Lake	Bt-granite dyke	61.459	-106.747	Davis et al., 2015
	2348	19	Inheritance	West	Zemlak	Hoidas	Hoidas Zircon	59.935	-107.812	Pandur et al., 2013
12PBA-S088B	2348	22	Meta	West	McCann	Labyrinth Rapids	Labyrinth rapids megacrystic	60.639	-106.699	Davis et al., 2015
T703	2345	11	Meta	West	McCann	Stephenson Lake	Diatexite migmatite	61.720	-105.872	Berman et al., 2013
11KA-250	2331	4	Crystal	East	Beaverlodge	Intermediate Pit	Pink leucogranite	59.580	-108.514	Ashton et al., 2017
15DJ476C	**2330**	**10**	**Meta**	**West**	**McCann**	**Insula Lake**	**Granodioritic gneiss**	**60.514**	**-106.843**	**This thesis**
RH98-46	2329	9	Detrital	East	Beaverlodge	Dunbar Bay	Dunbar Bay Psammitic Gneiss	59.469	-108.295	Ashton et al., 2013
4701-0765	2327	14	Detrital	East	Beaverlodge	Elliot Bay	Basal conglomerate	59.388	-108.723	Ashton et al., 2013
RH98-22	2326	15	Crystal	East	Beaverlodge	Moose Island	Mackintosh Bay Granite	59.465	-108.307	Hartlaub et al., 2007
4705-0007	2325	7	Crystal	West	Zemlak	Ena Lake	Ena Lake Granodiorite-Tonalite	59.929	-108.189	Ashton et al., 2007
12PBA-S056	2325	39	Crystal	West	McCann	Hostile Lake	Foliated quartz diorite	60.931	-106.156	Davis et al., 2015
4709-6006	2322	5	Crystal	East	Beaverlodge	Mackintosh Bay	Mackintosh Bay Porphyry Dyke	59.484	-108.270	Ashton et al., 2013
RH00-03	2321	3	Crystal	East	Beaverlodge	East of Gunnar Mine	Gunnar Granite	59.380	-108.865	Hartlaub et al., 2007
RH99-576	2320	44	Crystal	East	Beaverlodge	Geebee Lake	Geebee Lake Granite	59.549	-108.306	Hartlaub et al., 2007
4703-0006	2316	1	Crystal	East	Beaverlodge	Crackingstone Peninsula	Milliken Lake Pluton	59.451	-108.771	Ashton et al., 2007
C174	2315	11	Meta	West	McCann	Cronyn Lake	Granulite-facies diatexite migmatite	61.315	-106.966	Berman et al., 2013
	2311	7	Crystal	West	Zemlak	Hoidas	JAK zone	59.939	-107.801	Normand, C., 2014
B141	2298	21	Meta	West	McCann	Penylan Lake	Granulite-facies diatexite migmatite	61.842	105.873	Berman et al., 2013
J419	2283	22	Meta	West	McCann	Coventry Lake	Granulite-facies metatexite migmatite	61.042	-106.297	Berman et al., 2013
4707-0210	2171	31	Detrital	East	Beaverlodge	Mackintosh Bay	Mackintosh Bay Pelite	59.484	-108.269	Ashton et al., 2013

Table A-5. Compilation of available post-Arrowsmith U-Pb Ages in the Black Bay Fault Area

ID	Age (Ma)	Error (Ma)	Type	Side of Fault	Domain	Area	Rock Type	Lat	Lon	Reported By
4707-0210	2171	31	Detrital	East	Beaverlodge	Mackintosh Bay	Mackintosh Bay Pelit	59.484	-108.2695	Ashton et al., 2013
12PBA-S088A	2066	31	Crystal	West	McCann	Labyrinth Rapids	Fine Grained gabbro	60.639	-106.6994	Report, percival 2013
HUD84-317	1994	37	Crystal	East	Beaverlodge	Box Mine	Box Granite	59.456	-108.5222	Persons, 1983
4701-0299	1974	5	Crystal	West	Zemlak	Orbit Bay	Granite	59.530	-108.8925	Hartlaub et al., 2005
B141	1946	54	Meta	West	McCann	Penylan Lake	Granulite-facies diatexite migmatite	61.842	105.8727	Berman et al., 2013
B016	1936	10	Meta	East	Beaverlodge	Mackintosh Bay	Grt-St-Sil Schist, Grt	59.481	-108.2954	Bethune et al., 2013
4701-8025	1936		Meta	West	Zemlak	Wynert Lake	Psammopelitic gneiss	59.567	-108.7550	Ashton et al., 2009
B010a	1933	8	Meta	East	Beaverlodge	Mackintosh Bay	Grt-Bt-gibrolitic Sil schist, Grt	59.491	-108.2561	Bethune et al., 2013
RH01-06	1933	3	Crystal	West	Zemlak	ranium City Cemetar	Pink leucogranite	59.558	-108.6388	Hartlaub et al., 2005
B016	1932	16	Meta	East	Beaverlodge	Mackintosh Bay	Grt-St-Sil Schist, Matrix	59.481	-108.2954	Bethune et al., 2013
B002e	1931	11	Meta	West	Beaverlodge	Mackintosh Bay	Grt-bt schist	59.484	-108.3964	Bethune et al., 2013
14KA-095	1931	11	Meta	West	Zemlak	Bushell Inlet	Deformed meta-psammite, Rim	59.504	-108.7695	Shiels et al., 2016
RH99-354	1930		Crystal	East	Beaverlodge	Donaldson Lake	Donaldson Lake Pluton	59.600	-108.4151	Hartlaub et al., 2004
4705-0007	1922	16	Meta	West	Zemlak	Ena Lake	Ena Lake Granodiorite-Tonalite	59.929	-108.1891	Ashton et al., 2007
14KA-095	1917	15	Meta	West	Zemlak	Bushell Inlet	Deformed meta-psammite, rim	59.504	-108.7695	Shiels et al., 2016
	1917	12	Crystal	West	Zemlak	Hoidas	Hoidas Titanite	59.935	-107.8120	Pandur et al., 2013
4700-4541	1911	10	Meta	East	Beaverlodge	Elliot Bay	Mafic volcanic	59.383	-108.7514	Hartlaub, 2004
10CN326-1	1910	37	Meta	West	Zemlak	Bear Lake	Bear Lake REE Titanite	59.795	-108.4265	Normand, C., 2014
	1909	11	Crystal	West	Zemlak	Hoidas	Hoidas Monazite	59.935	-107.8120	Pandur et al., 2013
4700-0320	1908	1	Meta	West	Zemlak	Erickson Inlet	Meta-gabbro	59.507	-108.8043	Ashton and Hunter, 2003
	1906	34	Meta	West	Zemlak	Hoidas	Hoidas Zircon	59.935	-107.8120	Pandur et al., 2013
B010b	1904	8	Meta	East	Beaverlodge	Mackintosh Bay	Grt-Bt-gibrolitic Sil schist, Matrix	59.491	-108.2561	Bethune et al., 2013
12PBA-S056	1894	11	Meta	West	McCann	Hostile Lake	Foliated quartz diorite	60.931	-106.1556	Davis et al., 2015
	1870		Crystal	West	Zemlak	Hoidas	Hoidas REE dykes	59.935	-107.8120	Gunning and Card, 2005
J592	1855	17	Meta	East	Firedrake	Vermette Lake	Grt-bearing diatexite migmatite	61.259	-105.6688	Berman et al., 2013
10CN326-1	1848	20	Crystal	West	Zemlak	Bear Lake	Bear Lake REE Zircon	59.795	-108.4265	Normand, C., 2014
T902	1847	14	Meta	West	McCann	Andrecyk Lake	Grt-Crd metatexite migmatite	61.041	-105.3269	Berman et al., 2013
15EM81A	1846	5	Meta	East	Firedrake	Dunvegan Lake	Tonalite	60.072	-107.2541	Regis et al., 2017
15DJ468B	1844	4	Crystal	West	McCann	Labrinth Rapids	Granite	60.629	-106.6540	This thesis
	1841	5	Crystal	West	Zemlak	Hoidas	Hoidas Monazite	59.935	-107.8120	Pandur et al., 2013
12PBA-S014	1838	6	Crystal	West	McCann	Labyrinth Lake	Foliated hbl augen gneiss	60.730	-106.5276	Davis et al., 2015
12PBA-S084	1836	5	Meta	East	Firedrake	Abitau	Grt-bt migmatitic paragneiss,	60.314	-106.9368	Davis et al., 2015
RH99-354	1830		Meta	East	Beaverlodge	Donaldson Lake	Donaldson Lake Granite	59.600	-108.4153	Ashton et al., 2013
12PBA-S088A	1830	5	Meta	West	McCann	Labyrinth Rapids	Fine grained gabbro	60.639	-106.6994	Report, percival 2013
15PA390	1829	4	Crystal	East	Firedrake	Gemelo	Cpx-Syenite	60.744	-106.1315	Pehrsson et al., 2016
J592	1829	10	Meta	East	Firedrake	Vermette Lake	Grt-bearing diatexite migmatite	61.259	-105.6688	Berman et al., 2013
8311-74	1828	3	Meta	East	Train	Southern Train	Amphibolite	59.747	-107.2568	Ashton et al., 2009
	1828	6	Crystal	West	Zemlak	Hoidas	Hoidas Titanite	59.935	-107.8120	Pandur et al., 2013
15EM71A	1825		Meta	East	Firedrake	Gardiner Lake	Firedrake soup	60.534	-105.7533	Regis et al., 2017
15EM80B	1824	4	Meta	East	Firedrake	Smalltree Lake	Firedrake soup	60.864	-104.8646	Regis et al., 2017
	1820	25	Crystal	West	Zemlak	Hoidas	Hoidas Apatite	59.935	-107.8120	Pandur et al., 2013
4701-9042	1818	4	Crystal	West	Zemlak	Fold Island	Uranium City Dyke	59.513	-108.9298	Ashton and Hunter, 2003
12PBA092	1817	36	Meta	East	Firedrake	Gozdz Lake	Opx-Tonalite	61.192	-105.5353	Davis et al., 2015